1981

Effect of prestressing the deck in continuous bridge of composite construction.

Nabil Fouad Fanouse. Grace
University of Windsor

NOTICE

AVIS

The quality of this microfiche is heavily dependent upon the quality of the original thesis submitted for microfilming. Every effort has been made to ensure the highest quality of reproduction possible.

If pages are missing, contact the university which granted the degree.

Some pages may have indistinct print especially if the original pages were typed with a poor typewriter ribbon or if the university sent us a poor photocopy.

Previously copyrighted materials (journal articles, published tests, etc.) are not filmed.

Reproduction in full or in part of this film is governed by the Canadian Copyright Act, R.S.C. 1970, c. C-30. Please read the authorization forms which accompany this thesis.

La qualité de cette microfiche dépend grandement de la qualité de la thèse soumise au microfilmage. Nous avons tout fait pour assurer une qualité supérieure de reproduction.

S'il manque des pages, veuillez communiquer avec l'université qui a conféré le grade.

La qualité d'impression de certaines pages peut laisser à désirer, surtout si les pages originales ont été dactylographiées à l'aide d'un ruban usé ou si l'université nous a fait parvenir une photocopie de mauvaise qualité.

Les documents qui font déjà l'objet d'un droit d'auteur (articles de revue, examens publiés, etc.) ne sont pas microfilmés.

La reproduction, même partielle, de ce microfilm est soumise à la Loi canadienne sur le droit d'auteur, SRC 1970, c. C-30. Veuillez prendre connaissance des formules d'autorisation qui accompagnent cette thèse.

<div align="center">

THIS DISSERTATION
HAS BEEN MICROFILMED
EXACTLY AS RECEIVED

LA THÈSE A ÉTÉ
MICROFILMÉE TELLE QUE
NOUS L'AVONS REÇUE

</div>

EFFECT OF PRESTRESSING THE DECK IN CONTINUOUS
BRIDGE OF COMPOSITE CONSTRUCTION

by

Nabil Fouad Fanouse Grace

A Thesis
Submitted to the Faculty of Graduate Studies
through the Department of
Civil Engineering in Partial Fulfillment
of the Requirements for the Degree
of Master of Applied Science at
The University of Windsor

Windsor, Ontario, Canada
1981

To my wife Nadrine and our parents

ABSTRACT

A mathematical method is presented for the analysis of composite bridges by the more reliable orthotropic plate theory. The deflection of the composite bridge is assumed in the form of a Fourier series so as to satisfy the governing differential equation of equilibrium. The arbitrary constants in the deflection function are chosen to satisfy the appropriate boundary conditions. An available computer program for solving orthotropic plates or bridges subjected to lateral loads is modified to compute the strain and deflection of continuous composite bridges. An experimental study is carried out on two continuous two-span composite bridge models to obtain a better understanding of the behaviour of laterally loaded composite bridges. In this investigation, a solution for the elimination of undesirable transverse cracks in the negative moment region (over the intermediate support) is obtained. Theoretical expressions for determining the flexural and torsional rigidities of uncracked sections are established. The effect of the presence of diaphragms on the transverse distribution of the load is examined. The deflections, longitudinal and transverse moments at the middle of the span and the longitudinal moment at the intermediate support obtained from tests, are found to be in satisfactory agreement with the theoretical results. Furthermore, theoretical comparative studies are carried out on four different aspect ratios of prototype continuous composite bridges according to the proposed

rigidities and those according to the Ontario Highway Bridge Design Code (OHBDC), and the importance of the diaphragms is highlighted.

ACKNOWLEDGEMENTS

The level of appreciation and respect that I feel towards my advisor, Dr. J.B. Kennedy, Professor of Civil Engineering at the University of Windsor, cannot be expressed strictly in written form, but will be carried with me for the rest of my life. To him I say "Thank you."

The aid of Mr. F. Kiss and Mr. P. Feimer during the experimental work is greatly appreciated. Thanks are also due to the staff of the computer centre for their assistance and help.

Thanks are also due to Mrs. Barbara Denomey for typing the manuscript.

TABLE OF CONTENTS

LIST OF FIGURES

LIST OF TABLES

LIST OF APPENDICES

LIST OF NOTATION

$A_{j1}-A_{j8}$	Definite integrals (Appendix A).
A_n	Arbitrary function in n.
a	Semi-width of the bridge.
$B_{j1}-B_{j2}$	Definite integrals defined (Appendix A).
B_n	Arbitrary function in n.
b	Half span length of the slab.
$C_{1n}-C_{16n}$	Arbitrary functions dependent on n.
$C_{17}-C_{24}$	Arbitrary constants.
D	Flexural rigidity of the flange plate with respect to its middle plane.
$D_x,\ D_y$	Flexural rigidities of the bridge per unit width and length, respectively.
$D_{xy},\ D_{yx}$	Transverse and longitudinal torsional rigidities, respectively.
$D_1,\ D_2$	Coupling rigidities - contribution of bending to torsional rigidities of the bridge.
EI	Flexural rigidity of the edge beam.
$E_c,\ E_s$	Modulus of elasticity of concrete, steel.
$e_x,\ e_y$	Depths of neutral plane from top fibre for bending in the x-(y) directions.
f'_c	28 days compressive strength of concrete.
$G_{xy},\ G_{yx}$	Shear modulii of the orthotropic bridge.
GJ	Torsional rigidity of the edge beam.
H	Effective torsional rigidity of the bridge.
h	Thickness of flange plate.

I_x', (I_y')	Moment of inertia of transverse (longitudinal) girders with respect to the assumed N.A.
I_{xy}, I_{yx}	Torsional constants.
M_x, M_y, M_{xy}	Bending and torsional moments associated with the x and y axes.
m	Integer >1, number of harmonics.
n	Integer >1, number of harmonics.
Q_x	Shear force per unit width of the plate.
$q(x,y)$	Load function.
$S_x (S_y)$	Spacing of girders in transverse (longitudinal) direction.
W	Deflection function.
W_c	Complementary solution.
W_p	Particular solution.
x,y,z	Rectangular axes.
μ	Poisson's ratio of concrete.
α_m	Equals $m\pi/a$.
α_n'	Equals $n\pi/a$.
β_m	Equals $m\pi/b$.
β_n	Equals $n\pi/b$.
ε_x, ε_y	Strain in x and y directions.

CHAPTER I

INTRODUCTION

1.1 General

A typical composite slab-girder highway bridge structure consists of three major structural elements; namely, a reinforced concrete slab constructed over steel girders which are interconnected with lateral diaphragms spaced at intervals along the span. The transverse steel diaphragms are usually rigidly connected between all girders at a given location, so that the diaphragms and girders form a grid work. The concrete deck is attached to the top flange of the steel girders with mechanical shear connectors, which are assumed to eliminate relative movement between the girders and slab. Due to variations in the longitudinal and transverse rigidities, the bridge behaves like an orthotropic plate. Thus, it is essential to use an exact analytical solution in order to predict accurately the behaviour of such construction.

1.2 Objective

The overall objectives of this investigation are as follows:

1) Eliminate the undesirable transverse cracking of the deck in the negative moment region (slab in tension) in the vicinity of the intermediate support of a continuous bridge;

2) Develop theoretical expressions for determining flexural and torsional rigidities for the uncracked section

of the composite bridge, and verify the theoretical analysis by means of experimental results;

3) To determine the distributions for deflection, longitudinal and transverse moment for each longitudinal girder at the mid span section as well as at the intermediate support section of a composite bridge subjected to a concentrated lateral load.

1.3 Scope

Mathematical formulation of the problem using a Fourier series for lateral forces is derived. The test of a structural composite bridge, one-eighth scale in the horizontal direction and one-fourth scale in the vertical direction, "direct" model can simulate the behaviour of the prototype both before and after transverse cracking at the intermediate support. Analysis and discussion of the theoretical and experimental results from the two bridges are presented in this work.

The experimental work comprised of the construction and testing of two bridge models:

(I)   The first bridge was two-span continuous structure, each span consisting of five steel I-beams connected to five diaphragms. This bridge model was designed according to the Ontario Highway Bridge Design Code, (18), and was subjected to a concentrated lateral load;

(II)   The second bridge, with the same dimensions as the first bridge but with a portion of the concrete deck at the intermediate support prestressed.

CHAPTER II

HISTORICAL REVIEW

2.1 Review of Literature

Composite steel and concrete beams for bridges have been used extensively in Canada and the United States for a number of years. The popularity of composite bridge construction led to the adoption in 1944 of general specifications governing this type of construction. Extensive research leading to practical design rules for shear connectors and introduction of stud shear connectors resulted in the widespread use of composite design in bridges by the end of 1950's.

Composite design for bridges in Canada and the United States has been limited primarily to simple spans or the positive moment (slab in compression) regions of continuous spans. In 1953, Sies and Viest, (22), discussed the negative moment regions of continuous composite beam bridges in some detail. This discussion was based on the static behaviour of two composite bridge models (22). These models differed in that one had shear connectors throughout the beam while the second had shear connectors in the positive moment regions only. From these studies it was concluded that:

1) In the negative moment regions, only the slab reinforcement can act compositely with the steel beams;

2) in bridges with shear connectors throughout the beam, the slab reinforcement was fully effective; with connectors omitted from the negative moment region, the slab

was only partly effective;

    3) the action of both of these continuous composite bridges was about the same since the distribution of strains and of moments in both positive and negative moment regions were nearly the same.

    In 1958, Viest, Fountain, and Siess, (27), were able to conclude, based on the above studies, that the use of an elastic analysis in combination with the usual load distribution factors is justified, with no special provisions needed for the design of continuous composite bridges. In 1965, (23), Slutter and Driscoll found that in the positive moment region, the concrete contributed to the ultimate moment of the cross-section; in the negative moment region, only the steel beam plus the reinforcement was effective. In 1962, Iwamoto, (13), suggested that only the steel beam be considered effective over the negative moment regions, and suggested expansion joints in the slab to control cracking. In Japan, at that time (1962), eleven continuous composite-girder bridges had been constructed since 1958. In each bridge, the concrete slab in the negative moment region had been pre-compressed by prestressing with steel wires. In 1964, Tachibana, Kondo, and Ito, (25), discussed the behaviour of continuous composite beams prestressed with wire cables. The studies reported by Barnard, and Johnson, (3), investigated the behaviour of longitudinal reinforcements over the supports. Continuous composite design with discontinuous shear connection in the negative moment region was permitted

by the 1969 AASHO bridge specifications provided that addi-
tional connectors are placed in the vicinity of the dead
load inflection points to prevent overstressing of the shear
connectors in the positive moment regions. In 1967, a
report (6) proposed that connectors should be provided
throughout the length of the continuous beam, this was con-
sidered necessary because, in the negative moment regions of
composite beams with continuous longitudinal reinforcement,
the existing tensile forces must be carried by connectors
along the beam length. It was suggested that connectors
in the negative moment region were also required in order to
maintain flexural conformance and to prevent the sudden
transition from composite to a non-composite section. In
addition, these connectors would tend to minimize the large
differentials in slip deformation.

In 1972, Fisher, Daniels, and Slutter, (7), confirmed
the desirability of increasing the amount of longitudinal
reinforcing steel in the slab over the negative moment region
to at least 1% of the cross-section area of the concrete. It
was desirable for most of this reinforcement to be placed
near the top surface of the slab. It was suggested that this
assisted with controlling cracking at the negative moment
region.

The study of theory of plates goes back to the French
mathematician, Sophie Germain (1816), who obtained a differ-
ential equation for the vibration of plates, but she
neglected the work done by warping of the middle surface.

The first corrected differential equation for the free vibration of plates was used by Lagrange by adding the missing term in Sophie's equation. This work which was improved by researchers such as Navier, Poisson, and Kirchoff, is considered to be the basis for the classical thin plate theory. In 1956, Huffington (11) investigated theoretically and experimentally the method for the determination of rigidities for metallic rib-reinforced deck structures. Methods of analysing rectangular and skew deck plates with simple boundary conditions have been recently investigated by Kennedy (15,16). In 1968 Jackson, (14) proposed a method to estimate the torsional rigidities of concrete bridge decks, using the membrane analogy and the estimation of the junction effect. Mathematical analysis of grid systems with particular regard to bridge type was given by Bares and Massonnet (2) and Rowe (21) together with practical applications.

CHAPTER III

THEORETICAL FORMULATION

3.1 General Concept

In a composite bridge, the grid elements may be either reinforced or prestressed concrete beams or steel girders. The design of a composite bridge consisting of a reinforced concrete slab acting as a part of the upper flange of the longitudinal steel beams usually assumes that the entire system acts as a monolithic unit because the resistance to shear between the slab and the beams is provided by shear connectors. The effect of the composite action may be adequately included in the computation of the beam moment if the bridge deck is treated as an orthotropic plate with eccentric stiffeners, that is, a plate is stiffened only at the bottom by longitudinal and transverse members that are mutually perpendicular and may have different properties in each direction. In dealing herein with orthotropic concrete deck, it is assumed that orthotropy is a result of geometry and not of material, see Figure 3.1 and Figure 3.2.

3.2 Theoretical Background

Several methods have been developed to analyse such systems considering the deck either as a gridwork, or as an orthotropic plate, both approaches being permissible idealisations of the actual system. However, an analysis based on either assumption is only an approximation and not an exact solution. Both are based generally on Huber's theory of anisotropic plates with certain modifications.

Of the two possible approaches, the orthotropic plate concept is essentially simpler and possesses important practical advantages. The important feature in treating the deck system as an orthotropic plate is that the torsional rigidity of the system can be readily included. In this, it is assumed that the rigidities of both the longitudinal girders and diaphragms are uniformly distributed throughout the deck in the directions perpendicular to the respective members. Thus the actual discontinuous structure of the bridge is represented by an idealized substitute orthotropic plate of uniform thickness reflecting the characteristic properties of the actual system. The success of the orthotropic plate theory depends completely on defining the equivalent orthotropic plate. Since the orthotropic plate assumes a continuous medium, the load can be applied at any point to yield a true continuous influence surface over the entire deck area. The solution therefore is valid for any load position.

3.3 Assumptions

The analytical approach to the problem of the orthotropic plate has to be based on some simplifying assumptions related to the form and material of the plate and to the state of strain induced by the external loading. The assumptions for orthotropic plates are based on the same assumptions used in the analysis of isotropic plates, and they are as follows:

a) The materials of the plate are elastic, i.e.,

the stress-strain relationship is given by Hooke's law;

b) The material of the plate is considered to be homogeneous, by transforming the steel girder (area) into an equivalent area of concrete;

c) The plate thickness is uniform and small compared with lateral dimensions of the plate. Thus the shearing and normal stresses on the plane of symmetry are small enough to be neglected;

d) The deflections of the plate are small in comparison with its thickness, and are such that there is no normal strain on planes tangent to the middle plane;

e) Straight lines normal to the middle plane of the plate remain straight and normal to the middle plane of the plate after bending.

However, theoretical investigations and experimental data indicate that the orthotropic plate theory is applicable to structurally orthotropic plates under the following provisions:

a) Flexural and twisting rigidities do not depend on the boundary conditions of the plate or on the distribution of the lateral load;

b) A perfect interaction exists between plate and stiffeners.

3.4 Governing Differential Equation For Lateral Load

It is assumed that the material of the plate has three planes of symmetry with respect to its elastic properties. Taking these planes as the coordinate planes, the relations

between the moments and deflections are:

$$M_x = -(D_x W,_{xx} + D_1 W,_{yy})$$

$$M_y = -(D_y W,_{yy} + D_2 W,_{xx}) \qquad (3.1)$$

$$M_{xy} = D_{xy} W,_{xy}$$

where, D_x, D_y = flexural rigidities of the plate per unit width in x and y directions, respectively;

D_1, D_2 = coupling rigidities, measuring the contribution of bending to torsional rigidities of the plate;

D_{xy}, D_{yx} = torsional rigidities of the slab only, neglecting the effect of the steel girders.

According to Timoshenko (26), the general differential equation of equilibrium is:

$$M_{x,xx} + M_{y,yy} - 2 M_{xy,xy} = -q(x,y) \qquad (3.2)$$

Substituting expressions (3.1) into equation (3.2), the following fourth order differential equation governing the deflection of the orthotropic plate is obtained in rectangular coordinates:

$$D_x W,_{xxxx} + 2H W,_{xxyy} + D_y W,_{yyyy} = q(x,y) \qquad (3.3)$$

where, $H = (D_1 + D_2 + D_{xy} + D_{yx})/2$

and known as the effective torsional rigidity of the plate and characterizes the resistance of the plate element to

twisting. The rigidities D_x and D_y expressed in terms of lb.in^2/in. characterize the resistance to flexure of a plate strip having unit widths in the x and y directions. The torsional rigidity D_{xy} of the plate is defined as the reciprocal value of the angle of twist of a plate element with the side lengths $d_x = d_y = 1$ under the action of a twisting moment $M_{xy} = -M_{yx} = 1$.

3.5 Relation of Stress and Strain For Bending Action

According to Timoshenko (26), solving 3.1 and 3.3 to find $W,_{xx}$ and $W,_{yy}$ and substituting these two terms in the following formulae relating strain to curvature,

$$\varepsilon_x = -z\ W,_{xx}$$
$$\varepsilon_y = -z\ W,_{yy} \tag{3.4}$$
$$\gamma_{xy} = -2z\ W,_{xy}$$

Or, in terms of the rigidities and moments:

$$\varepsilon_x = z(M_x D_y - M_y D_1)/(D_x D_y - D_1 D_2)$$
$$\varepsilon_y = z(M_y D_x - M_x D_2)/(D_x D_y - D_1 D_2) \tag{3.5}$$
$$\gamma_{xy} = z\ M_{xy}/D_{xy}$$

where, z is the depth of the neutral axis from the top fibre.

3.6 Elastic Properties of the Continuous Composite Bridge Model

Since the thickness of the slab is constant and the slab material is continuous, as assumed before, the different

elastic properties in two principal directions must be due to different moments of inertia per unit width of the slab. The moduli of elasticity in two perpendicular directions are equal ($E_x = E_y = E$) as well as Poisson's ratio ($\mu_x = \mu_y = \mu$). As mentioned earlier, the condition of orthotropy for the bridges treated herein, is mainly due to geometry. The problem is idealized by assuming that the bridge is model of a homogeneous material with different elastic properties in two mutually perpendicular directions.

In addition to the basic assumptions in deriving the governing differential equation for an orthotropic plate, the following assumptions are made with respect to composite bridge construction:

1) The area of the flange plate is magnified by the factor $1/(1-\mu^2)$ due to the effect of Poisson's ratio μ;

2) The number of shear connectors is sufficient to ensure that the slab is connected rigidly to the main girder, i.e., 100% interaction is assumed;

3) The diaphragms are connected to the main girders rigidly;

4) The number of girders and diaphragms is enough for the real structure to be replaced by idealized one with continuous properties;

5) The neutral plane in each of the two orthogonal directions coincides with the centre of gravity of the total section in the corresponding direction;

6) As a result of assumptions (2,3), it is assumed

that the slab and the diaphragms in the transverse direction
are working together as one section although there is a
clearance of one inch in-between; this assumption is checked
by experimental results.

While there is no difficulty in determining the
flexural rigidities D_x and D_y of the composite bridge models,
there is one in finding an accurate estimate for the torsional
rigidities. A method for the determination of rigidities was
suggested by Huffington and others (11,14) for the restricted
case of equally spaced stiffeners of rectangular cross-section
disposed symmetrically with respect to its middle plane.
Various methods of estimating the load distribution in con-
crete bridge deck (19,21) have been proposed to date.

3.7 Rigidities of Uncracked Sections

3.7.1 Flexural Rigidities

The neutral planes for bending in each of the two co-
ordinate directions are assumed at the center of gravity of
the total section. This is an approximation only, since it
can be shown that the location of the neutral surface is a
function of the deflection as well as geometry of the section;
however, for most practical problems of this kind, the
approximation is very close. In the determination of D_y and
D_x, one may assume that the neutral planes for the bending
stresses are parallel to the middle plane of the plate and
located at distances e_y and e_x, respectively, from the top
fibre. These distances are determined from the condition
that the resultant force on a repeating cross-section must

zero. Based on the assumptions made before, the orthotropic flexural rigidities D_y and D_x, as well as the coupling rigidities D_2 and D_1 due to the Poisson's effect (16) can be put in the following forms (see Figure 3.2):

$$D_x = \{[4bD + 4bh\ E_c(e_x-h/2)^2/(1-\mu^2)] + [nm_1 E_c\ I_x']\}/4b$$

$$D_y = \{[2aD + 2ah\ E_c(e_y-h/2)^2/(1-\mu^2)] + [nm_2 E_c\ I_y']\}/2a$$

$$D_1 = \mu D_x' \tag{3.6}$$

$$D_2 = \mu D_y'$$

where, D = the flexural rigidity of the flange plate with respect to its middle plane, $E_c h^3/12(1-\mu^2)$;

E_c = modulus of elasticity of the concrete

f_c' = 28 day concrete cylinder strength in psi;

h = thickness of the flange plate;

μ = Poisson's ratio of concrete, $\sqrt{f_c'}/350$ (9,15);

n = modular ratio = E_s/E_c;

m_1 = number of diaphragms;

m_2 = number of the longitudinal girders;

S_y = spacing of longitudinal girders;

S_x = spacing of diaphragms;

e_x = depth of neutral plane from top fibre for bending about an axis perpendicular to the x direction;

e_y = depth of neutral plane from top fibre for bending about an axis perpendicular to the y direction;

$$e_x = \{nm_1A_D(\frac{dx}{2}+e+h) + 4bh^2/2(1-\mu^2)\}/\{nm_1A_D+4bh/(1-\mu^2)\}$$

$$\text{(3.7)}$$

$$e_y = \{nm_2A_G(\frac{dy}{2}+h) + 2ah^2/2(1-\mu^2)\}/\{nm_2A_G+2ah/(1-\mu^2)\}$$

I'_x = moment of inertia of transverse diaphragm with res-

pect to the assumed neutral plane of the gross

cross-section;

I'_y = moment of inertia of longitudinal girder with

respect to the assumed neutral plane of the gross

cross-section;

$$I'_x = I_x + A_D(\frac{dx}{2}+e+h-e_x)^2$$

$$I'_y = I_y + A_G(\frac{dy}{2}+h-e_y)^2$$

in which,

I_x = moment of inertia of transverse diaphragm with

respect to its middle plane;

I_y = moment of inertia of longitudinal girder with

respect to its middle plane;

A_D = cross-section area of transverse diaphragm;

A_G = cross-section area of longitudinal girder;

e = clearance distance between the slab and diaphragm;

b = half-span of the composite bridge;

a = half-width of the composite bridge;

d_y = depth of the longitudinal girder;

d_x = depth of the transverse diaphragm;

D'_x = flexural rigidities of the flange plate with respect

to the neutral plane of gross section associated

with bending about an axis perpendicular to the x

direction;

D_y' = flexural rigidities of the flange plate with respect to the neutral plane of the gross section associated with bending about an axis perpendicular to the y direction.

3.7.2 Torsional Rigidities

The effective torsional rigidity H, in equation (3.3) is given by:

$$H = (D_{xy} + D_{yx} + D_1 + D_2)/2$$

An approximate value recommended by Huber for the analysis of reinforced concrete slabs with different reinforcement in the two perpendicular directions is, $H = \sqrt{D_x D_y}$; such an expression gives a too high an estimate for a T-beam section. In determining the torsional parameter, the main problem lies in finding the values D_{xy} and D_{yx}, which are given by:

$$D_{xy} = G_{xy} \cdot I_{xy}$$

$$\text{(3.9)}$$

$$D_{yx} = G_{yx} \cdot I_{yx}$$

in which,

Shear modulus = $G_{xy} = G_{yx} = E/2(1 + \mu)$

E and μ refer to the equivalent transformed material. I_{xy} and I_{yx} are the torsional constants.

A number of investigators have obtained the torsional constants for structural steel and aluminum-alloy sections, using membrane analogy and/or numerical methods. Rowe (21) has determined the torsional constants by dividing open section into a number of rectangular areas. Thus the

torsional constant is given by:

$$I_{xy}S_x \quad \text{or} \quad I_{yx}S_y = (\tfrac{1}{2}k_1 a_1^3 b_1) + \sum_{i=2}^{n}(k_i a_i^3 b_i) \qquad (3.10)$$

where, S_x, S_y = spacing of transverse (longitudinal) girders;

a_1, b_1 = the smaller and the larger dimension of the slab portion;

k = factor depending on the ratio b_i/a_i, as given in any standard textbook on torsion (26).

It should be mentioned here that in the analysis of composite bridges consisting of steel I-section girders and a concrete slab it is customary to neglect the torsional stiffness of the girders, since this usually is very small compared to their flexural stiffness and therefore has little effect on the lateral distribution of the loads.

3.8 Boundary Conditions

Figure 3.3 shows the co-ordinate system for a two span continuous composite bridge; the two spans are of identical dimensions and elastic properties.

Observing the polar symmetry of the slab and its boundaries about the center of the intermediate support, the loading on the slab is divided into symmetric and anti-symmetric components. For the symmetric loading system, the deflection surfaces of both spans are identical. That is, the deflection or the moment at any point $x = x_1$, $y = y_1$ in span I (Figure 3.3) is equal to that in span II at the point $x' = x_1$ and $y' = y_1$, both in magnitude and sense. For

the anti-symmetric loading system, the deflection or moment at any point $x = x_1$ and $y = y_1$ in span I is equal to that in span II at the point $x' = x$ and $y' = y$ in magnitude but opposite in sense. Hence it is necessary to analyse only span I (or span II) for each loading system.

A solution for the deflection function $W(x,y)$ in cartesian coordinates to the plate problem must be consistent with the conditions at the edges of the plate. The boundary conditions have to be re-formulated first in terms of the deflection, if the solution is to be based on the deflection. Thus a rectangular composite bridge has 8 boundary conditions which are to be satisfied by the solution of the governing partial differential equation, equation (3.3).

3.8.1 Bridge Slabs

The continuous bridge-type shown in Figure 3.3 is simply supported along edge, $y = +b$, continuously supported at $y = -b$ and free or elastically supported at the remaining two edges ($x = \pm a$).

1) Along the elastically supported edge $x = +a$, following Timoshenko and Woinwsky-Krieger (26) in making Kirchoff modification, i.e., combining the forces replaced by the twisting couples with the shear force along the edge and equating the same to the pressure transmitted from the plate to the supporting edge beam,

$$-V_x = -(Q_x - M_{xy,y}) = EI\, W,_{yyyy} \qquad (3.11)$$

which becomes,

$$D_x W,_{xxx} + (D_1 + D_{xy} + D_{yx}) W,_{xyy} = EI\, W,_{yyyy} \, ,$$

at $x = +a$ for $-b \leqslant y \leqslant +b$

where, Q_x = the lateral shear force;

$M_{xy,y}$ = additional shearing forces at the edges, produced by the torsional moment M_{xy};

EI = flexural rigidity of the edge beam.

Also, along the elastically supported edge $x = -a$, the equality of the reactive forces gives:

$$+V_x = +(Q_x - M_{xy,y}) = -EI\, W,_{yyyy} \qquad (3.12)$$

which becomes,

$$D_x W,_{xxx} + (D_1 + D_{xy} + D_{yx}) W,_{xyy} = -EI\, W,_{yyyy}$$

at $x = -a$ for $-b \leqslant y \leqslant +b$

Similarly, at $x = +a$, the equality of the moment normal to the edge in the plate with the twisting moment in the beam gives,

$$-M_n = -M_x = -GJ(W,_{xy}),_y \qquad (3.13)$$

which becomes,

$$D_x W,_{xx} + D_1 W,_{yy} = -GJ\, W,_{xyy}$$

at $x = +a$ for $-b \leqslant y \leqslant +b$

Similarly, at $x = -a$,

$$M_n = M_x = GJ(W,_{xy}),_y \qquad (3.14)$$

which becomes,

$$D_x \, W_{,xx} + D_1 \, W_{,yy} = GJ \, W_{,xyy}$$

$$\text{for } -b \leqslant y \leqslant +b$$

where, GJ = Torsional rigidity of the edge beam.

The boundary conditions for the bridge slab where the two edges are free are obtained by putting the rigidities for the edge beam EI and GJ equal to zero.

2) Along the simple support $y = +b$, the deflections and moments normal to the edge must be zero; at the same time this edge can rotate freely with respect to the edge line,

$$W = 0 \text{ at } y = +b \quad \text{for } -a \leqslant x \leqslant +a \qquad (3.15a)$$

$$M_y = 0 \text{ at } y = +b \quad \text{for } -a \leqslant x \leqslant +a \qquad (3.15b)$$

which becomes,

$$D_y \, W_{,yy} = 0 \text{ at } y = +b \text{ for } -a \leqslant x \leqslant +a$$

after observing that $W_{,xx} = 0$ because $W = W_{,x} = 0$ on the simple support.

3) At the intermediate support, the deflections must be zero, which gives:

$$W = 0 \text{ at } y = -b \quad \text{for } -a \leqslant x \leqslant +a \qquad (3.16)$$

at the intermediate support, the compatibility of slope and moments between the two slabs leads to the following two equations.

a) <u>Symmetric Load System</u>

Referring to Figure 3.3, consider the compatibility

of slope at any point $x = x_1$, $y = -b$ of span I.

$$W,_n \text{ at } x = x_1, y = -b \text{ in span I}$$

$$= -W,_n' \text{ at } x' = -x_1, y' = -b \text{ in span II}$$

$$= -W,_n \text{ at } x = -x_1, y = -b \text{ in span I}$$

Here the negative sign is necessary because, the co-ordinate of the two slabs are opposite in direction. Since the odd part of $W,_n$ in span I is already satisfied,

$$\text{Even part of } W,_n = 0 \text{ at } y = -b$$

which becomes,

$$\text{Even part of } W,_y = 0 \text{ at } y = -b \text{ for } -a \leqslant x \leqslant +a \qquad (3.17)$$

Similarly, considering the compatibility of moments,

$$M_n \text{ at } x = x_1, y = -b \text{ in span I}$$

$$= M_n' \text{ at } x' = -x_1, y' = -b \text{ in span II}$$

$$= M_n \text{ at } x = -x_1, y = -b \text{ in span I}$$

Since the even part of M_n is already satisfied:

$$\text{Odd part of } M_n = 0 \text{ at } y = -b.$$

which becomes,

$$\text{Odd part of } D_y W,_{yy} = 0 \text{ at } y = -b \text{ for } -a \leqslant x \leqslant +a \qquad (3.18)$$

b) Anti-Symmetric Load System

Considering the compatibility of slopes and observing that the deflections in the two spans are identical in magnitude but opposite in direction at the corresponding points,

$$W_{,n} \text{ at } x = x_1, \quad y = -b \text{ in span I}$$

$$= -W'_{,n} \text{ at } x' = -x_1, \quad y' = -b \text{ in span II}$$

$$= W_{,n} \text{ at } x = -x_1, \quad y = -b \text{ in span I}$$

Since the even part of W_n is already satisfied,

$$\text{Odd part of } W_{,y} = 0 \text{ at } y = -b \text{ for } -a \leqslant x \leqslant +a \qquad (3.19)$$

Similarly,

$$M_n \text{ at } x = x_1, \quad y = -b \text{ in span I}$$

$$= M'_n \text{ at } x' = -x_1, \quad y' = -b \text{ in span II}$$

$$= -M_n \text{ at } x = -x_1, \quad y = -b \text{ in span I}$$

which becomes,

$$\text{Even terms of } D_y W_{,yy} = 0 \text{ at } y = -b, \quad -a \leqslant x \leqslant +a \qquad (3.20)$$

CHAPTER IV

ANALYTICAL SOLUTION

4.1 General

A complete mathematical solution for the composite bridge is obtained by combining the particular and complementary solutions which satisfy the boundary conditions and the governing equation, (3.3), as follows:

$$W = W_c + W_p \qquad (4.1)$$

where, W = the total deflection at a point on the plate;

W_c = deflection found from the complementary solution of the homogeneous equation;

W_p = deflection from the particular solution of the non-homogeneous equation.

4.2 Complementary Solution

Following the approach similar to Levy, the deflection surface of the plate is assumed to be represented in a Fourier series as:

$$W_c = \sum_{n=1}^{\infty} e^{\lambda_n x} (P_n \sin \beta_n y + Q_n \cos \beta_n y)$$

where, n = some integer chosen to enable the series to represent as closely as desired a convergent solution;

$\beta_n = n\pi/b$

λ_n, P_n and Q_n are basic functions of the elastic properties and geometry of the plate.

Substituting equation 4.1 in equation 3.3 and putting

23

q(x,y) equal to zero, separating and equating the coefficients of $\sin \beta_n y$ and cos $\beta_n y$, yield two equations in P_n and Q_n. According to Gupta (9), the final expression for λ_n is:

$$\lambda_n = \pm [(H \pm \sqrt{H^2 - D_x D_y})/D_x]^{1/2} \beta_n \qquad (4.3)$$

It can be observed, from equation 4.3, that there are four possible values for λ_n which give rise to four possible solutions.

For the bridge model considered herein, it is assumed that the slab is flexurally stiff and torsionally weak, i.e., ($H^2 < D_x D_y$). This case includes the more common type of open decks and T-beam bridges. The case of gridwork where the torsional rigidity is negligible also falls into this case.

4.2.1 Composite Bridge Which is Flexurally Strong and Torsionally Weak

The value of λ_n in equation 4.3 is written in a simplified form as shown below, (9):

$$\lambda_n = (\pm K_1 \pm i K_2) \beta_n \qquad (4.4)$$

where,

$$K_1 = \sqrt{(\sqrt{D_x D_y} + H)/2D_x}$$

$$K_2 = \sqrt{(\sqrt{D_x D_y} - H)/2D_x}$$

from equation 4.3, and considering the linear combination of all the roots and transforming the exponential function into hyperbolic and trigonometric function, a possible solution of W for the orthotropic plate can be taken as:

$$W_{C1} = \sum_{n=1}^{\infty} (C_{1n} \cosh K_1\beta_n x + C_{2n} \sinh K_1\beta_n x) \cos(K_2 x+y)\beta_n$$

$$+ \quad (C_{3n} \cosh K_1\beta_n x + C_{4n} \sinh K_1\beta_n x) \sin(K_2 x+y)\beta_n$$

$$+ \quad (C_{5n} \cosh K_1\beta_n x + C_{6n} \sinh K_1\beta_n x) \cos(K_2 x-y)\beta_n$$

$$+ \quad (C_{7n} \cosh K_1\beta_n x + C_{8n} \sinh K_1\beta_n x) \sin(K_2 x-y)\beta_n \quad (4.5)$$

where, C_{1n} to C_{8n} are arbitrary constants dependent on n and adjusted to satisfy the boundary conditions. For a more general representation of the deflection, a Fourier series in $\sin \alpha_n x$ and $\cos \alpha_n x$ is also considered where,

$$\alpha_n = \frac{n\pi}{a}$$

Proceeding as before, the values of λ_n' would be

$$\lambda_n' = \frac{\alpha_n}{(\pm K_1 \pm iK_2)}$$

$$= (\pm K_1 \pm iK_2) x_1 \alpha_n \quad (4.6)$$

where,

$$x_1 = \frac{1}{(K_1^2 + K_2^2)}$$

Hence another possible complementary solution of W can be taken as:

$$W_{C2} = \sum_{n=1}^{\infty} (C_{9n} \cosh x_1 K_1 \alpha_n y + C_{10n} \sinh x_1 K_1 \alpha_n y) \cos(x_1 K_2 y+x)\alpha_n$$

$$+ \quad (C_{11n} \cosh x_1 K_1 \alpha_n y + C_{12n} \sinh x_1 K_1 \alpha_n y) \sin(x_1 K_2 y+x)\alpha_n$$

$$+ \quad (C_{13n} \cosh x_1 K_1 \alpha_n y + C_{14n} \sinh x_1 K_1 \alpha_n y) \cos(x_1 K_2 y-x)\alpha_n$$

$$+ \quad (C_{15n} \cosh x_1 K_1 \alpha_n y + C_{16n} \sinh x_1 K_1 \alpha_n y) \sin(x_1 K_2 y-x)\alpha_n$$

$$(4.7)$$

It will be observed later that the boundary conditions used in the solution of this problem are eight in number, two for each edge of the plate, and when the deflection function W is made to satisfy the boundary conditions, it becomes necessary to expand the function of x and y in Fourier series, yielding three equations for each boundary condition or 24 equations for the eight boundary conditions. In order to have the same number of arbitrary constants in the deflection function as there are equations, a polynomial function of the form:

$$W_{C3} = C_{17} + C_{18}\frac{x}{a} + C_{19}\frac{y}{b} + C_{20}\frac{x^2}{a^2} + C_{21}\frac{y^2}{b^2}$$

$$+ C_{22}\frac{x^3}{a^3} + C_{23}\frac{y^3}{b^3} + C_{24}\frac{Tx^4-y^4}{b^4} \qquad (4.8)$$

which satisfies the homogeneous equation is added to the deflection function, where,

$$T = D_y/D_x$$

and, C_{17}, C_{18},..........,C_{24} are arbitrary constants. Thus the total complementary solution becomes:

$$W_C = W_{C1} + W_{C2} + W_{C3} \qquad (4.9)$$

4.3 Particular Solution

The particular solution, involving the load function, has to be determined and added to the complementary solution of homogeneous equation, and then must satisfy the boundary conditions. The concentrated load acting on a limited area of (rxs) whose center is at (x,y) is expanded into double

Fourier series over the entire area of the bridge. Following

Gupta (9) the particular solution can be taken as:

$$W_p = (a_o/4D_y)(y^4/24 - y^2b^2/4 + 5b^4/24)$$

$$+ \sum_1^\infty [T_{5m}\cos \alpha_m x + T_{7m}\sin \alpha_m x]$$

$$+ \sum_1^\infty [T_{6n}\cos \beta_n y + T_{8n}\sin \beta_n y]$$

$$+ \sum_1^\infty \sum_1^\infty [K_{mn}\cos \alpha_m x \cos \beta_n y + P_{mn}\sin \alpha_m x \cos \beta_n y$$

$$+ Q_{mn}\cos \alpha_m x \sin \beta_n y + L_{mn}\sin \alpha_m x \sin \beta_n y]$$

$$(4.10)$$

4.4 Symmetric and Anti-Symmetric Loading

The loading on the structure is divided into symmetric

and anti-symmetric components. This division is clear in

Figure 4.1. For symmetric loading odd terms vanish, i.e.,

$$C_{2n} = C_{3n} = C_{6n} = C_{7n} = C_{10n} = C_{11n} = C_{14n} = C_{15n}$$

$$= C_{18} = C_{19} = C_{22} = C_{23} = Q_{7m} = Q_{8n} = Q_{3mn} = Q_{4mn} = 0$$

$$(4.11)$$

For anti-symmetric loading, all even terms vanish, i.e.,

$$C_{1n} = C_{4n} = C_{5n} = C_{8n} = C_{9n} = C_{12n} = C_{13n} = C_{16n}$$

$$= C_{17} = C_{20} = C_{21} = C_{24} = a_o = Q_{5m} = Q_{6n} = Q_{1mn} = Q_{2mn}$$

$$= 0 \qquad\qquad (4.12)$$

When either even or odd terms of the deflection func-

tion are considered at a time, the boundary conditions at

the opposite edges would become identical and the number of

boundary conditions would reduce to four in number for each

loading system.

4.5 Satisfaction of Boundary Conditions

The arbitrary constants of the deflection function are
determined from the matrix equation derived by making the
deflection satisfy the appropriate boundary conditions. Here
one of the boundary conditions for the bridge under symmetric
component of the loading is considered.

From the boundary condition that the deflection must
be zero at the edge $y = -b$, the following equation is
obtained,

$$f_O(x) + \sum_1^\infty [\, f_n(x) + A_n \cos \alpha_n x + B_n \sin \alpha_n x] =$$

$$-\sum_1^\infty T_{5m} \cos \alpha_m x - \sum_1^\infty (-1)^n T_{6n} - \sum_1^\infty \sum_1^\infty (-1)^n K_{mn} \cos \alpha_m x$$

$$(4.13)$$

in which,

$$f_O(x) = C_{17} + C_{20} x^2/a^2 + C_{21} + C_{24} [\,(T_x^4/b^4)-1]$$

$$f_n(x) = (-1)^n (C_{1n} \cosh \mu_{3n} \cos \mu_{4n} + C_{4n} \sinh \mu_{3n} \sin \mu_{4n}$$

$$+ C_{5n} \cosh \mu_{3n} \cos \mu_{4n} + C_{8n} \sinh \mu_{3n} \sin \mu_{4n})$$

$$A_n = C_{9n} K_{1n} + C_{12n} K_{2n} + C_{13n} K_{1n} + C_{16n} K_{2n}$$

$$B_n = -C_{9n} K_{4n} + C_{12n} K_{3n} + C_{13n} K_{4n} - C_{16n} K_{3n}$$

In which, μ_{3n}, μ_{4n} and K_{1n} to K_{8n} are defined in Appendix
(A).

The function $f_O(x)$ and $f_n(x)$ must be expanded in

Fourier series to satisfy the boundary condition, thus:

$$f_o(x) = a_{oo} + \sum_1^\infty (a_{om} \cos \alpha_m x + b_{om} \sin \alpha_m x)$$

$$f_n(x) = c_{no} + \sum_1^\infty (c_{nm} \cos \alpha_m x + d_{nm} \sin \alpha_m x)$$

(4.14)

where, a_{oo}, a_{om}, b_{om}, c_{no}, c_{nm} and d_{nm} are Fourier coefficients and defined in Appendix (B). Substituting equation 4.14 in equation 4.13 and equating the coefficients of $\sin \alpha_m x$ and $\cos \alpha_m x$ and the constant term to zero, the following three equations are obtained:

$$a_{oo} + \sum_1^\infty c_{no} = - \sum_1^\infty (-1)^n T_{6n}$$

$$a_{om} + \sum_1^\infty c_{nm} + A_m = -T_{5m} - \sum_1^\infty (-1)^n K_{mn} \quad \text{for each } m$$

(4.15)

and, $\quad\quad B_m = 0$, for each m

From equation 4.15, it should be noted that if n harmonics of the series are considered, the second and third equations yield (2n) equations and together with the first one yields (2n+1) equations for one boundary condition. Thus for eight boundary conditions altogether (16n+8) equations are obtained and a matrix equation of (16n+8) dimension must be solved for each loading component whether symmetric or anti-symmetric. Once the matrix equation is formulated and solved for the unknown constants, the deflection function is known over the entire area of the slab. The moment and the strains can be computed readily as follows:

$$M_x = -(D_x W,_{xx} + D_1 W,_{yy})$$

$$M_y = -(D_y W,_{yy} + D_2 W,_{xx})$$

$$M_{xy} = 2D_{xy} W,_{xy}$$

The strains can be obtained from equation 3.5 by substituting for M_x and M_y.

CHAPTER V

EXPERIMENTAL PROGRAM

5.1 Scope of the Experimental Program

To verify and substantiate the analytical approach proposed in Chapters III and IV, tests were carried out on two models of composite bridge. The two models were identical and consisting of reinforced concrete slab and steel girders except that the portion of the slab of the second model was prestressed in the vicinity of the intermediate support, (negative moment region). The tests were aimed at: obtaining the deflections, stresses and bending moments at various points; determining the cracking load; studying the feasibility of prestressing the slab in the negative moment region of a continuous composite bridge. The composite bridges tested were scaled one-to-eight in the horizontal direction, and one-to-four in the vertical direction, the two different scales were to ensure successful prestressing of the slab to tailor the experiment to the available space in the laboratory.

The two bridge models I and II were two-span continuous structures, each span being 5 ft. (1520 mm), consisting of five steel I-beams spaced at 1.0 ft. (304.8 mm) intervals, and supporting a reinforced concrete slab $2\frac{1}{2}$ in. (63.5 mm) thick. These dimensions were dictated by several requirements, the most important of which was the necessity for making the two bridges identical except that the slab of bridge model II was prestressed in the negative moment region. Certain details in the models were omitted in order to facilitate the

31

interpretation of the test results, e.g., the usual sidewalks, curbs, and handrails were not incorporated, and the roadway was built without a crown, or wearing surface and the outside beams were placed at the edges of the slab. The five diaphragms between the main girders were located over each support and at the middle of each span; the diaphragms were welded to the main girder webs and were set at a constant depth equal to 3/4 the depth of the main girders; the diaphragms did not bear against the underside of the slab. Shear connectors were provided throughout the entire length of the main girders. The layout of shear connectors is shown in Figure 5.1.

5.2 Materials

5.2.1 Concrete

High Early Strength Portland cement (CSA) manufactured by Canada Cement Company was used in both bridge models. This type of cement provides high strength within a week. The combined aggregate was prepared according to the ACI Code (1) by mixing 40 to 60% fine aggregates of the total aggregates. This combination gave a well-graded aggregate mix with a fineness modulus equal to 2.50. The coarse aggregates used were crushed stones with hard, clean and durable properties. The maximum size of aggregate was restricted to 0.25 in. (6 mm) since the narrowest dimension between the sides of the formwork was equal to 1.0 in. (25.4 mm) and the concrete cover to reinforcing wires was 0.25 inch (6.5 mm). Clean sand free of impurities was used. Natural water having no impurities

was used to obtain different concrete pastes of varying
maximum strength for concrete specimens. Two trial mixes of
air-entrained concrete of medium consistency and different
water-cement ratio varying between 40% to 70% were examined.

Mixing was done in a manually operated Eirich Counter
Current Mixer, Model EA2 (2W) with five cu. ft. charging
capacity. Three batches of concrete mix were required for
each bridge model. The compressive strengths of all specimens
were measured after seven, fourteen and twenty-eight days as
shown in Appendix (C).

5.2.2 Steel Girders

The main girders were W 8 x 13 steel of G 40.21-M 300 W
grade; the diaphragms had a section of W 6 x 15.5 of the same
grade of steel. A test program was conducted to determine the
mechanical properties of both the steel and concrete used in
the two bridge models. Properties of the structural steel
were determined from tensile coupons cut from the steel sup-
plied. The mechanical properties of the steel girders are
shown in Table D.1. The coupons were tested in a 120 kip
Tinus Olsen Universal machine at a speed of 0.025 inch per
minute up to first yielding and then at 0.3 inch per minute
until fracture occurred. For all coupon tests the yield
stress, tensile strength, modulus of elasticity and the per-
centage of elongation referred to gauge length of 2 inch
(50.8 mm) were determined. In addition a plot of applied
stress versus elongation was obtained, Figure D.1.

5.3 Reinforcing Steel

5.3.1 Steel Mesh for Reinforced Concrete Slab

A mesh of smooth welded wire fabric was chosen to be used as a reinforcing steel in the reinforced concrete slab of bridge I and in the reinforced concrete slab portions of bridge II. The sectional properties of the mesh were as follows: the spacing was 2 inch (50.8 mm) center to center, the cross-sectional area was 0.36 sq. in/ft of width, the diameter was 0.276 inch (7.01 mm) and the nominal weight was 0.204 lb/lin. ft. The yield strength was found to be 65,000 psi (448.00 MPa) and the tensile strength was 75,000 psi (517.00 MPa).

5.3.2 High Tensile Steel for the Post-Tensioned
Concrete Part in Bridge Model II

High tension steel wire of 0.27 inch in diameter was used for prestressing the concrete deck in bridge model II, Figure 5.7. Tensile tests on the wire indicated an ultimate strength of 262,500 psi (1810 MPa), and a yield stress of 240,000 psi (1655 MPa). This wire exhibited good resistance against slippage from the grips.

5.4 Formwork

The formwork consisted of 3/4 inch (19.1 mm) thick plywood supported on the grillage system by brackets as shown in Figure 5.2. The brackets were spaced about $2\frac{1}{2}$ feet (762.0 mm) apart and consisted of 2 x 2 x 3/8 inch equal angle bent at 90°. The arrangement proved very satisfactory and the resulting form was rigid, Figure 5.3 shows the slab formwork with the longitudinal and transverse reinforcement mesh.

5.5 Experimental Equipment

5.5.1 Support System

The steel section of each longitudinal girder was supported on rollers at the extremities and hinged at the intermediate support. Each one of the girders was instrumented with a load cell. The results obtained from these load cells were disregarded because its contact area was too small to be stable at the supports. The details of support bearings are shown in Figures 5.4, 5.5. The roller support consisted of a steel shaft, of 2 inch (50.8 mm), diameter resting on a steel plate as shown in Figure 5.4. The hinged support consisted of two plates and the shaft in between, with the two plates grooved to accommodate the shaft as shown in Figure 5.5; the main purpose of the hinged support was to allow the girders to rotate freely as well as prevent lateral movement.

5.5.2 Prestressing Equipment

The prestressing equipment used in prestressing the wires in bridge model II, was manufactured by Cable Covers Ltd., England. A hydraulic jack of twenty kips (89 kN) capacity was used for post-tensioning. The mechanical gripping devices were of the open grip type and washers were very simple and quick to use. Black wax lubricant was applied to the wedges to make it easier to release the grips after completing the prestressing operation.

5.5.3 End Bearing Plate

Eighteen end bearing plates 2 x 4 x 0.5 inch (51 x 101

x 12.7 mm) thick, with holes of 0.25 inch (6.4 mm) diameter were used in bridge model II to distribute the prestressing force as shown in Figures 5.6 and 5.7.

5.6 The Construction of Bridge Model I

Figures 3.1 and 3.2 show the dimension of the cross-section and the layout of the bridge model I. The five I-beams for each bridge together with the end, intermediate and mid-span diaphragms were assembled into a single frame by fillet welding to ensure proper interaction between the longitudinal girders and diaphragms; the shear connectors were welded next. The shear connectors were 2 x 2 x 3/8 inch equal angles welded to the top flange of each of the longi-tudinal girders through their heels, i.e., each leg was making an angle 45° with the top flange as shown in Figure 5.7. The shear connectors were distributed uniformly throughout the length of the bridge and the distance between each connector was 2 inch (50.8 mm) as shown in Figure 5.1. The fillet welding was continuous along both sides of the heel of the angle. The number of shear connectors was enough to ensure 100% interaction between the slab and the longitudinal girders. The model was placed on the supports next as shown in Figure 5.1.

The required form was prepared as shown in Figures 5.2 and 5.3 and then painted with grease material, Vitrea Oil 150, for easy form release after the concrete has set. All of the reinforcement for the slab was assembled into a single mesh; this mesh was supported on steel wire chairs

which provided a clear cover of 0.4 inch (10.2 mm) from the
bottom. Another piece of the reinforcement mesh, 4.0 feet
(1219.2 mm) long, was placed at the intermediate support
area near the top of the slab to cater for the negative
support moment as shown in Figure 5.3. Air-entrained con-
crete of 5000 psi compressive strength was placed, progress-
ing from one end of the bridge model. The concrete was
vibrated using a high frequency needle vibrator; in addition,
the sides were tamped with a tamping rod. The sides of the
forms were also lightly hammered to avoid honeycombing.

The top of the concrete slab was worked with a wooden
screed to obtain a level surface and the location areas for
the concrete strain gauges were worked with a steel trowel
for extra smooth surface. To determine the compressive
strength of the concrete, six 3 x 6 inches (76 x 152 mm)
cylinders were cast at the time of placing the concrete slab.
The forms were removed 48 hours after casting. The concrete
slab was then covered with four layers of moist burlap, with
a polyethylene sheet on top. The polyethylene sheet effect-
ively prevented the escape of moisture from the concrete
slab and burlap. Consequently, water was sprinkled on the
burlap only at 2-day intervals to keep the concrete continu-
ously moist. Water curing of the concrete slab continued for
14 days. The slab was then air-cured until test day (35th
day after casting). The curing of the concrete test cylin-
ders was done by immersing them in a water tank; water-curing
was discontinued for the test cylinders and the composite

bridge model on the same day.

A view of the composite bridge model after curing can be seen in Figure 5.8. To avoid any uplift of the structure at the supports due to loading, the two ends of the composite bridge model were held down by steel cables as shown in Figures 5.8 and 5.9 .

5.7 The Construction of Bridge Model II

Figure 5.10 shows the dimension and the layout of bridge model II. The same procedures were followed to connect the main girders with the diaphragms, and the shear connectors to the top flange of the main girders as bridge model I. The main difference between model I and model II was prestressing the slab in the negative moment region.

The required forms, for prestressing the slab in the negative moment region, were prepared as shown in Figure 5.11. Rubber hoses having an inner diameter of 0.25 inch (6.4 mm) and 0.62 inch (15.7 mm) outside diameter were used to cover the prestressing wires during casting of the concrete as shown in Figure 5.12. Nine prestressing wires were used for prestressing the slab in the negative moment region. Two strain gauges were mounted on each prestressing wire to mea-sure the prestressing force and to record the reading during the testing of the bridge model. The prestressing wires were placed at the mid-thickness of the slab, transverse reinforcement were used at the bottom of this slab as shown in Figure 5.13.

Air-entrained concrete of 8000 psi (55.00 MPa) compressive strength was placed. This high strength, low slump mix was used to obtain a minimal amount of shrinkage. Compaction of the concrete was accomplished by internal vibration and the final finish was obtained by hand-trowelling. The concrete in the slab was moist-cured for seven days by covering the exposed surface with wet burlap and a polyethylene sheet. After seven days, the slab was allowed to cure under dry conditions for five days. After the concrete had reached the desired strength, the slab was prestressed. The prestress force was applied in two stages, to each wire to minimize the prestress losses due to the jacking sequence and to minimize the in-plane bending of the slab. A view of the prestressing slab portion after prestressing can be seen in Figure 5.14.

A formwork was prepared to cast the right and left parts of the reinforced concrete slab as shown in Figure 5.15. The prestressing wires were extended to the right and the left of prestressing slab and embedded in the reinforced concrete slab. The arrangement of the reinforcement for the reinforced concrete slab is shown in Figure 5.16. The procedures for casting and curing the reinforced concrete slab were the same as described earlier.

5.8 Instrumentation

5.8.1 Strain Gauges on the Prestressing Wires

The longitudinal prestressing wires were instrumented with strain gauges, type EA-06-125AC-350. The surface of

the prestressing wire was prepared by cleaning it using fine
silicon carbide paper and acetone. The gauge was mounted
using Eastman M-Bond 200 adhesive with 200 catalyst as bond-
ing agent according to the manufacturer's recommendations.
The strain gauges, consisting of a stabilized constant etched
foil grid mounted on a flexible polymide backing, had a gauge
factor of 2.07, a gauge resistance of 350 ohms, and a gauge
length of 0.125 inch. These gauges are capable of measuring
strains up to 0.3% elongation. The temperature coefficient
of the gauges when bonded to steel is zero at 75°F. The
gauges had integral terminals of one-piece high-endurance
beryllium copper. The lead wires were then soldered to the
gauges and water-proofed by coating them with the protective
coating Gagekote Five. After curing for 24 hours at room
temperature, a layer of wax was applied on the gauge as well
as plastic tape for further protection.

5.8.2 Strain Gauges on the Steel Girders

To measure the strain on the top and the bottom
flanges of the main girders, strain gauges of type EA-06-500
BH-120 were used. All gauges had a nominal gauge length of
0.50 inch (12.7 mm). The locations of the strain gauges
are shown in Figure 5.17. The steel surface at the locations
of the gauges were smoothed using sandpaper, all dust was
removed and then the surfaces were cleaned with acetone. The
strain gauges were mounted, soldered with lead wires, covered
by M-coating and water-proofed by coating them with the
protective coating Gagekote Five. The gauges were then
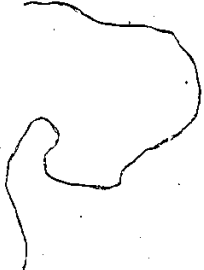
connected to the electronic strain indicator, shown in Figure 5.18.

5.8.3 Strain Gauges on the Concrete

To measure the strain on the top and bottom surface of the slab, electric strain gauges of type EA-06-500 BH-120 were used. All gauges had a nominal gauge length of 0.50 inch (12.7 mm). The locations of the strain gauges are shown in Figure 5.17. The concrete surface at the locations of the gauges were smoothed using sandpaper, all dust was removed and then the surfaces were cleaned with acetone. Surface cavities were then filled by applying an epoxy of high strength (RTC). This epoxy was mixed by one volume activator B, and the same volume of resin A. After the surface was dry, it was again smoothed and the gauge was mounted, soldered with lead wires and covered by coating it with epoxy M coat. Figures 5.19 and 5.20 show the strain gauges on the top and the bottom of the slab.

5.8.4 Mechanical Dial Gauges

The deflections were measured using mechanical dial gauges having 0.001 inch (0.025 mm) travel sensitivity; they were also used to measure slip at the ends of the bridge models as shown in Figure 5.9 . The locations of the dial gauges are shown in Figure 5.21. In both bridge models, the dial gauges were placed at the top surface of the slab and supported by a light steel beam.

5.8.5 Load Cells

5.8.5 a) Universal Flat Load Cell

Two universal flat load cells, having capacities of 50 kips (222.40 kN), and 150 kips (667.00 kN), were used to measure the load for working and cracking loads conditions, respectively, (the working load refers to the load at which the first crack appears); the concentrated load being applied through the hydraulic jack as shown in Figure 5.22. The calibrations of these load cells are given in Appendix (E).

5.8.5 b) Cylindrical Load Cell

Thirty-four cylindrical load cells were used to measure the reactions. Figure 5.4 shows the cylindrical load cells in position.

5.9 Experimental Set-Up and Test Procedure

Figure 5.21 shows the experiment set-up for both bridge models I and II.

5.9.1 Bridge Model I

Shims were provided under each support so that uniform contact was maintained between the supports and the girders. Seventy-three strain gauges, were mounted on the steel girders and on the concrete at mid-span and intermediate support sections; the arrangement of the strain gauges is shown in Figure 5.17. Five dial gauges were used to measure the deflections at the middle of each span, as shown in Figure 5.21.

The bridge model was tested under transverse concentrated loads, applied through a rigid portal frame supporting

a cross I-beam and a hydraulic jack of 50,000 lbs (222 kN) capacity. The arrangement was such that the concentrated load could be applied anywhere without moving the bridge; see Figure 5.21. The transfer of the load from the hydraulic jack to the slab was made through a small rectangular steel plate, 1 inch (25.4 mm) thick and 5 x 6 inches (127 x 152 mm) in plan. Grooves were made on the bottom of the steel loading plate to avoid contact with the strain gauges located at loading positions. Loading and unloading were applied three times before starting the test, to minimize the residual strains and for proper seating of the bridge model on the supports. The readings from loading and unloading were recorded and averaged.

The bridge was tested under one concentrated load at four locations and under two-point load at one location, as shown in Figures 5.22 and 5.23.

5.9.2 Bridge Model II

Bridge model II was identical to bridge model I in its dimension, number of strain gauges, dial gauges and locations of the applied load. The only difference in bridge model II was the prestressing of the concrete slab in the region of the intermediate support as shown in Figure 5.16. All care and adequate precautions were taken during the prestressing process.

To avoid any distortion in the exterior edge and/or local failure, the wires were tensioned in a sequence starting with the odd-numbered wires and followed by tensioning

the even-numbered wires. The model was tested under concentrated load through a universal load cell of 50 kips (222 kN) capacity. Figure 5.22 shows the load location for the exterior girder; Figure 5.23 shows the two-points load and the one-point load on an intermediate girder. Each test was performed approximately one month after the slab was cast. Approximately 60 hours were required for testing which was carried out on 7 consecutive days. Load increments of five kips were applied throughout each test until a load of 50 kips (222 kN) was reached causing the first crack in bridge model I; in this case subsequently, load increments were ten kips until the conclusion of testing.

CHAPTER VI

DISCUSSION OF RESULTS

6.1 General

According to the Ontario Highway Bridge Design Code
(OHBDC) (18), there are two methods to calculate the rigidi-
ties in the transverse direction: the first one is to
neglect the effect of the diaphragms and this one will be
referred to herein as OHBDC-1; the second method is to take
the effect of the diaphragm by adding its rigidity to the
slab rigidity and this one will be denoted as OHBDC-2. The
theoretical results based on the rigidities assumed herein
and on OHBDC-1 and OHBDC-2 rigidities as well as the experi-
mental results, for the distribution of deflections,
longitudinal bending moment (M_y), and transverse bending
moment (M_x) at the mid-span section of composite concrete
bridges are compared in Figures 6.2 to 6.17 for each load
location. Figure 6.1 shows the strain distribution of the
composite section under prestressing force and under the
working load. Table D.3 shows the comparison between the
rigidities according to the various methods.

6.2 Results for Bridge Models I and II

6.2.1 One Concentrated Load on Beam C

The lateral distribution of deflections at the middle
of the span was studied by expressing the deflection of the
individual girders as a percentage of the total deflection
of all five girders at the cross-section under consideration.

45

In this way, it was possible to make a direct comparison of the experimental deflection behaviour of the bridge model with that predicted by the theory herein as well as by OHBDC. Figure 6.2 shows the comparison between the experimental deflections of bridge models I and II and the theory herein, OHBDC-1 and OHBDC-2 proposal under working load of 50 kips (222 kN). Close agreement is observed between the theory herein and the experimental results, and significant differences are observed between the results based on OHBDC-1, OHBDC-2 and the experimental results. These discrepancies are mainly due to improper accounting of the effect of the diaphragms.

The distribution of bending moments was taken to be the same as the distribution of strains measured at the center of the bottom face of the steel girders at the section under consideration. The distribution of bending moments, measured in this manner, is compared with the theoretical distribution of moment at the mid-span and the intermediate sections as shown, respectively, in Figures 6.3 and 6.4. The close agreement between theory and experiment and the discrepancies between OHBDC and experiment also apply to the results in Figure 6.3.

In Figure 6.4, the theoretical longitudinal bending moment at the intermediate support due to the applied prestressing force, the increase of prestressing force caused by the negative bending moment, secondary moment (due to continuity), and applied loads is denoted as theory II. The

secondary bending moment due to continuity caused by the

prestressing force is taken to be equal to zero. The dis-

crepancies between bridge model II and theory II results,

Figure 6.4, are mainly due to increasing of the prestressing

force which is caused by the loading system. The distribution

of transverse bending moment (M_x) at the middle of the span

has been studied by expressing the transverse bending moment

of individual girders, at the cross-section under considera-

tion, as a percentage of the total absolute transverse

bending moment of all five girders. The distribution of

(M_x) is taken to be the same as the distribution of strains

measured at the bottom face of the concrete slab at each

girder at the section under consideration. Figure 6.5 shows

the comparison between the experimental distribution of bend-

ing moment and those according to the various theories.

6.2.2 One Concentrated Load on Beam B

Figures 6.6, 6.7 and 6.8 show comparisons between the

experimental distribution of deflections, longitudinal

bending moment (M_y) and transverse bending moment (M_x) at

the middle of the loaded span and those due to the various

theories; close agreement is observed between the theory

herein and the experimental results, with large discrepancies

between the results based on OHBDC-1 proposals and the other

results. The same observation is noted in Figure 6.9 which

shows the comparisons for the distribution of longitudinal

bending moment (M_y) at the intermediate support. It is

interesting to observe that the bending moment (M_y) shifts

from negative to positive due to the prestressing force in bridge model II and theory II under the working load.

6.2.3 One Concentrated Load on Beam A

The third case of loading was one concentrated load applied to the exterior girder A; however, because this part of the bridge model is susceptible to cracking, the load was limited to a maximum of 25 kips (111.0 kN), i.e., half of the working load to avoid any cracks at the middle of the span. Figures 6.10, 6.11, 6.12 and 6.13 show comparisons between the experimental and theoretical results for the distribution of deflection, longitudinal bending moment (M_y), transverse bending moment (M_x) at midspan and longitudinal bending moment (M_y) at the intermediate support. Close agreement is observed between theory and experimental results. OHBDC results are in poor agreement with the experimental results.

6.2.4 Two Concentrated Loads, Beam C

The last loading case was two concentrated loads, each load being placed at the middle of each span; Figures 6.14, 6.15 and 6.17 show the comparison of the results for the distribution of deflections, longitudinal moment (M_y), transverse moment (M_x) at the midspan and longitudinal moment (M_y) at the intermediate support for a total applied load of 50 kips (222 kN). At the intermediate support of bridge model I, transverse cracks appeared at a load of 50 kips (222 kN); it was observed that the majority of the cracks occurred in the transverse direction due to the negative longitudinal bending

moment, while only hairline cracks appeared in the longitu-
dinal direction. Figures 6.18, 6.19 and 6.20 show the crack
patterns at the intermediate support of bridge model I under
a load of 50 kips (222 kN).

At the intermediate support of bridge model II no
cracks were observed at a load of 50 kips (222 kN). In fact,
the first crack was detected at a load of 180 kips (799 kN).
Figure 6.21 shows the crack pattern at the intermediate
support of bridge model II under an applied load of 200 kips
(888 kN). The maximum load that was applied was 240 kips
(1066 kN) because of limitations in the loading facilities
available in the laboratory. However, the predicted failure
load, by using a plastic analysis of continuous bridge, may
be in the range of 320 kips (1420 kN).

6.3 Comparison Between the Behaviour of Bridge Models

I and II

It was found that transverse cracks at the inter-
mediate support reduce the rigidities of the slab by
approximately 70%; thus, after cracks appeared in bridge
model I, the model possessed two sets of rigidities, one
based on a cracked section at the intermediate support and
the other one based on an uncracked section at the middle of
the span. By comparing the deflection distribution at the
mid-span section of bridge model I and bridge model II,
Figure 6.22, it can be observed that the values of the
deflection of bridge model II are less than those in bridge
model I, under the working load condition, 50 kips (222 kN),

this difference being due to the two sets of rigidities.
Also, it is clear that the cracks at the intermediate support
do not influence the distribution of deflections, longitudinal
moment and transverse moment at mid-span.

Figure 6.23 shows the distribution of the longitudinal
strain at the bottom face of the steel girders under working
load for both bridge models I and II. Figure 6.24 shows the
distribution of the longitudinal strain at the top of the
concrete deck at the intermediate support for each girder due
to two concentrated loads. It is observed that the experimen-
tal load strain relationship of bridge model II is approxi-
mately parallel to that calculated from the theory, the former
being shifted to the left by the amount of strain caused by
the prestressing. Whereas the strains of bridge model I go
from tension to compression due to the formation of transverse
cracks at the intermediate support. The magnitude of slip in
both bridge models was found almost equal to zero.

6.4 Sources of Error

The discrepancies between the experimental and
theoretical results can be attributed to several sources of
error such as:

1) The assumptions made in the theory;

2) Estimates of Poisson's ratio and modulus of
elasticity of concrete by means of empirical formulas;

3) Estimating the strength of the concrete from tests
on 3 x 6 inches cyliner;

4) Distortion in the formwork due to effect of water,

and lack of complete contact between the support and the
test model;

5) Residual stresses in the main girders due to high
temperature of arc-welding;

6) Positioning of reinforced and prestress wires;

7) The calibration of load cells, sensitivity and
drag in mechanical dial gauges, the stability of strain
gauges and the strain gauge measuring devices.

CHAPTER VII

PARAMETRIC STUDY

7.1 General

Four aspect ratios of two equal span continuous composite bridge prototypes were studied, to examine the effect of the presence of transverse diaphragms on the distribution of deflections, longitudinal moments (M_y) and transverse moments (M_x) at mid-span and the distribution of longitudinal moments (M_y) at the intermediate support. All the bridges had the same length, but with a varying width as shown in Table F.1; the aspect ratios, (b/a), were 0.5, 1.0, 1.5 and 2.0, where (2a) is the width of the bridge, and (2b) is the span.

Three cases of loading were considered: the first case of loading was a concentrated load acting on the exterior girder; the second case was a concentrated load acting on the first interior girder and the last one was a concentrated load acting on the centre girder. The location of the diaphragms were, one at each support and one at the middle of each span as shown in in Figure 7.1. The slab thickness was kept constant at 11 inch (279.4 mm); the main girders were of W 36 x 160 size and the diaphragms were of W 30 x 116 size, Figure 7.1.

According to Article A5.5 of the OHBD Code (18), "For shallow superstructure type bridge, the effect of diaphragms and cross frames between supports on the structural response may be ignored"; thus, in this parametric study, two sets of

results were obtained: one was based on OHBDC recommending neglecting diaphragms in the calculations of the rigidities and the other set of results in which the diaphragms and the slab are assumed acting together as one section; see Appendix F for details regarding the two methods of calculating the orthotropic rigidities for different aspect ratios.

7.2 Comparison Between the Results

The results for the three cases of loading were obtained. For brevity, however, results for only one case of loading, a concentrated load acting on the central girder, are presented herein. Figures 7.2 to 7.5 show the deflections distribution at the mid-span section for different aspect ratios. In Figure 7.2, the difference between the two deflection curves is quite large; however, it becomes smaller with increase in the aspect ratio, b/a, Figures 7.3 to 7.5. Thus for wider bridges, the presence of transverse diaphragms does significantly affect the load distribution characteristics; whereas for longer bridges, the effect of diaphragms between supports may be ignored.

Figures 7.6 to 7.17 show the distributions of the longitudinal bending moments (M_y) at the intermediate support and the longitudinal bending moments (M_y) and transverse bending moments at mid-span. These figures indicate that in wider bridges (say for b/a = 0.5), more than one diaphragm is required in order to increase the distribution of the longitudinal moment transversely; Figure 7.6 shows that the loaded girder carried about 60% of total moment (M_y) according

to the theory while according to the OHBDC, it carries about 78% of the moments. For a longer bridge (say for b/a = 2.0), Figure 7.9, the loaded girder carries 28% and 40% of total moment according to the theory herein and to the OHBDC, respectively; this indicates the importance of diaphragms in wider bridges and to lesser extent in longer bridges.

Finally, the presence of diaphragms in the super-structure of slab-on-girder bridges does significantly affect the deflections, the longitudinal moment and the transverse moment distribution characteristics.

CHAPTER VIII

SUMMARY, CONCLUSIONS AND RECOMMENDATIONS

8.1 Summary

The overall objective of this study was to eliminate the unavoidable transverse cracks at the intermediate support of continuous two-span composite bridges, and to obtain a better understanding of the load distribution characteristics due to the presence of the transverse diaphragms. A Fourier series method of analysing two-span continuous composite bridges by orthotropic plate theory was presented; concentrated load was considered. Proposed theoretical formulae for calculation of the various orthotropic rigidities were used. The theoretical results were verified and substantiated by tests on two bridge models. An analytical study and comparison between the behaviour of such bridges using the rigidities proposed by OHBDC and those proposed herein were undertaken.

8.2 Conclusions

The following conclusions are based on the results obtained from the theoretical and experimental studies:

1) Composite action of the full transformed section can be realized in the negative moment region of a continuous composite bridge by placing shear connectors throughout the negative moment region and applying a suitable prestressing force to the slab;

2) Prestressing can be used to effectively control slab cracking in the negative moment region. Cracks can be

eliminated up to certain load levels depending upon the amount of prestress force applied;

3) The good agreement between the experimental and theoretical results supports the reliability of the proposed formulae for estimating the orthotropic rigidities;

4) The torsional rigidity of the slab plays an important part on the behaviour of a continuous composite bridge when a concentrated load is close to the unsupported edge;

5) Transverse cracks produced at the intermediate support in reinforced concrete slab can reduce the stiffness of the bridge by as much as 25 to 30%;

6) In the superstructure of slab-on-girder bridges, the presence of transverse diaphragms can significantly affect the load distribution characteristics;

7) If the transverse diaphragms are connected rigidly to the main girders and with 100% interaction between the slab and the longitudinal girders, then the transverse diaphragms and the slab act as one section;

8) Orthotropic plate theory as presented provides an effective method of predicting the distribution of load to the different members of the multibeam-girder bridge.

8.3 Suggestions for Future Research

The following suggestions are recommended for future research as an extension of this investigation:

1) Consideration should be given to the placement of shear connectors before or after the prestressing operation;

2) A further investigation is required to answer the following question: what is the effect of increasing the number of transverse diaphragms beyond a certain limit on further improving the load distribution characteristics?, e.g., optimization on the number of transverse diaphragms;

3) Consideration should be given to the continuity of connection between the prestressing concrete slab in the negative moment region and the ordinary reinforced concrete slab portions.

FIGURES
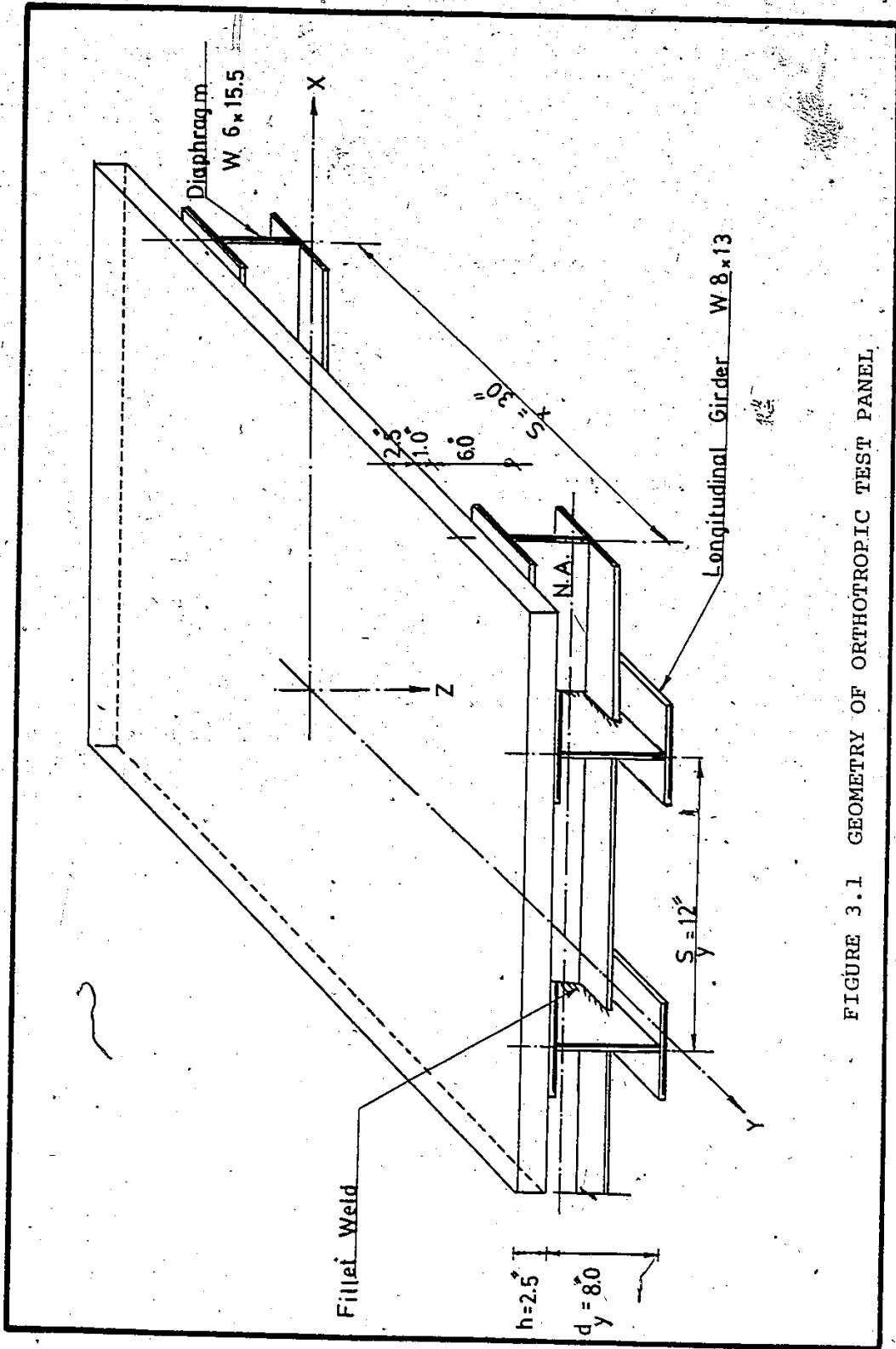
FIGURE 3.1 GEOMETRY OF ORTHOTROPIC TEST PANEL

TRANSVERSE SECTION AT MID SPAN

PLAN

LONGITUDINAL SECTION
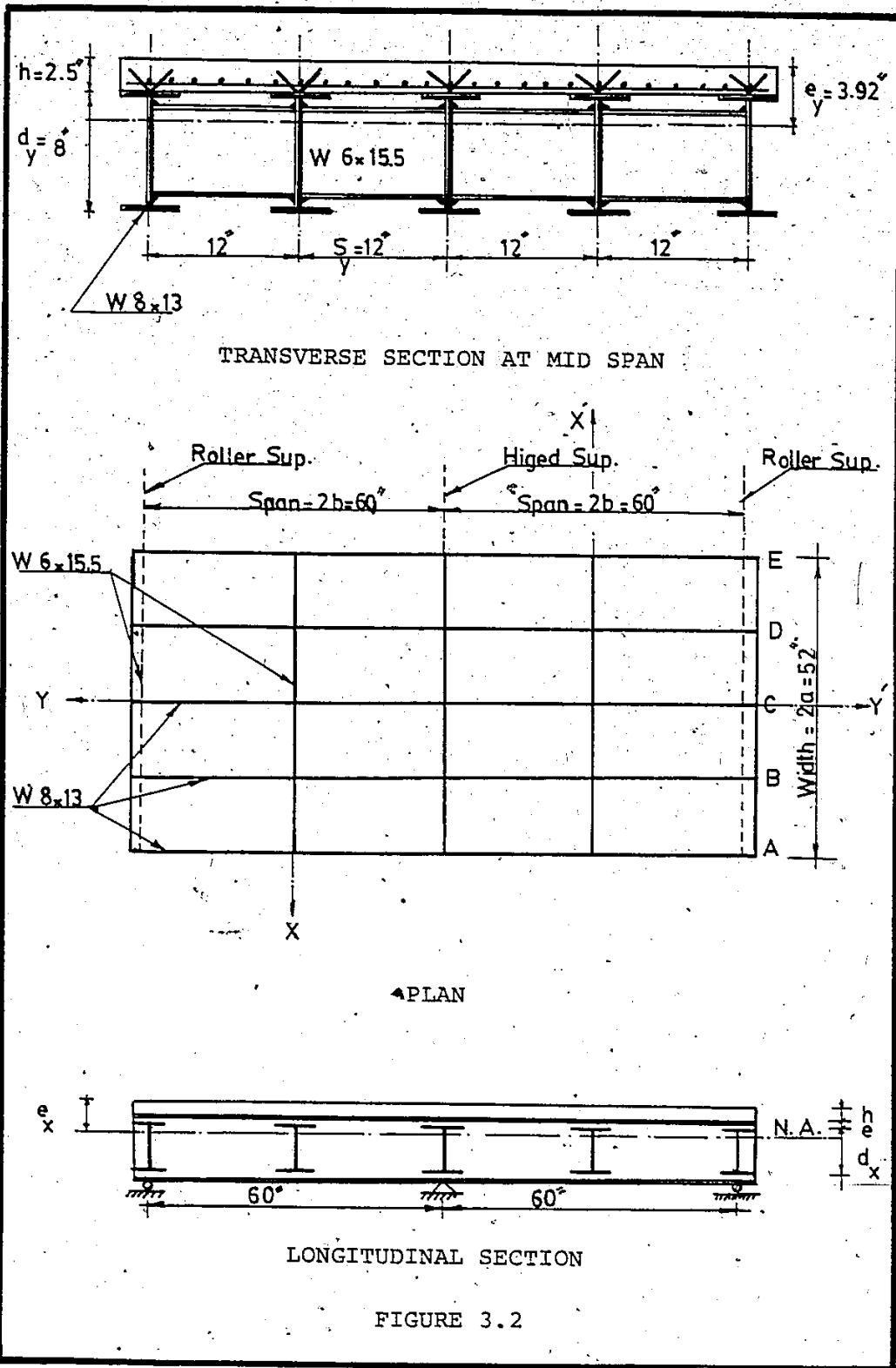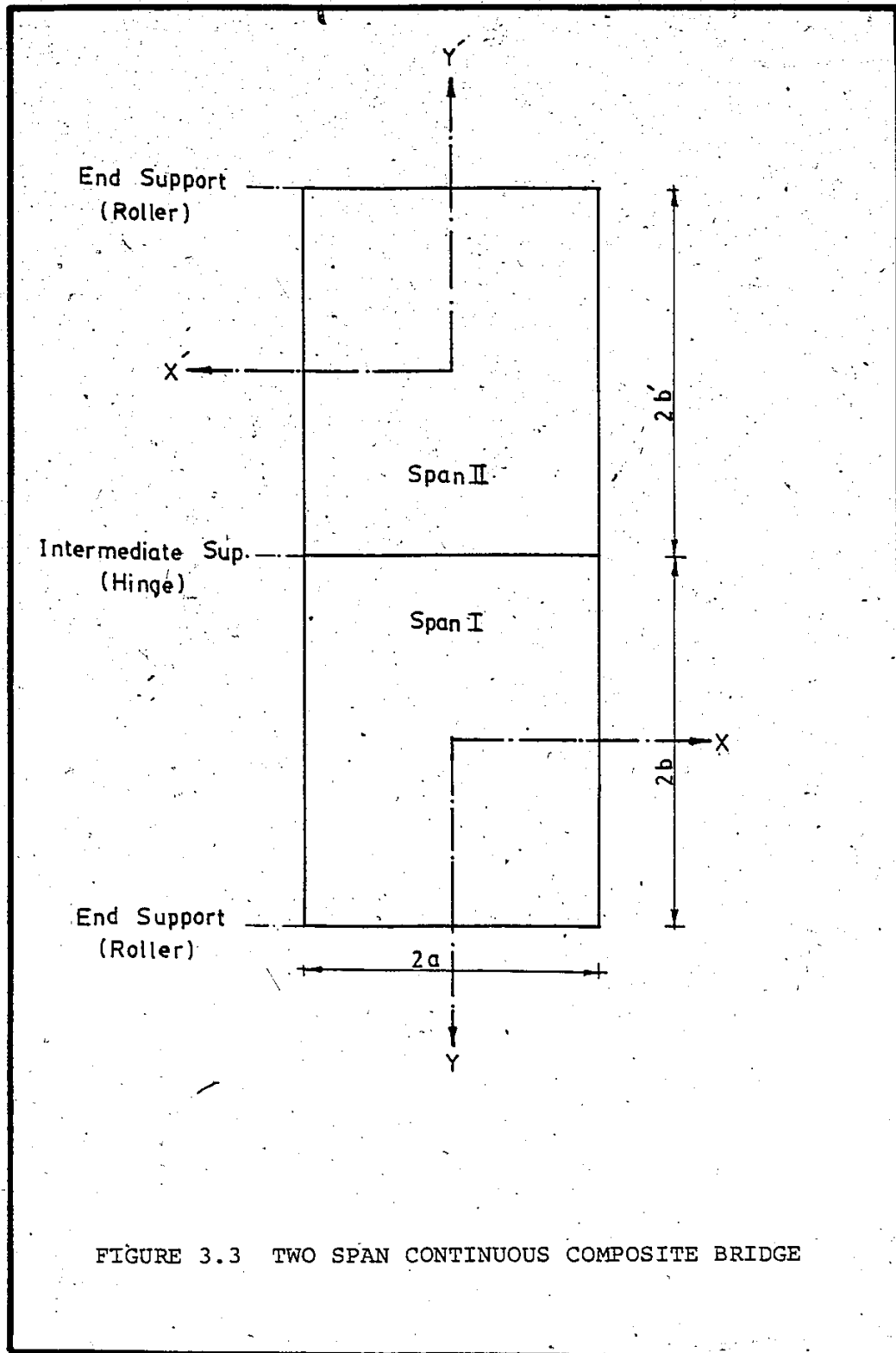
FIGURE 3.2

FIGURE 3.3   TWO SPAN CONTINUOUS COMPOSITE BRIDGE

62
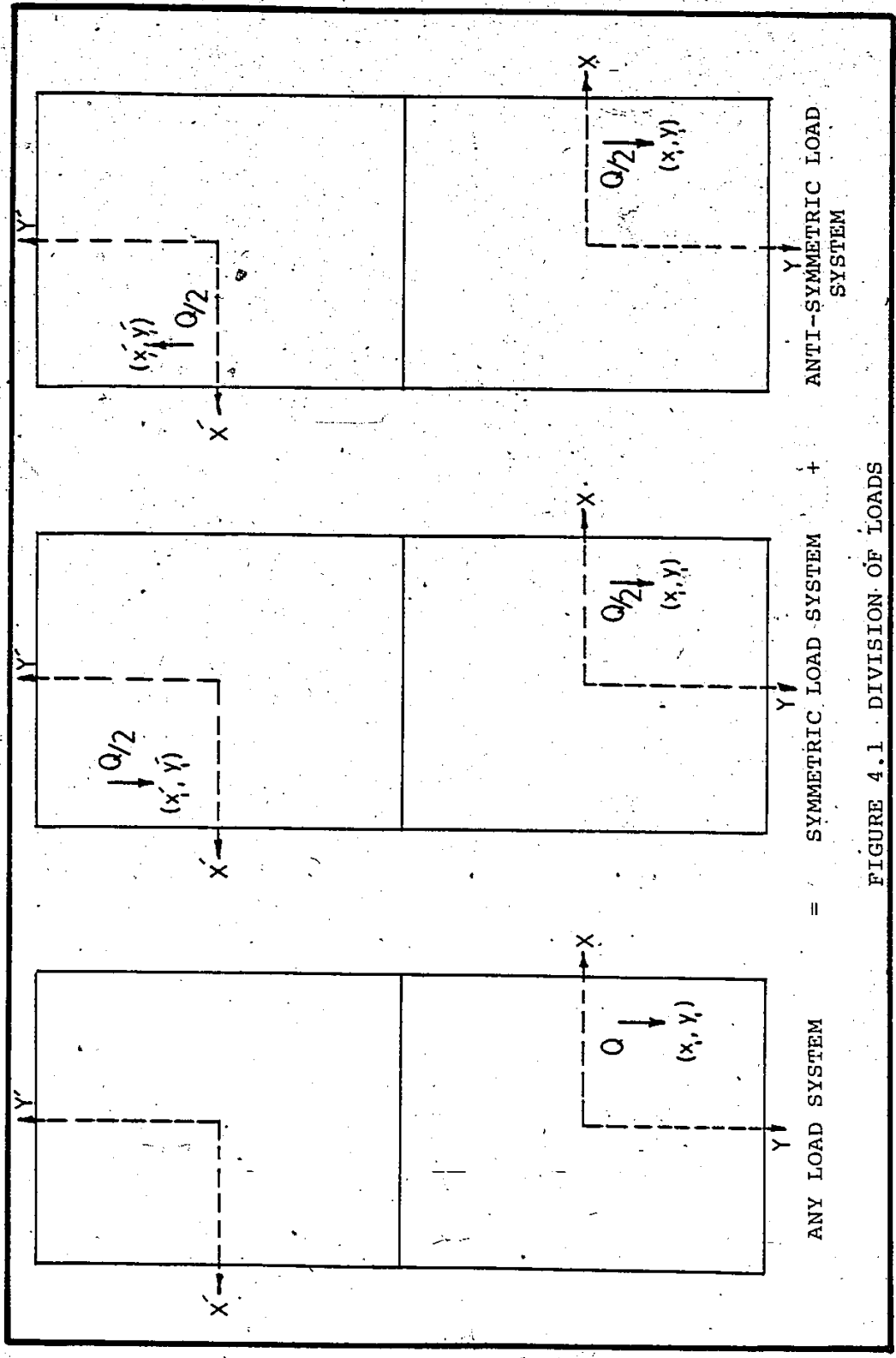
FIGURE 4.1 DIVISION OF LOADS

ANY LOAD SYSTEM = SYMMETRIC LOAD SYSTEM + ANTI-SYMMETRIC LOAD SYSTEM
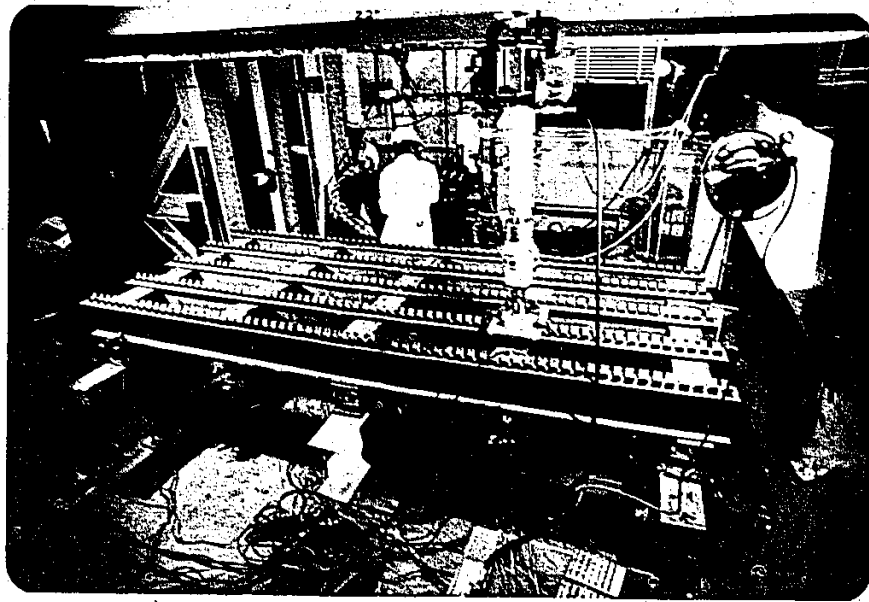
FIGURE 5.1   THE LAYOUT OF SHEAR CONNECTORS,
             MAIN GIRDERS AND DIAPHRAGMS.
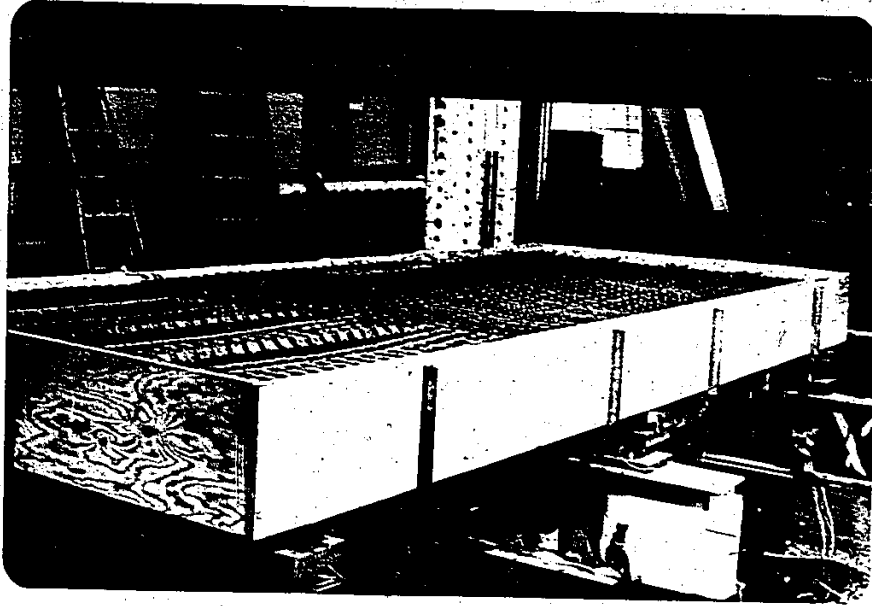
FIGURE 5.2   FORMWORK FOR THE CASTING OF THE
             REINFORCED CONCRETE SLAB, BRIDGE
             MODEL I.
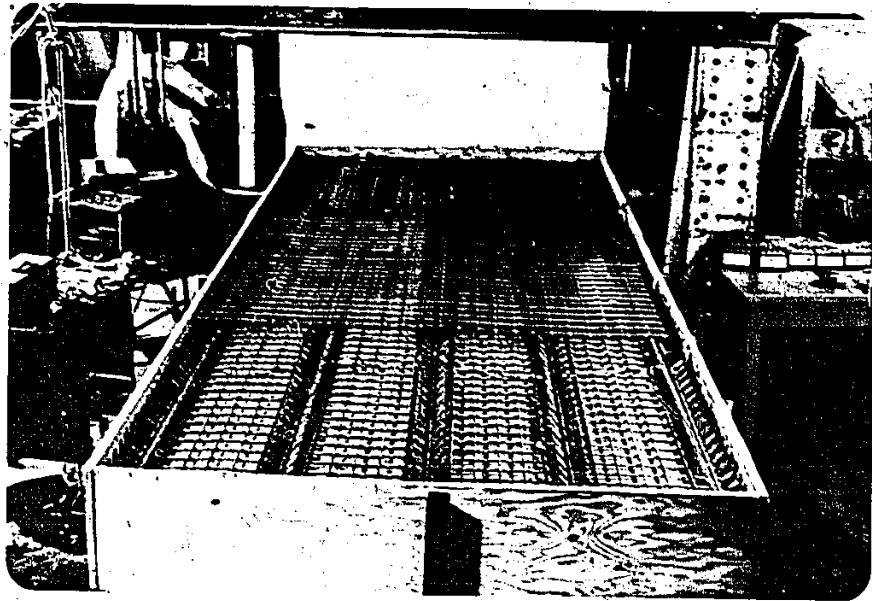
FIGURE 5.3   SLAB REINFORCEMENT LAYOUT AND THE
             FORMWORK, BRIDGE MODEL I.
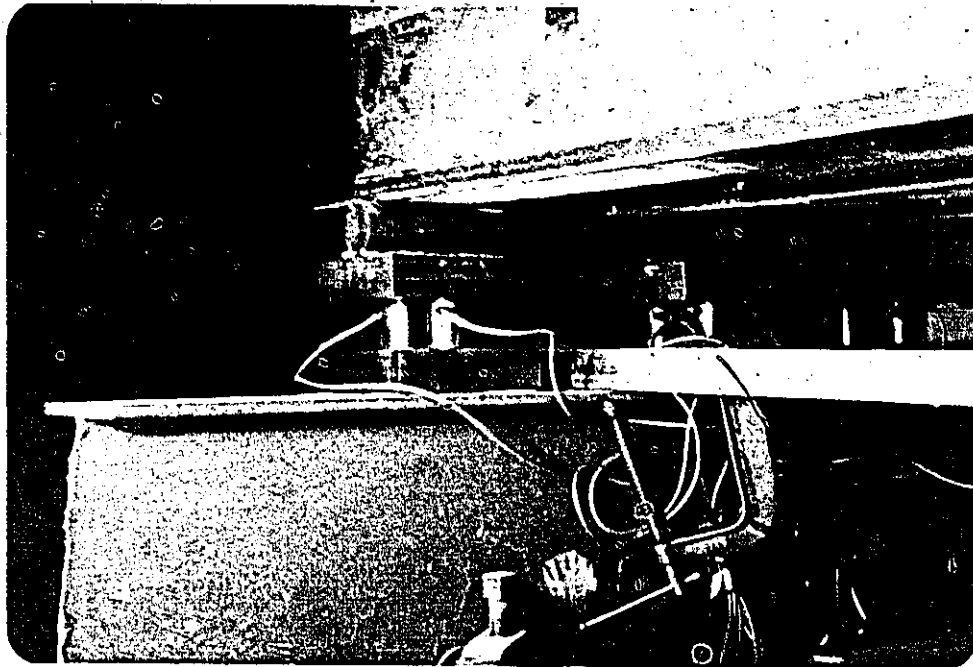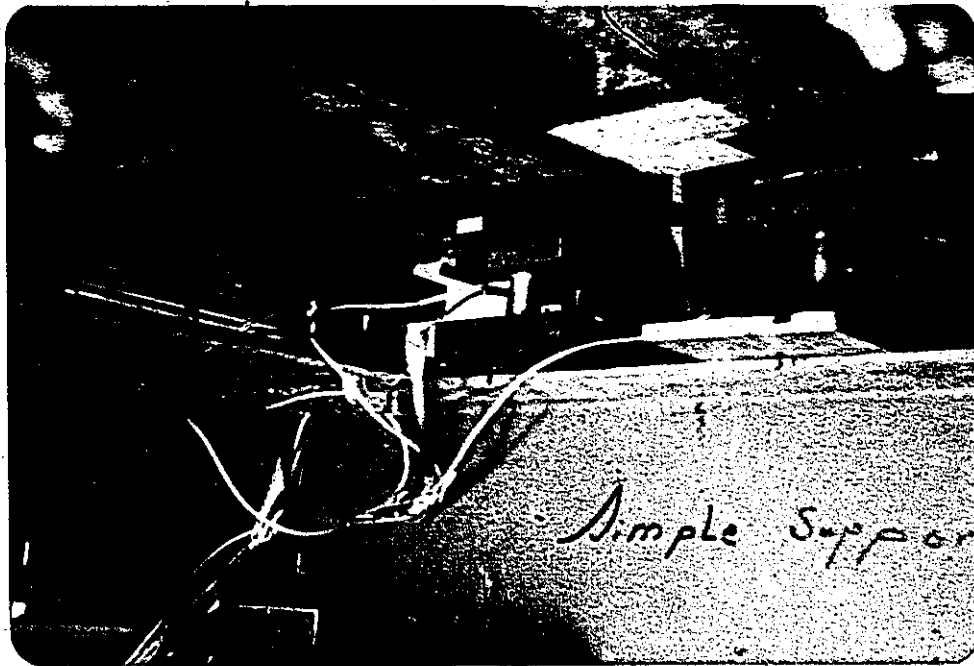
FIGURE 5.4   THE ROLLER SUPPORT INSTRUMENTED
WITH THE LOAD CELLS.
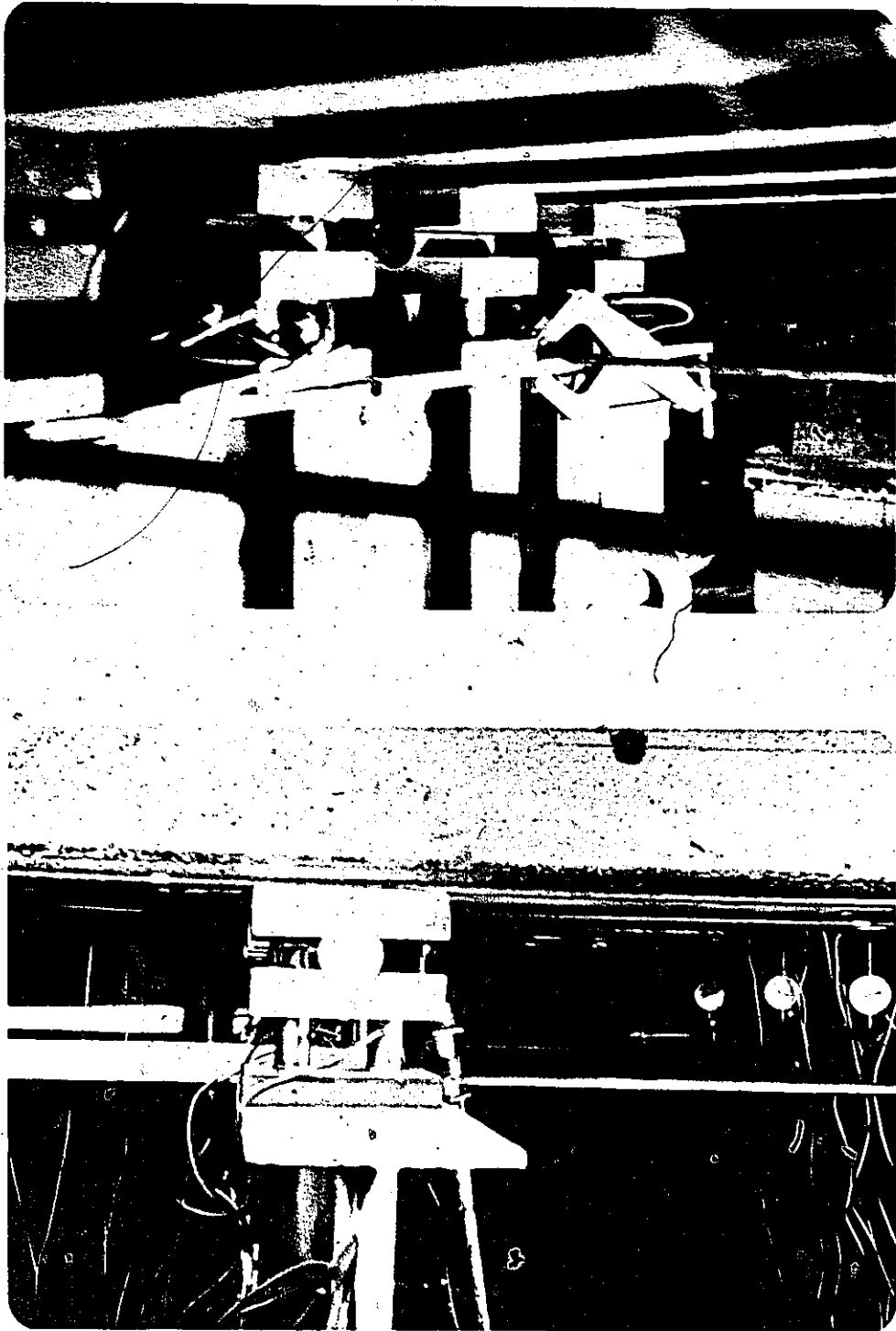
FIGURE 5.5 THE HINGED SUPPORT INSTRUMENTED WITH
THE LOAD CELLS.

FIGURE 5.6 END BEARING SYSTEM, BRIDGE MODEL
          II.

FIGURE 5.7 DISTRIBUTION OF END BEARING PLATES
            THROUGH THE CROSS-SECTION, BRIDGE
            MODEL II.
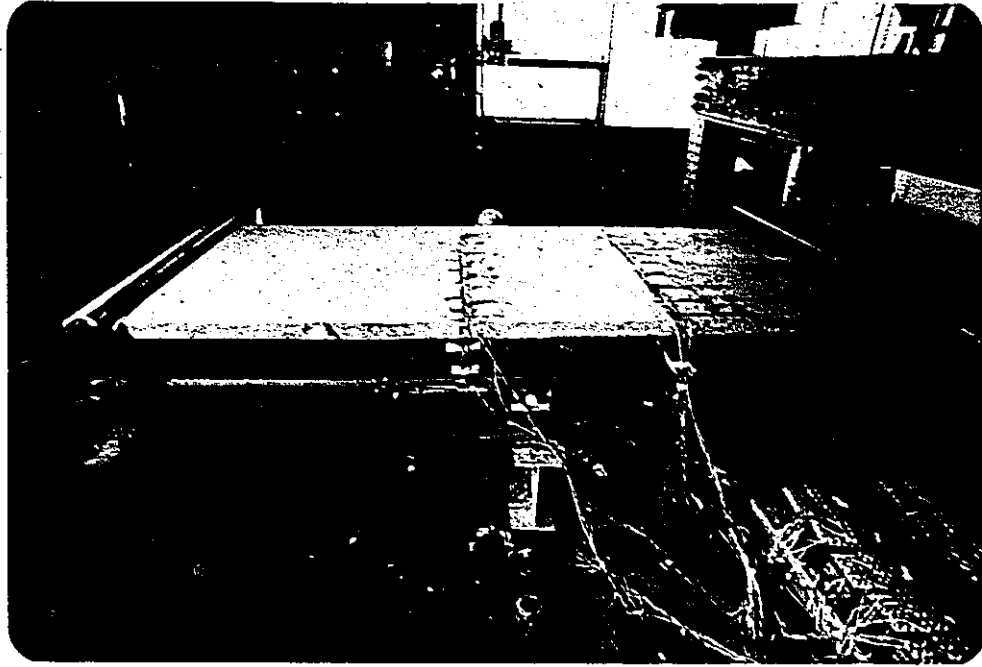
FIGURE 5.8   A VIEW OF THE CONCRETE SLAB AFTER
             CASTING, BRIDGE MODEL I.

FIGURE 5.9 STEEL CABLE ANCHORS, BRIDGE MODEL I.

PLAN

ELEVATION
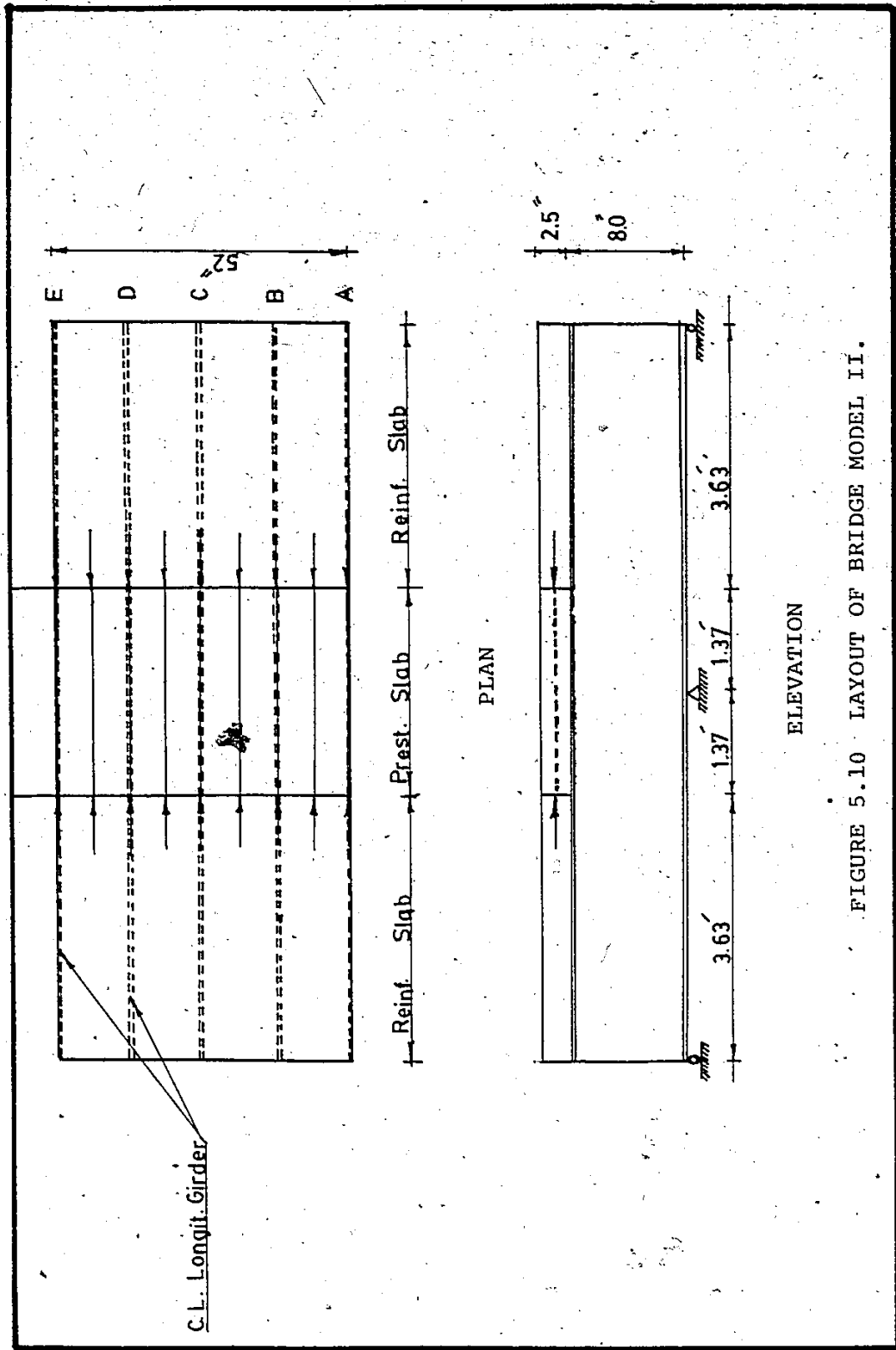
FIGURE 5.10 LAYOUT OF BRIDGE MODEL II.
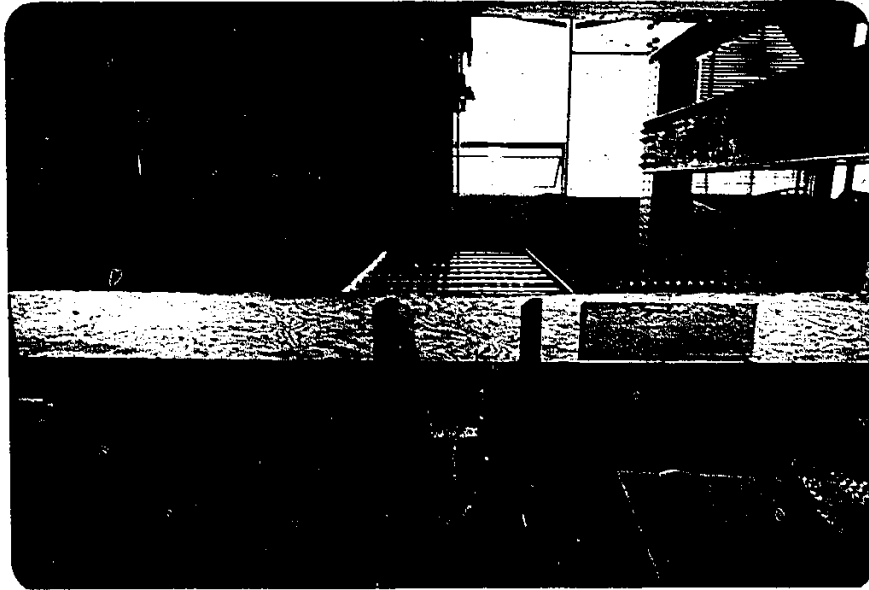
FIGURE 5.11   FORMWORK FOR PRESTRESSING SLAB
              AT THE INTERMEDIATE SUPPORT.
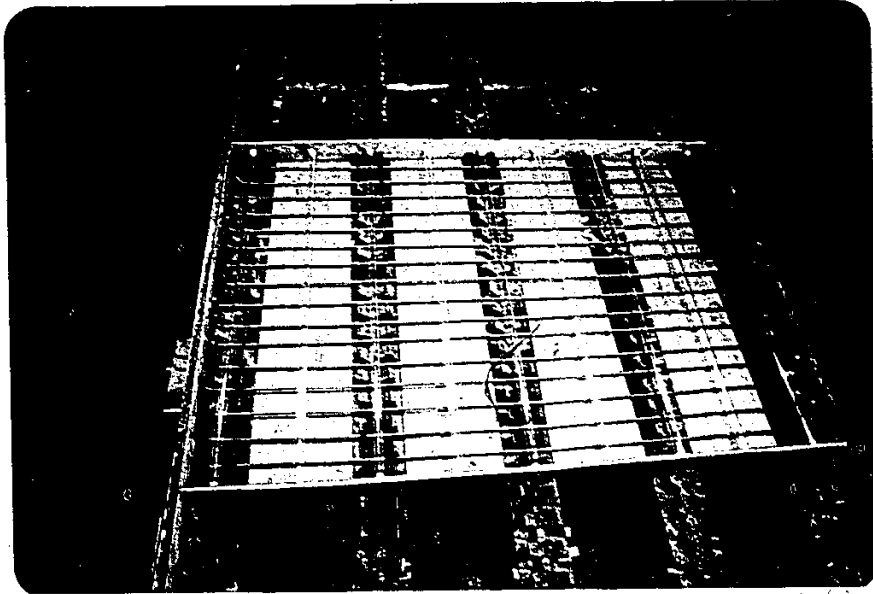
FIGURE 5.12   RUBBER HOSES TO COVER THE PRESTRESSING
WIRES DURING CASTING.
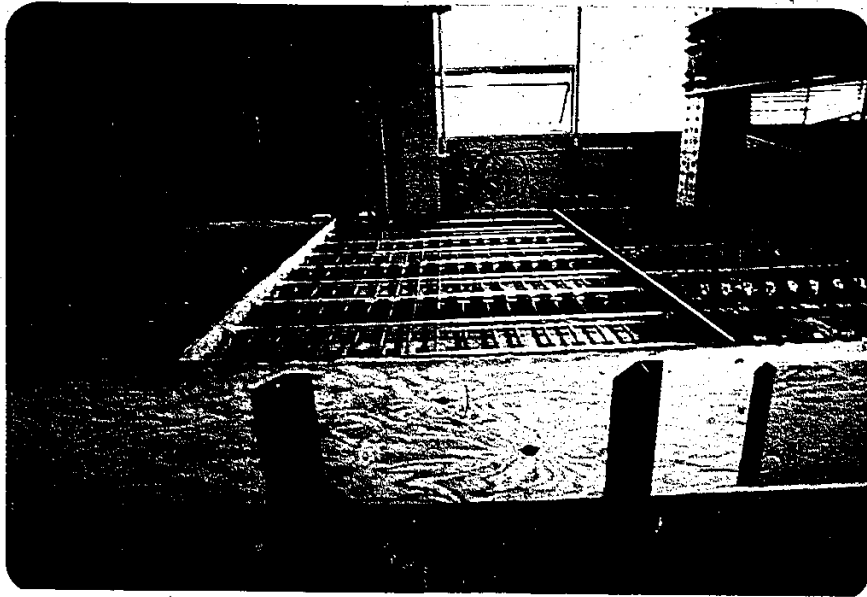
FIGURE 5.13   TRANSVERSE REINFORCEMENT IN PRE-
             STRESSING SLAB.
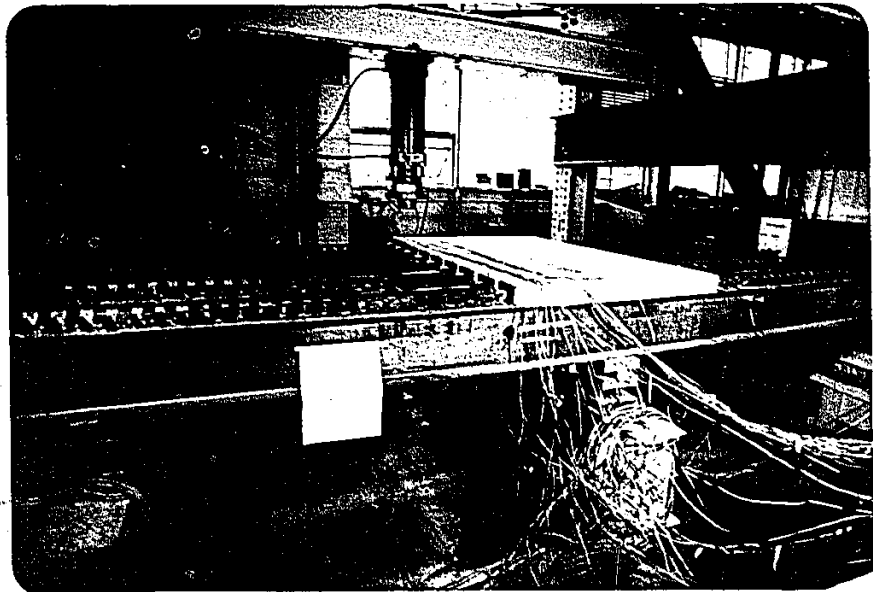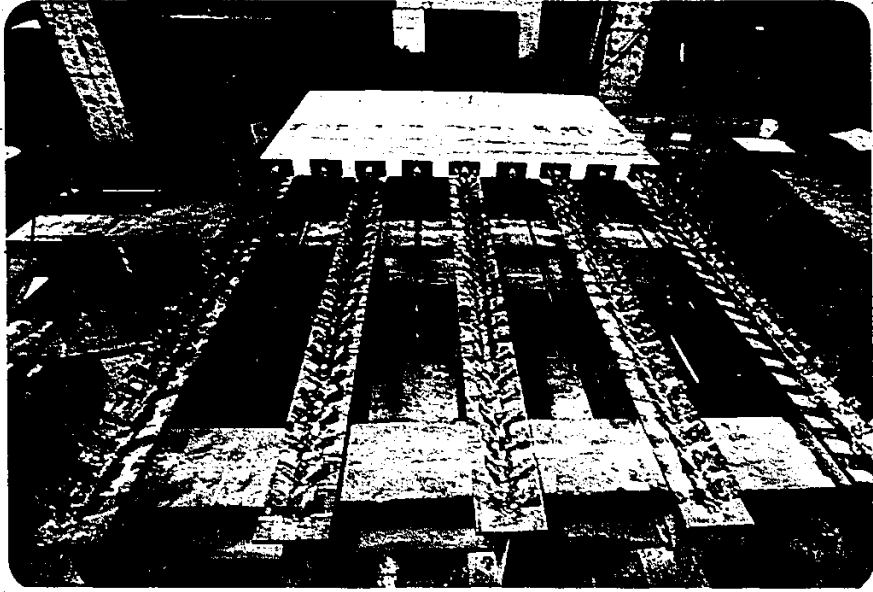
FIGURE 5.14 A VIEW OF PRESTRESSED SLAB PORTION
            AFTER PRESTRESSING.
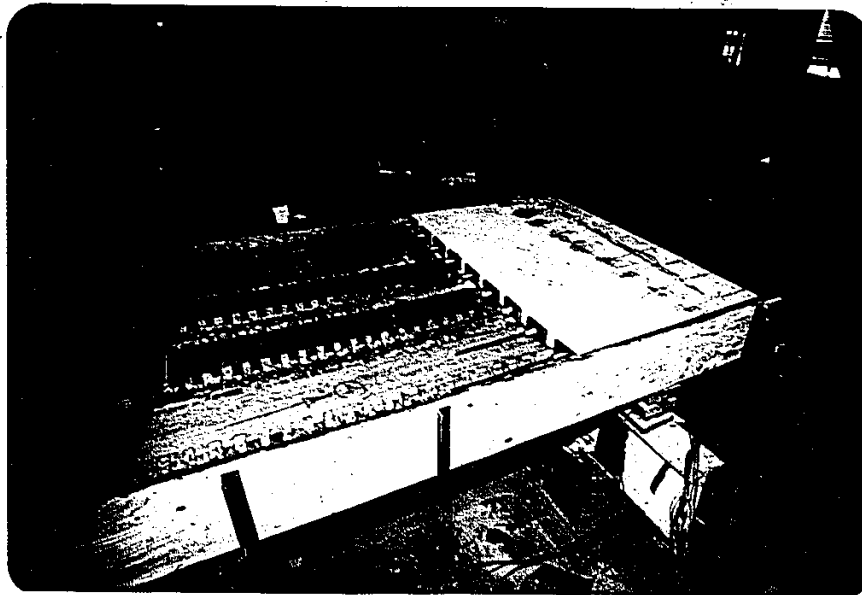
FIGURE 5.15 FORMWORK FOR THE REMAINING RIGHT
AND LEFT PORTIONS OF THE SLAB.
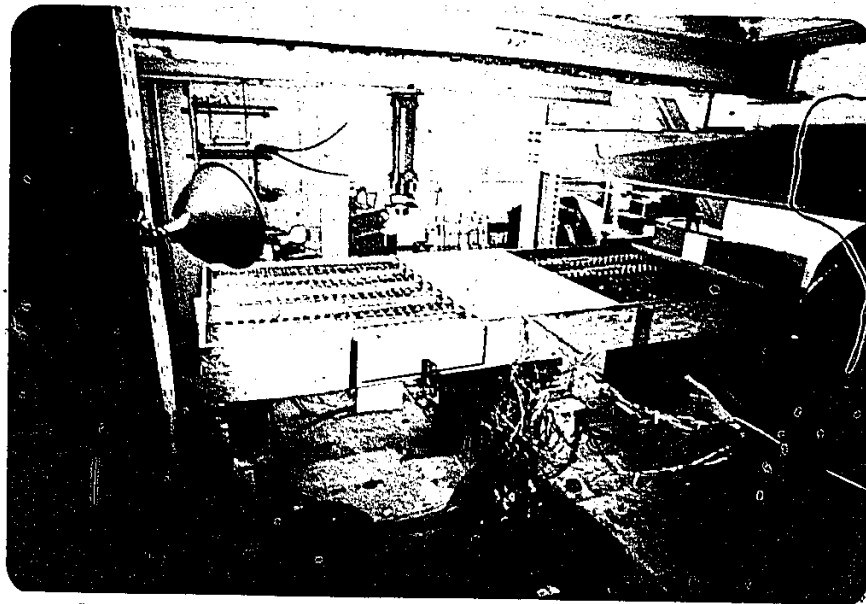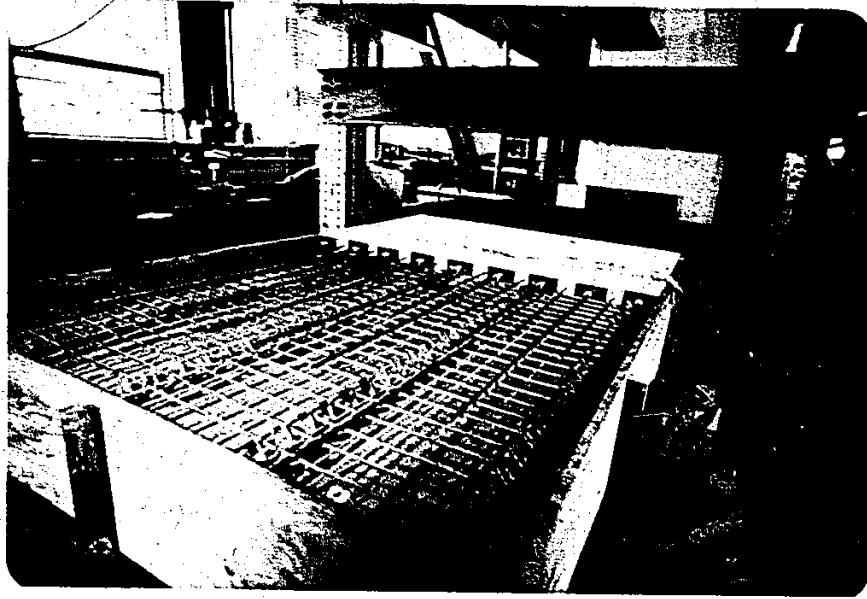
FIGURE 5.16   REINFORCEMENT STEEL FOR THE NON-
              PRESTRESSED PORTION OF THE SLAB.
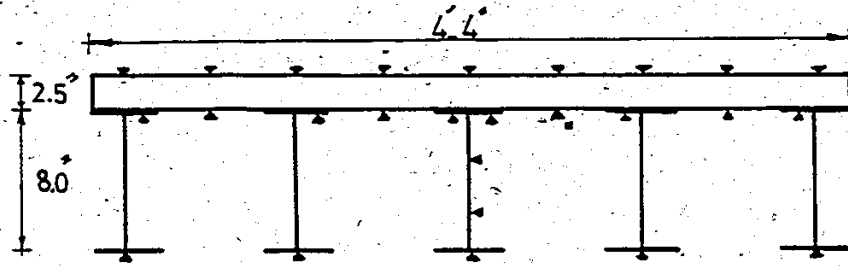
LOCATION OF LONGITUDINAL STRAIN GAUGES AT MID SPAN
AND INTERMEDIATE SUPPORT SECTIONS
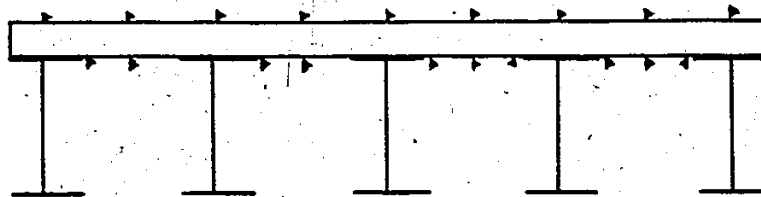
LOCATION OF TRANSVERSE STRAIN GAUGES AT MID SPAN
SECTION
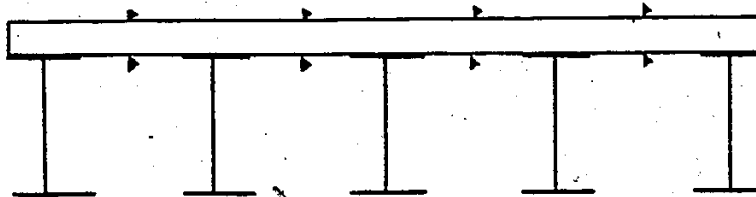
LOCATION OF TRANSVERSE STRAIN GAUGES AT INTERMEDIATE
SUPPORT SECTION

FIGURE 5.17 LOCATION OF STRAIN GAUGES
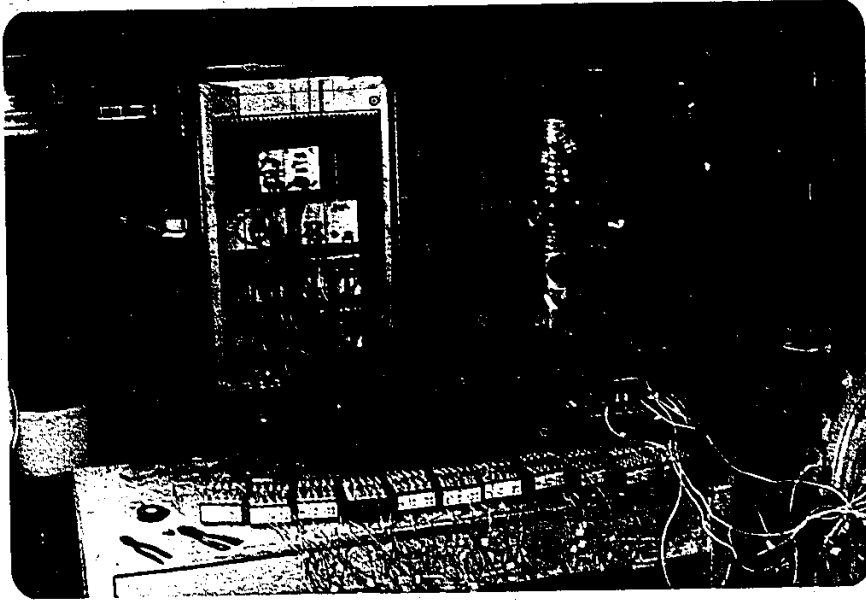
FIGURE 5.18 ELECTRONIC STRAIN INDICATOR.
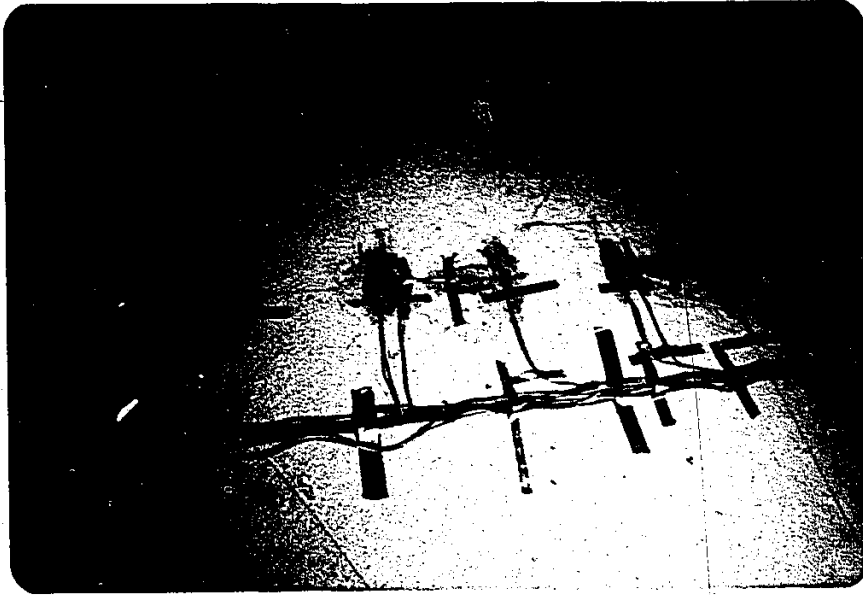
FIGURE 5.19   STRAIN GAUGES ON THE TOP OF THE
              SLAB.

FIGURE 5.20   STRAIN GAUGES ON THE BOTTOM OF THE
              SLAB.
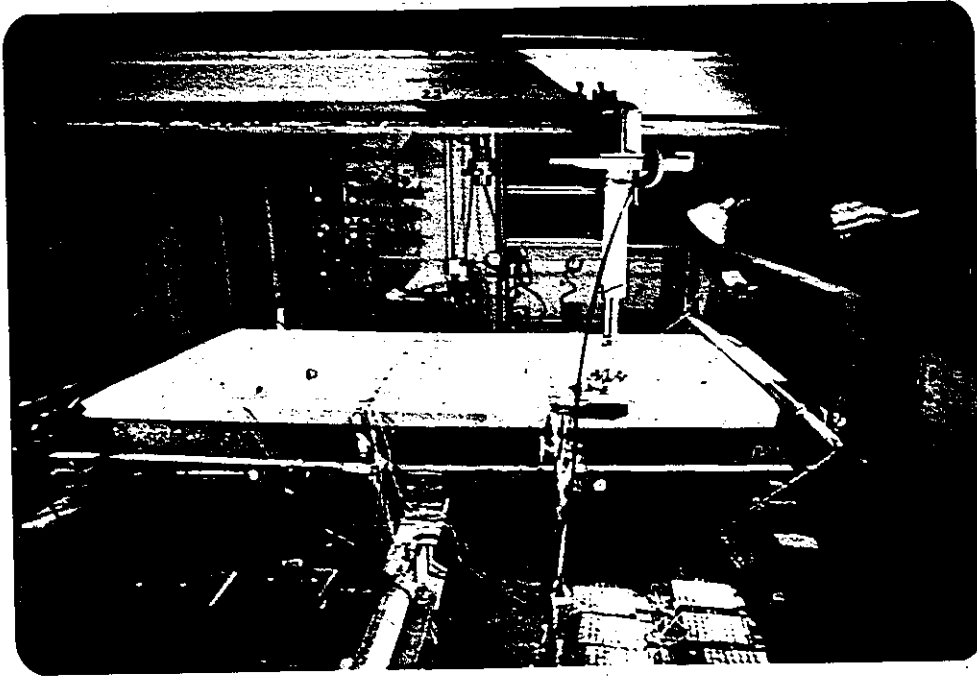
FIGURE 5.21   LOCATION OF DIAL GAUGES.
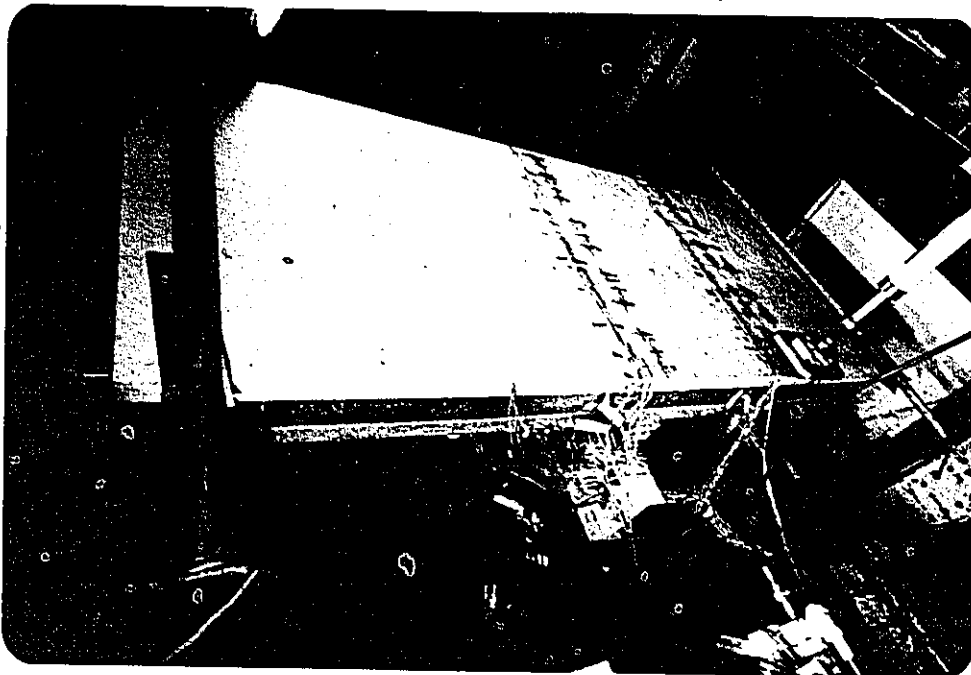
FIGURE 5.22   CONCENTRATED LOADING SYSTEM.
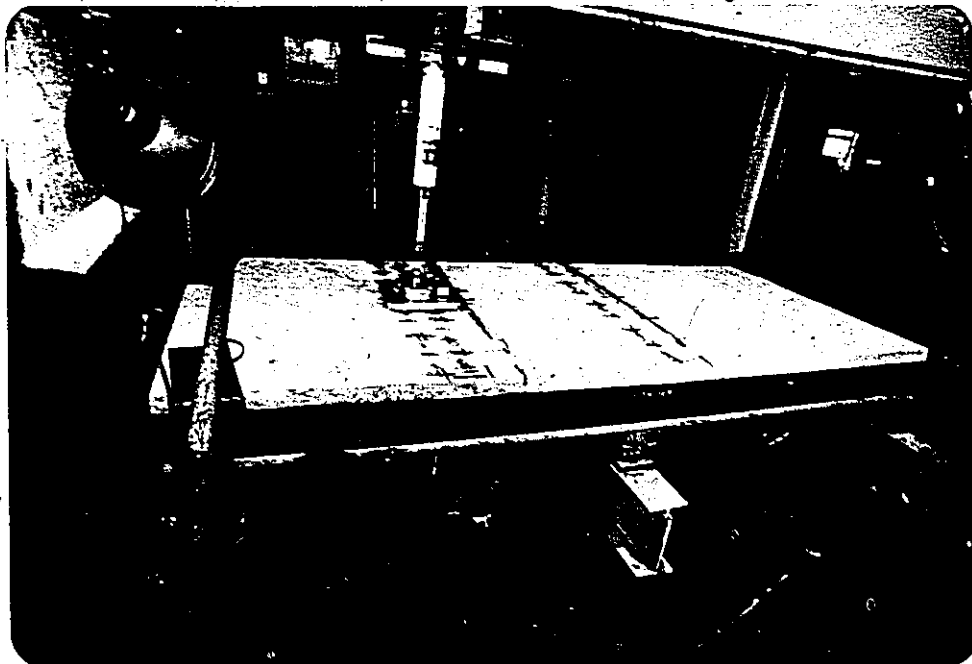
ONE POINT LOAD ON INTERMEDIATE GIRDER, BEAM C
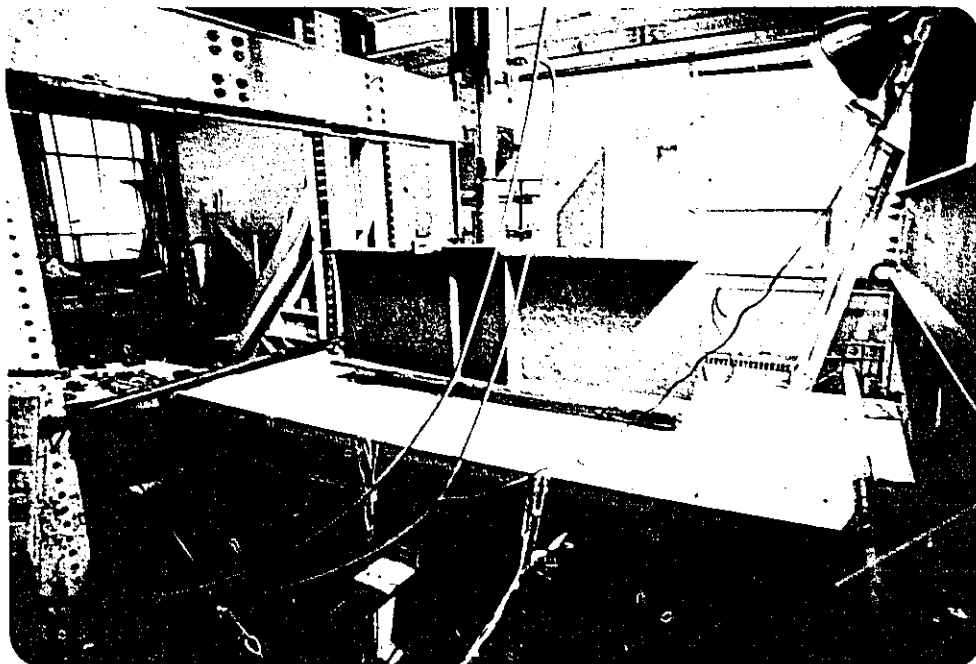
FIGURE 5.23: TWO POINTS LOAD ON INTERMEDIATE GIRDER

CROSS-SECTION AT THE INTERMEDIATE SUPPORT
BRIDGE MODEL II

Under
Working Load

Just After Transfer

Girder C, At
Intermediate Support
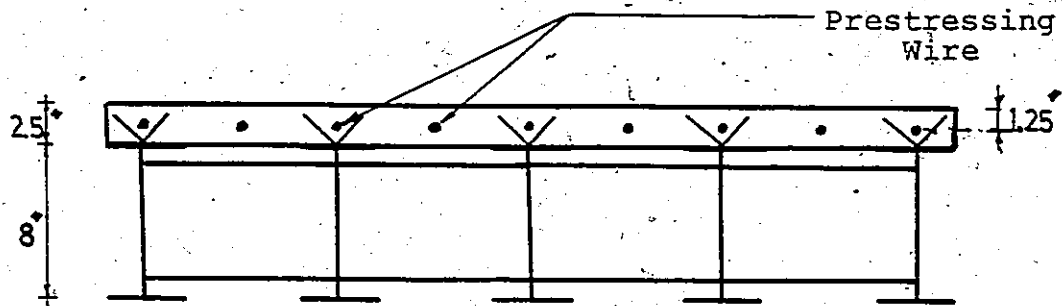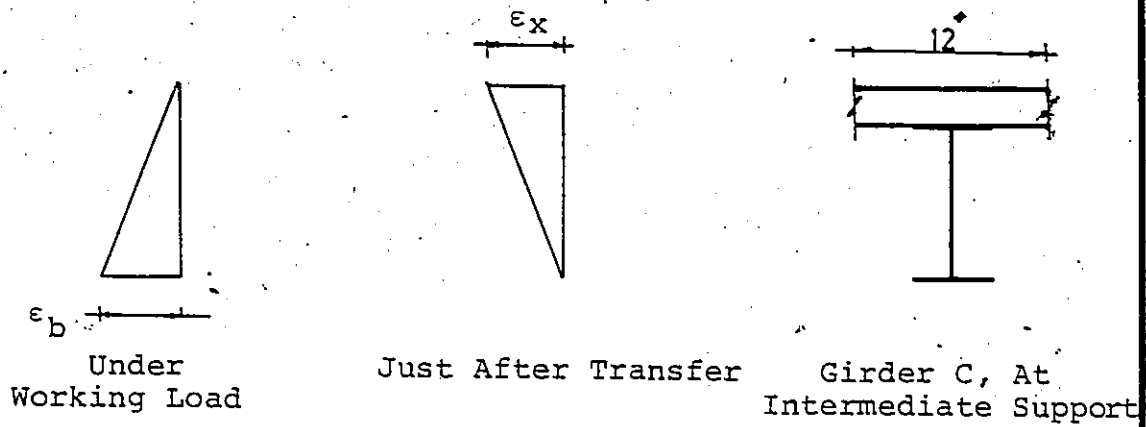
FIGURE 6.1   STRAIN DISTRIBUTION AT THE INTERMEDIATE
SUPPORT.
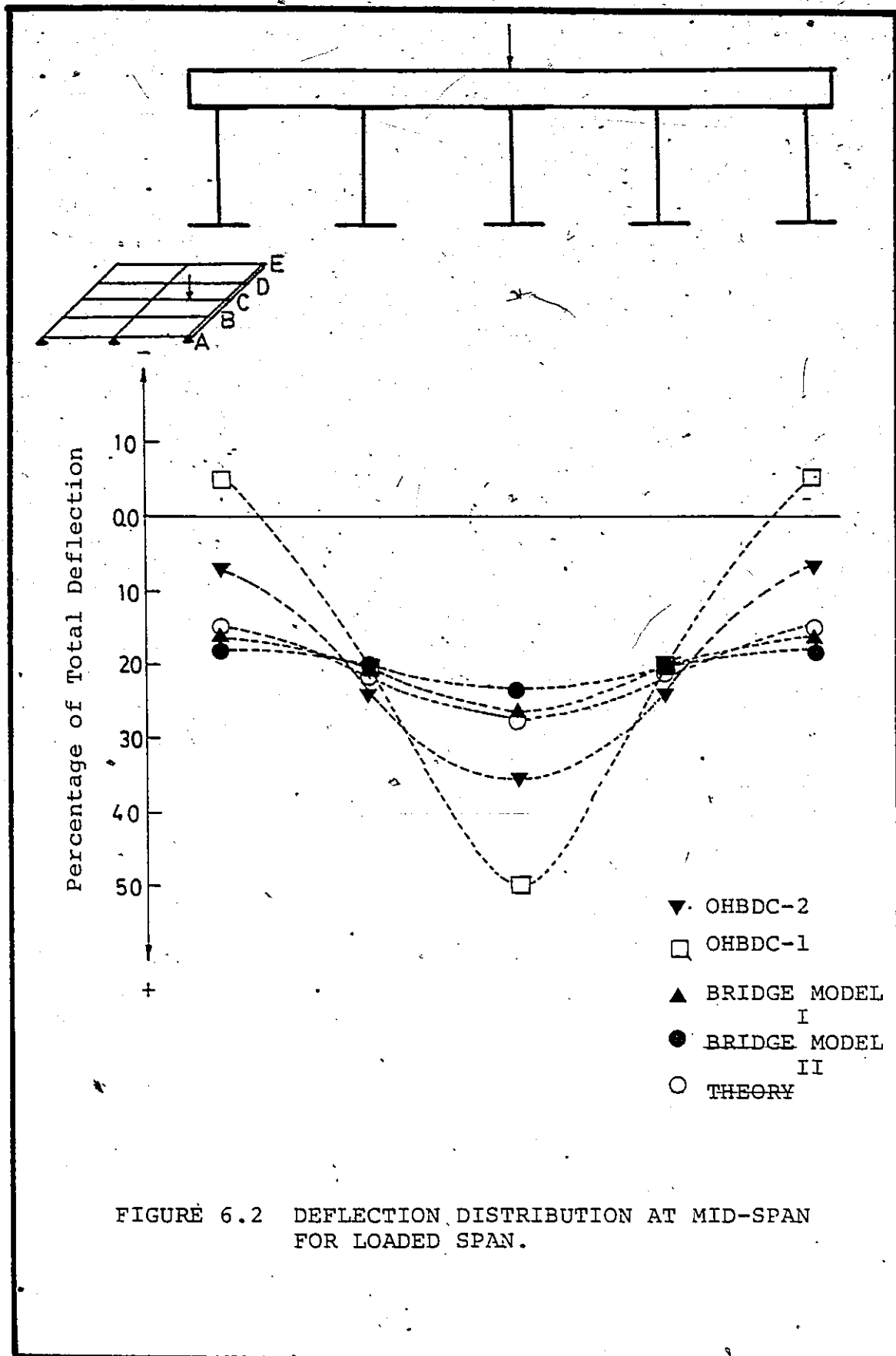
FIGURE 6.2   DEFLECTION DISTRIBUTION AT MID-SPAN
FOR LOADED SPAN.
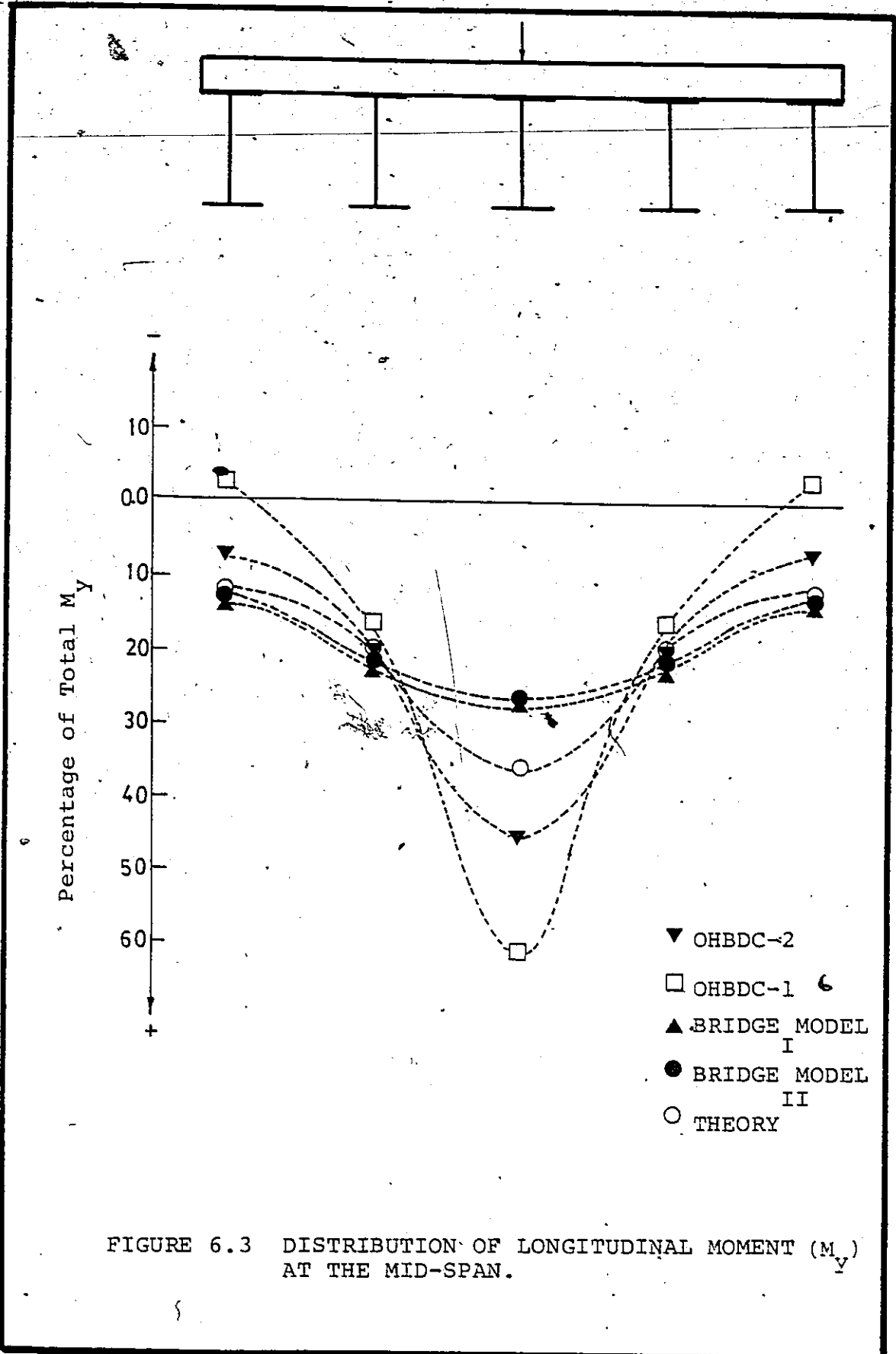
FIGURE 6.3   DISTRIBUTION OF LONGITUDINAL MOMENT (M_y) AT THE MID-SPAN.
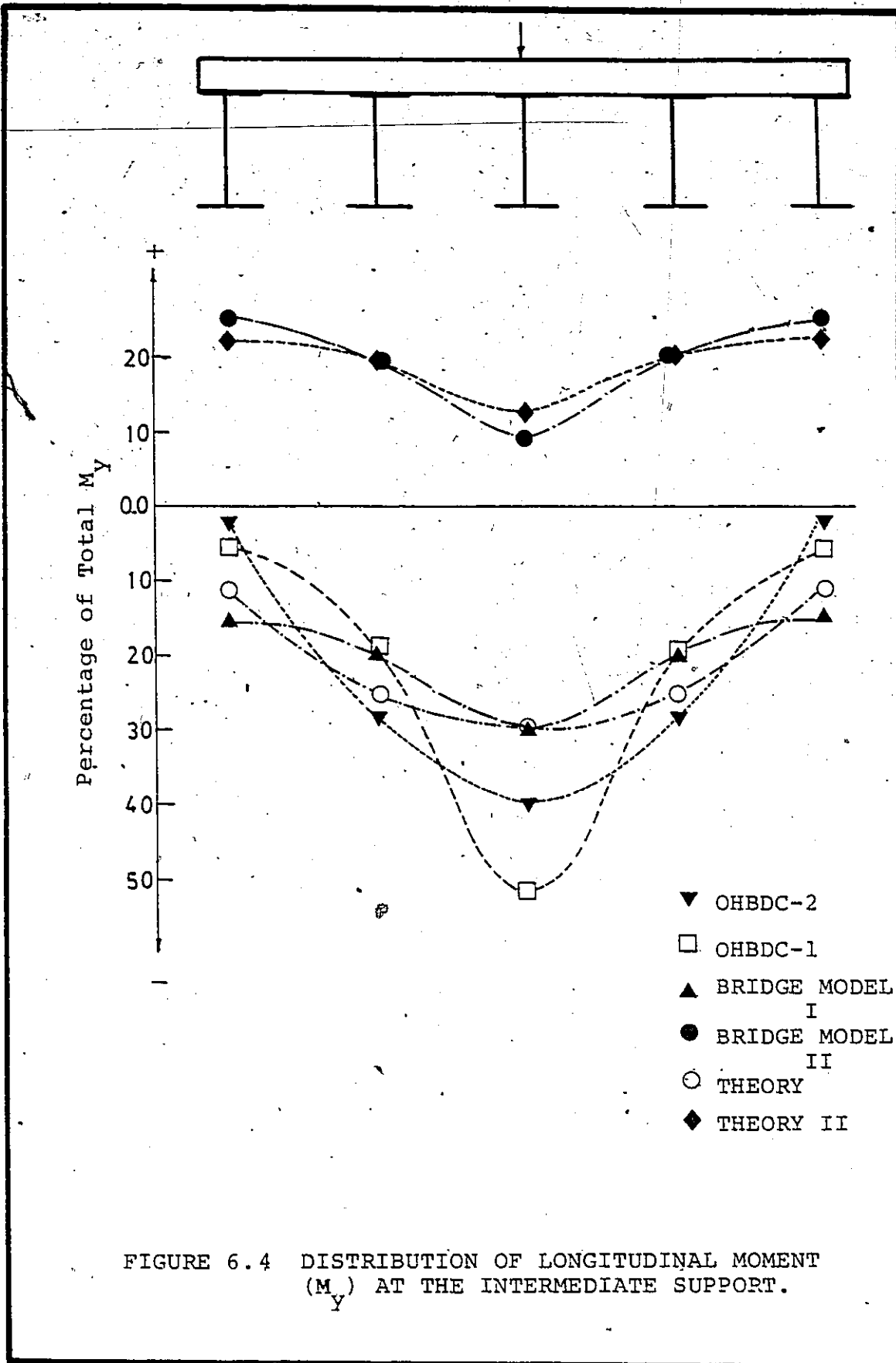
FIGURE 6.4 DISTRIBUTION OF LONGITUDINAL MOMENT
(M_y) AT THE INTERMEDIATE SUPPORT.
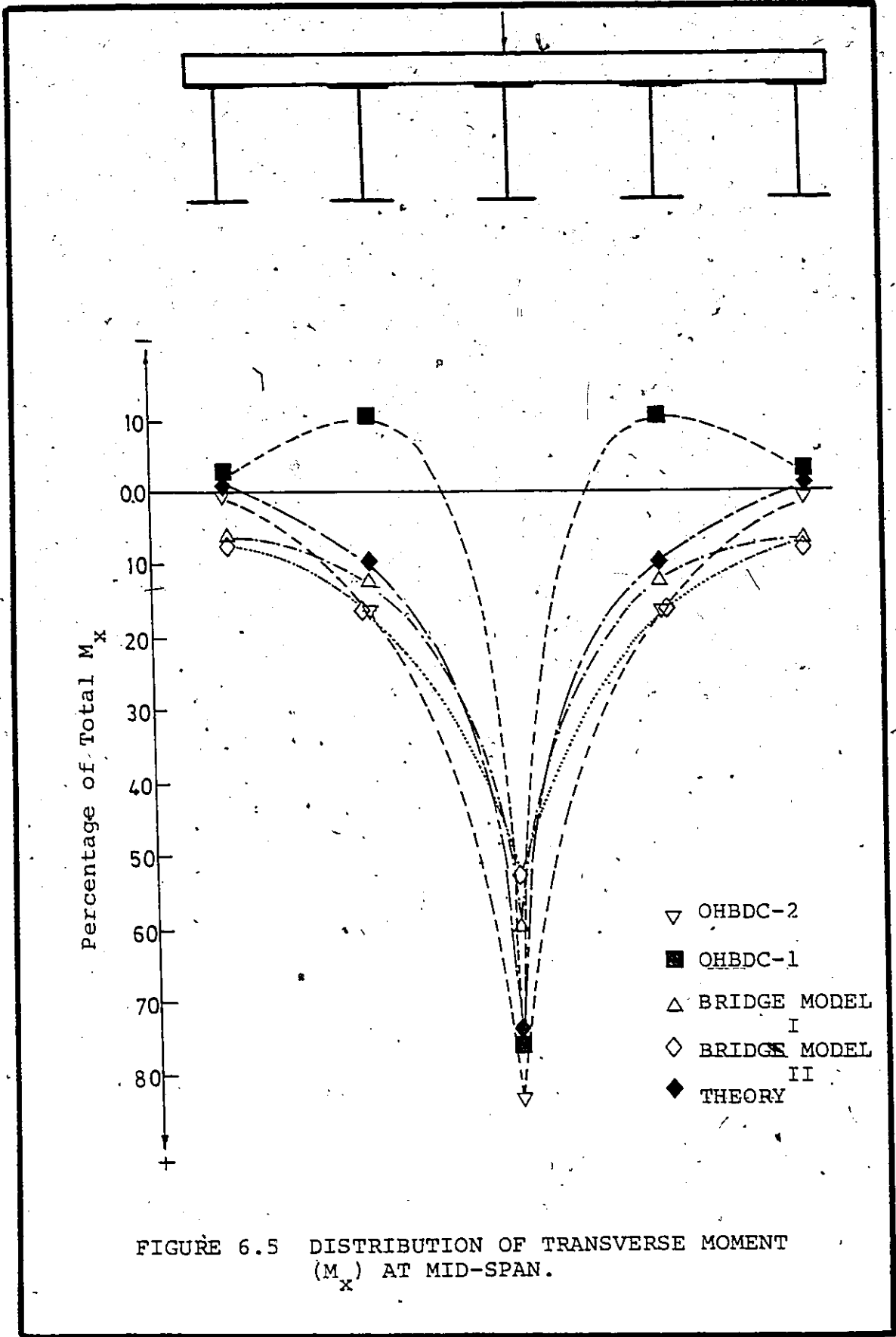
FIGURE 6.5 DISTRIBUTION OF TRANSVERSE MOMENT
            (M_x) AT MID-SPAN.
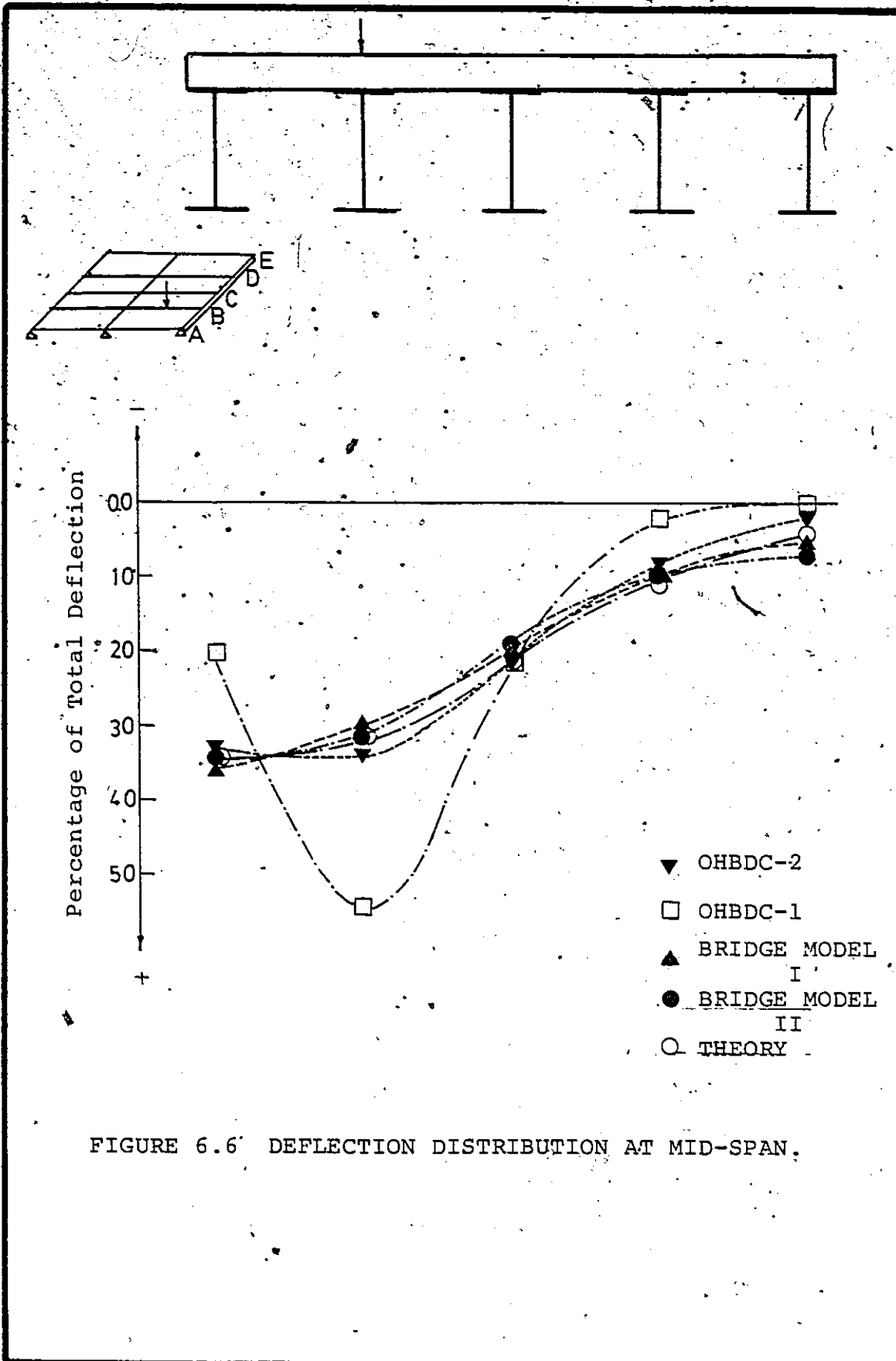
FIGURE 6.6 DEFLECTION DISTRIBUTION AT MID-SPAN.
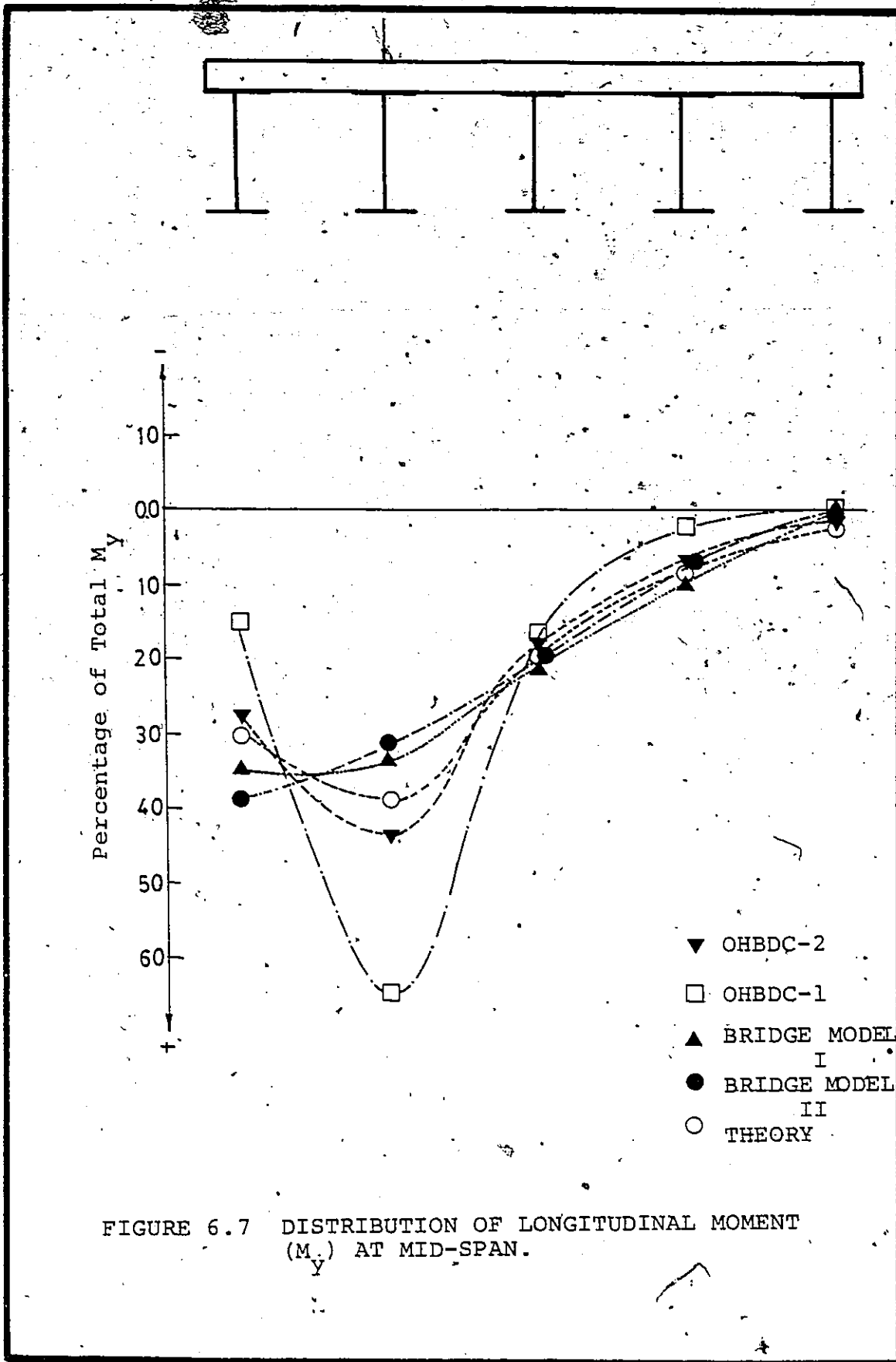
FIGURE 6.7   DISTRIBUTION OF LONGITUDINAL MOMENT
              (M_y) AT MID-SPAN.
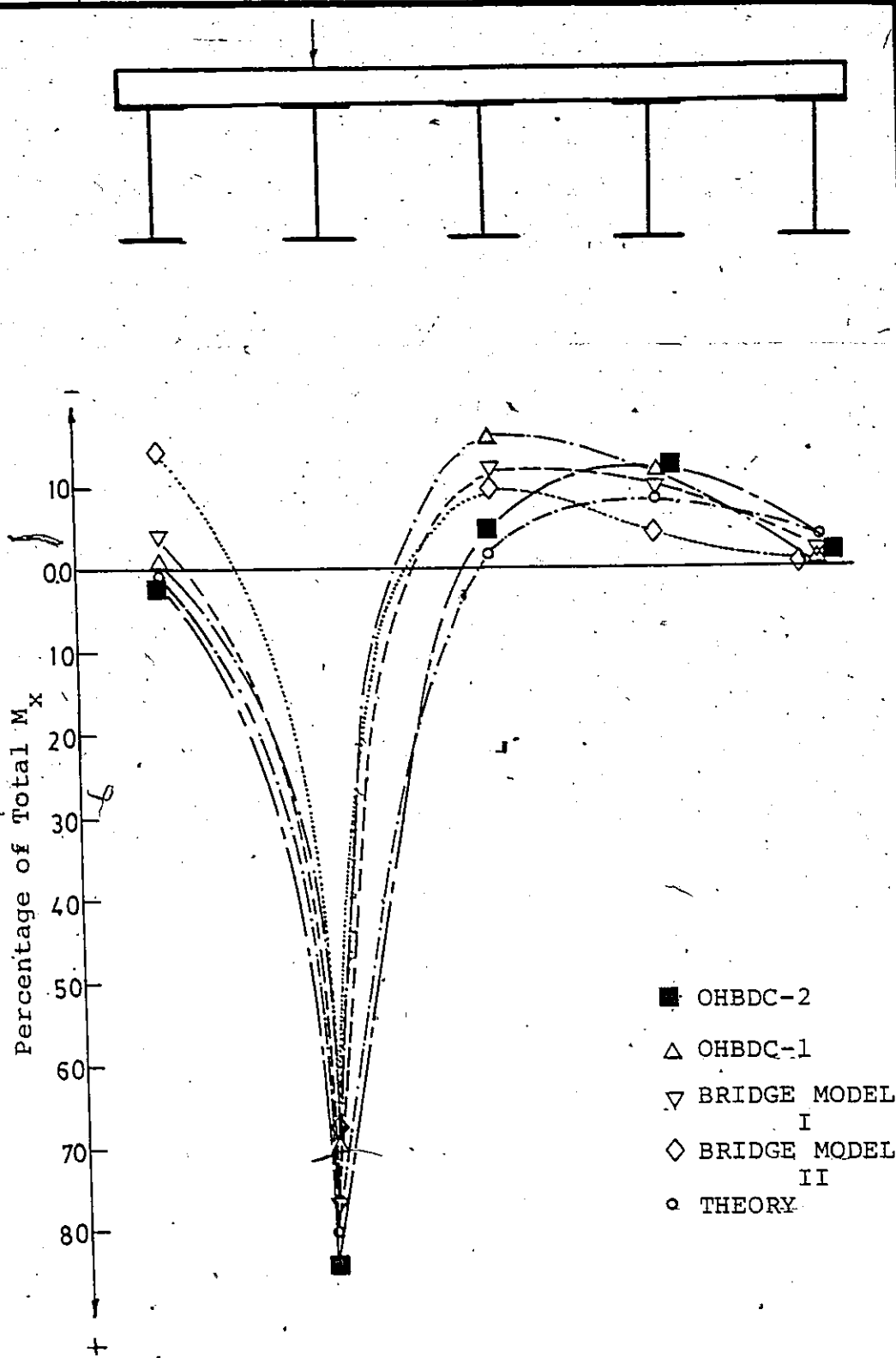
FIGURE 6.8   DISTRIBUTION OF TRANSVERSE MOMENT (M_x)
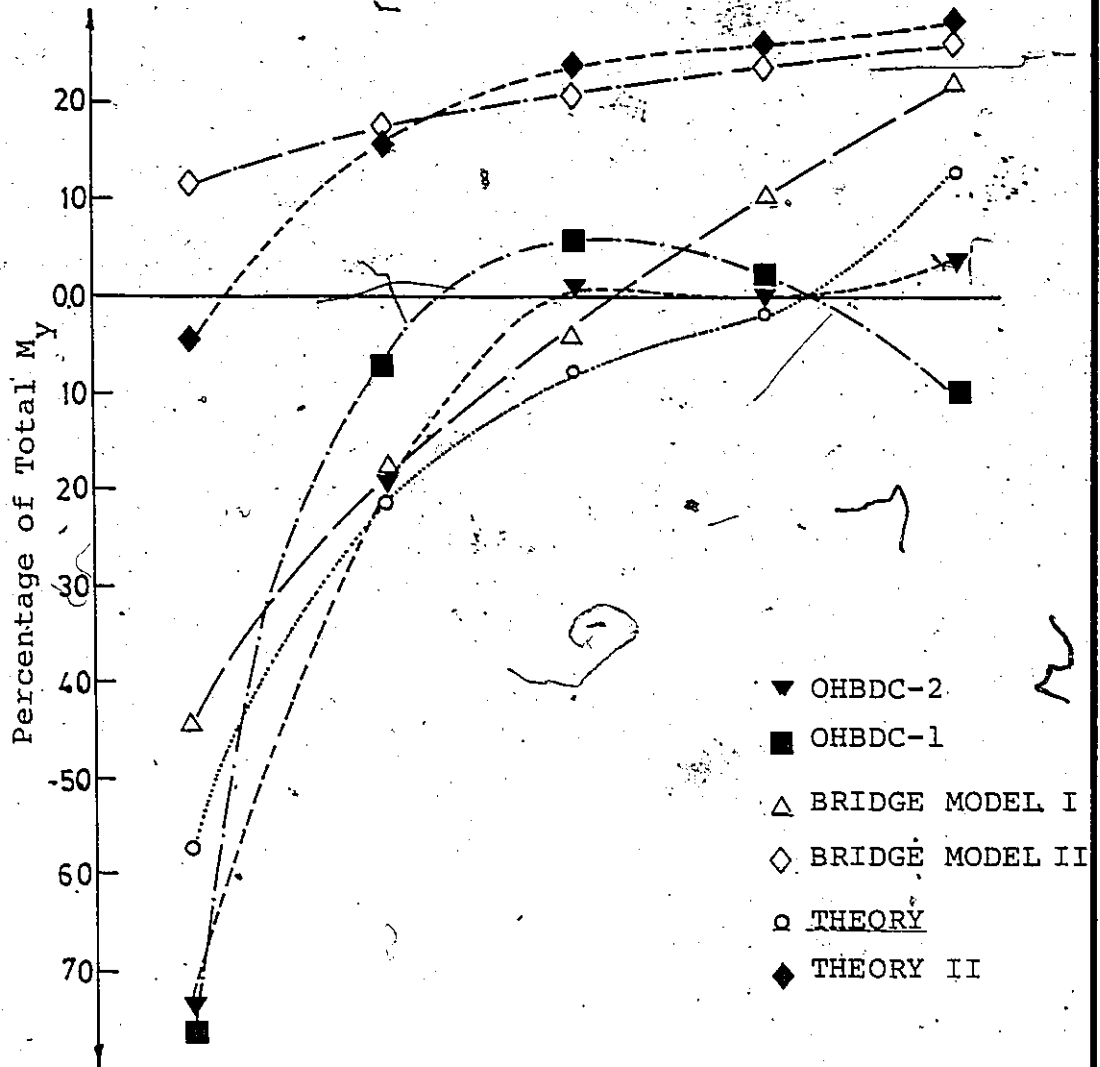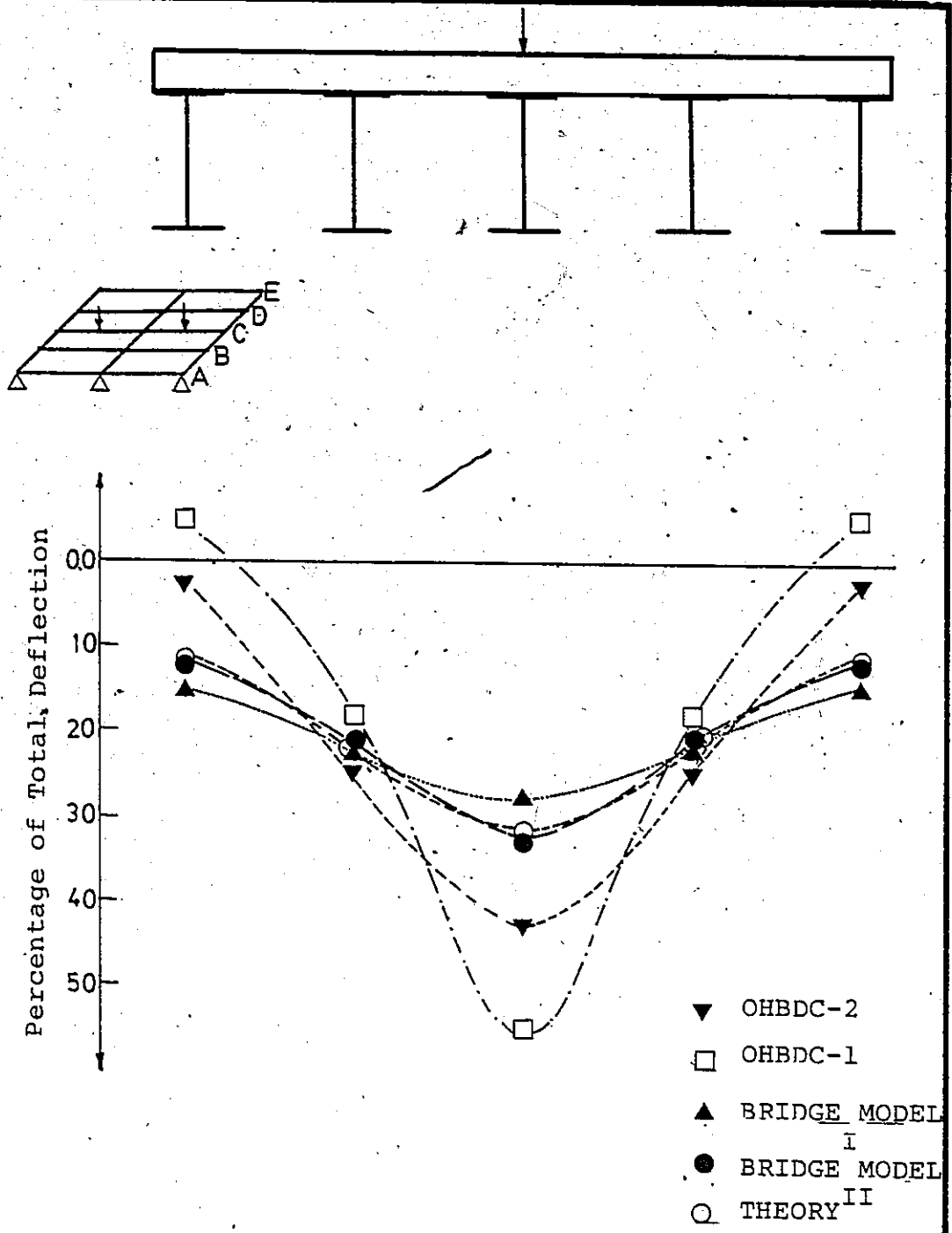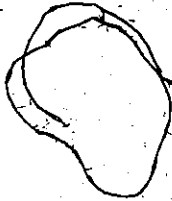   AT MID-SPAN.
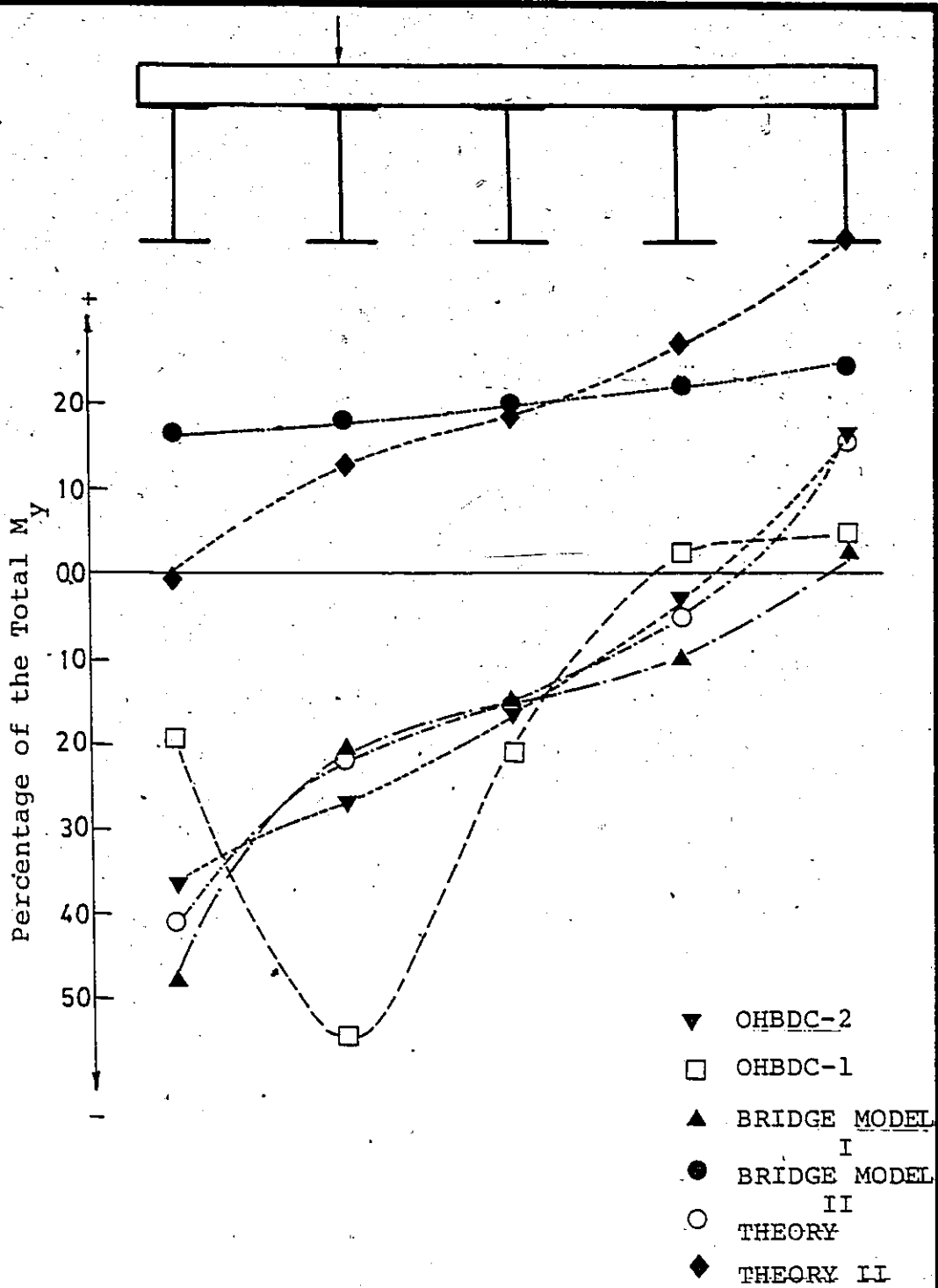
FIGURE 6.9   DISTRIBUTION OF LONGITUDINAL MOMENT
(M$_y$) AT THE INTERMEDIATE SUPPORT.
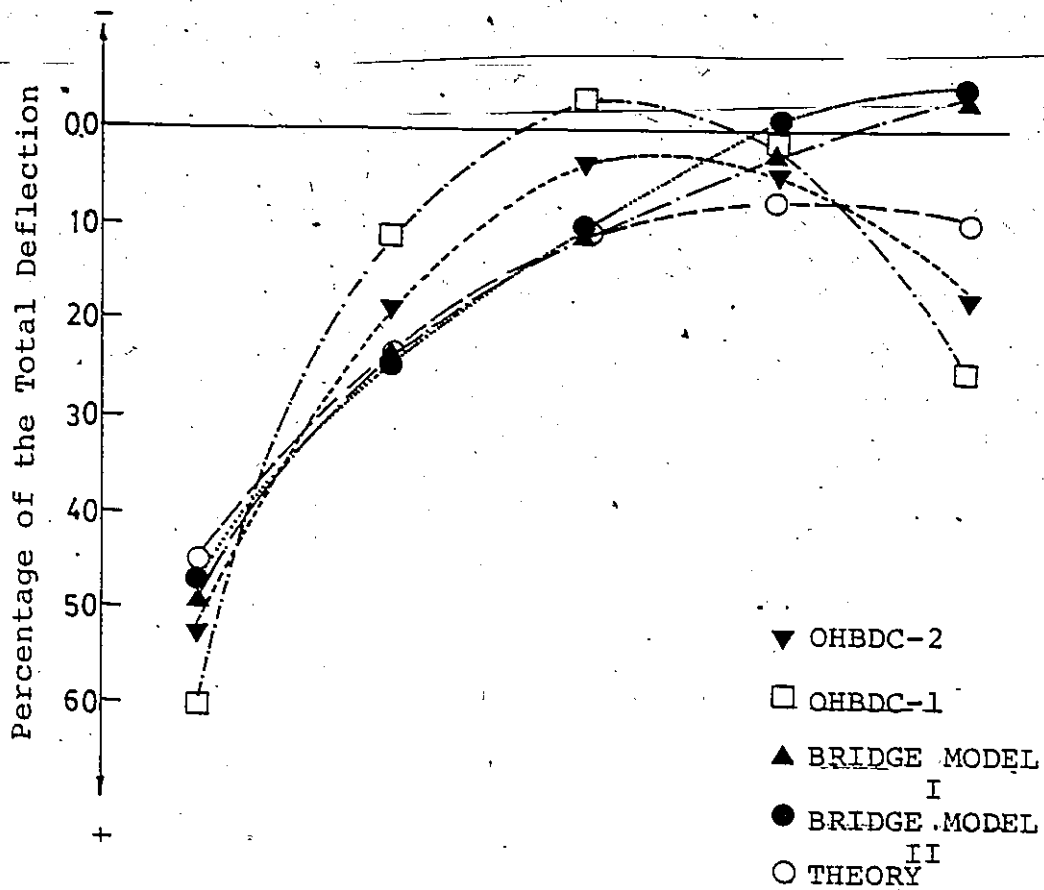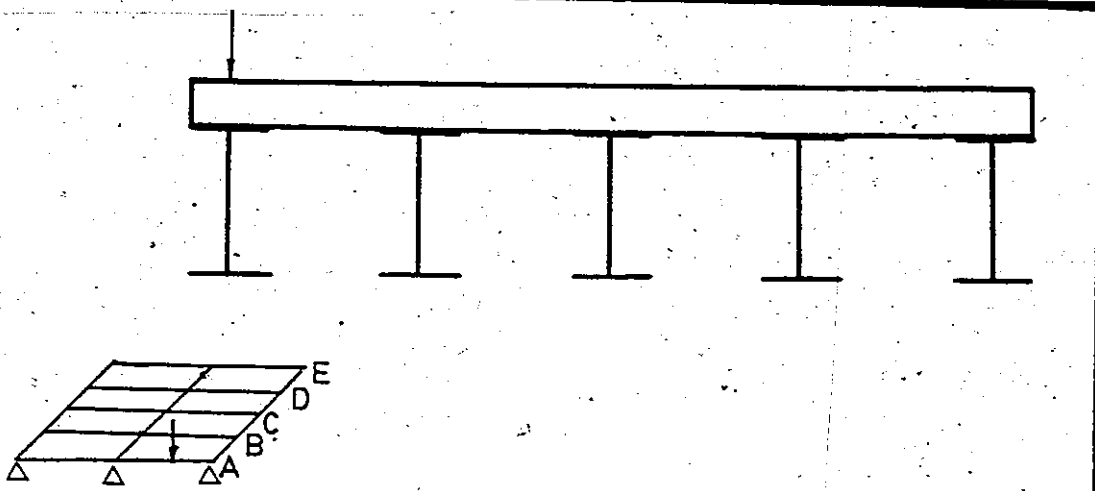
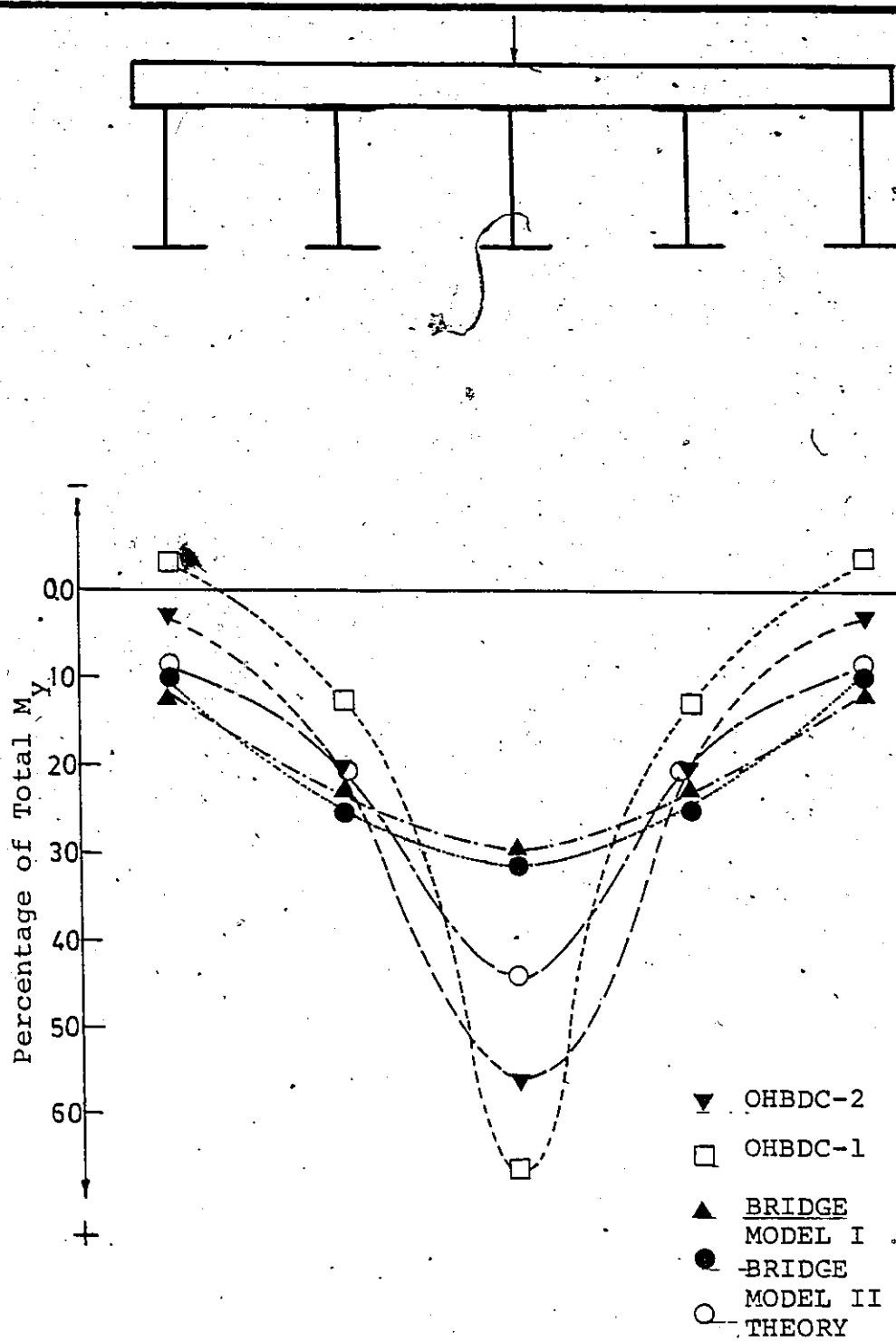FIGURE 6.10   DEFLECTION DISTRIBUTION AT THE MID-
SPAN.
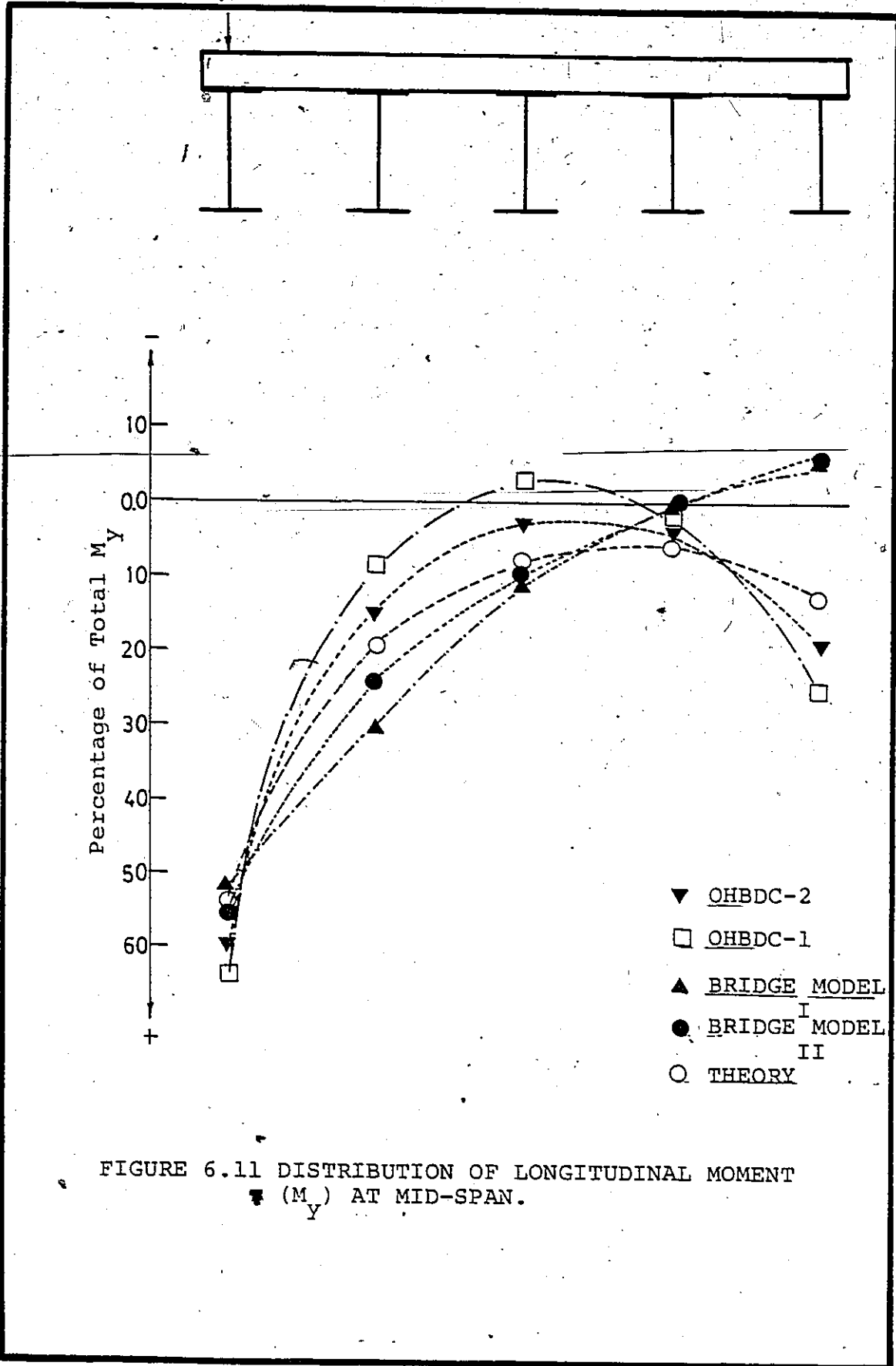
FIGURE 6.11 DISTRIBUTION OF LONGITUDINAL MOMENT
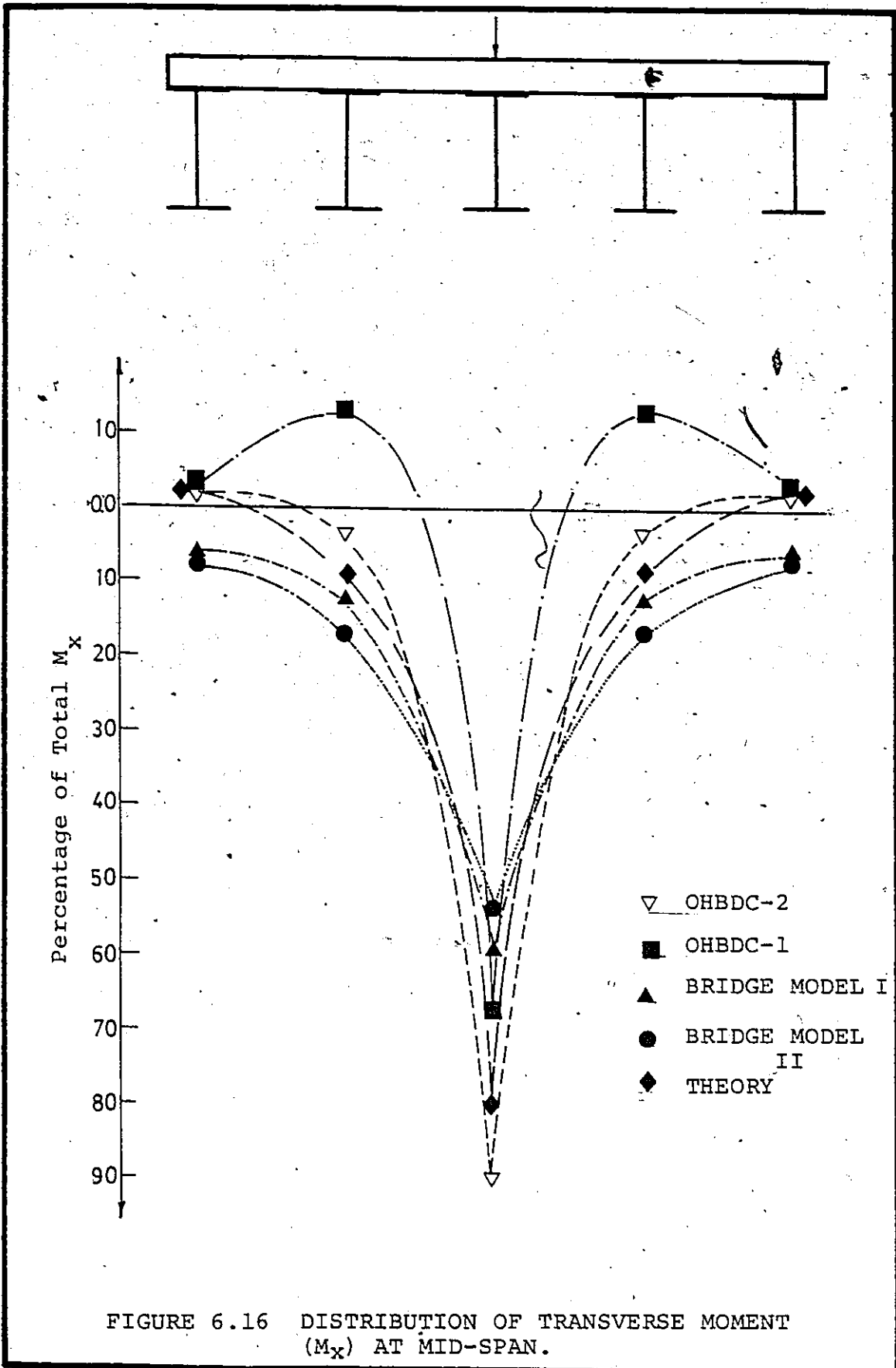(M_y) AT MID-SPAN.
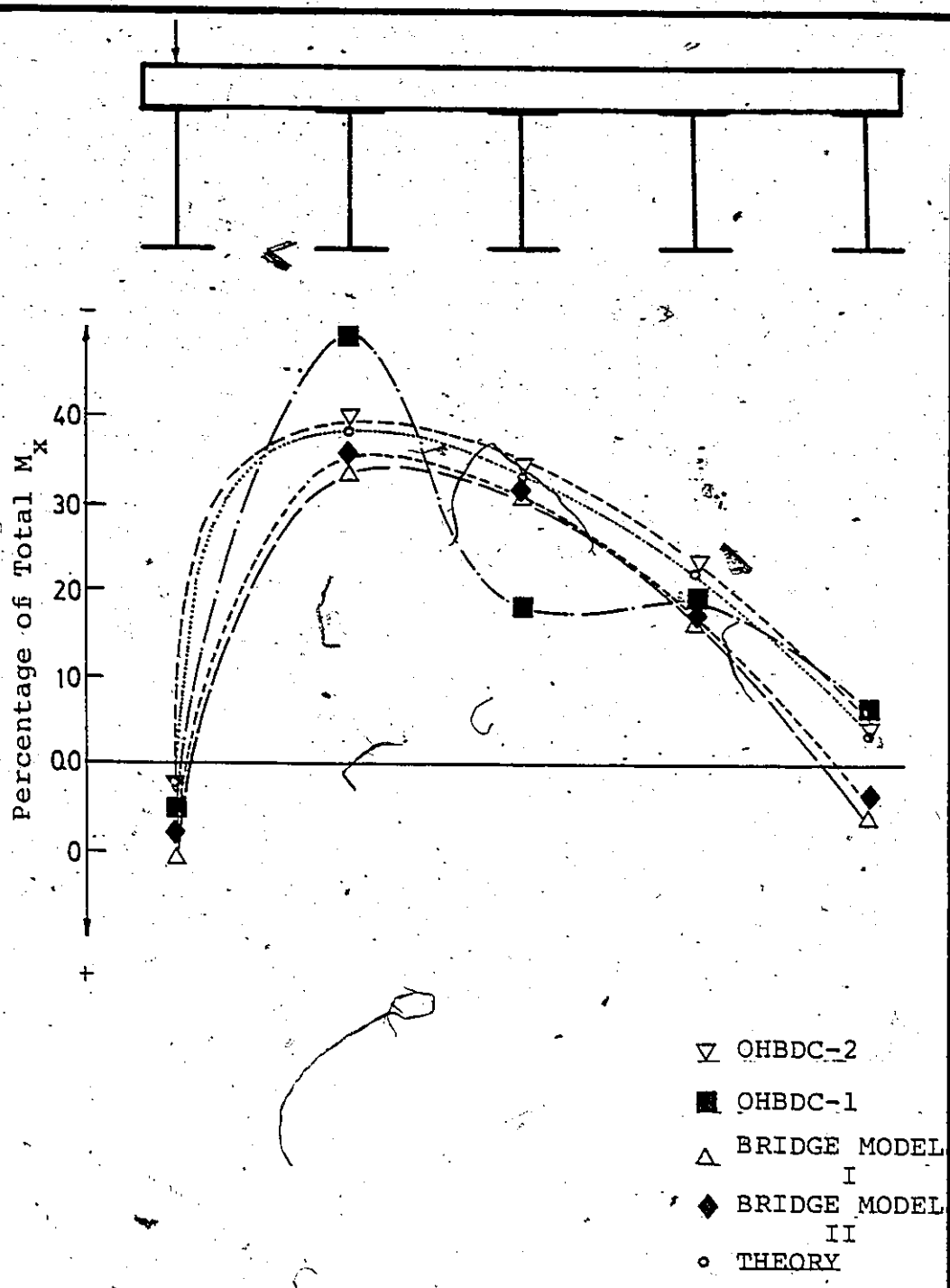
FIGURE 6.12   DISTRIBUTION OF TRANSVERSE MOMENT
(M$_x$) AT MID-SPAN.

FIGURE 6.13 DISTRIBUTION OF LONGITUDINAL MOMENT
(M_y) AT INTERMEDIATE SUPPORT.

FIGURE 6.14   DEFLECTION DISTRIBUTION AT MID-
SPAN.

FIGURE 6.15   DISTRIBUTION OF LONGITUDINAL MOMENT
(M$_y$) AT MID-SPAN.

FIGURE 6.16   DISTRIBUTION OF TRANSVERSE MOMENT
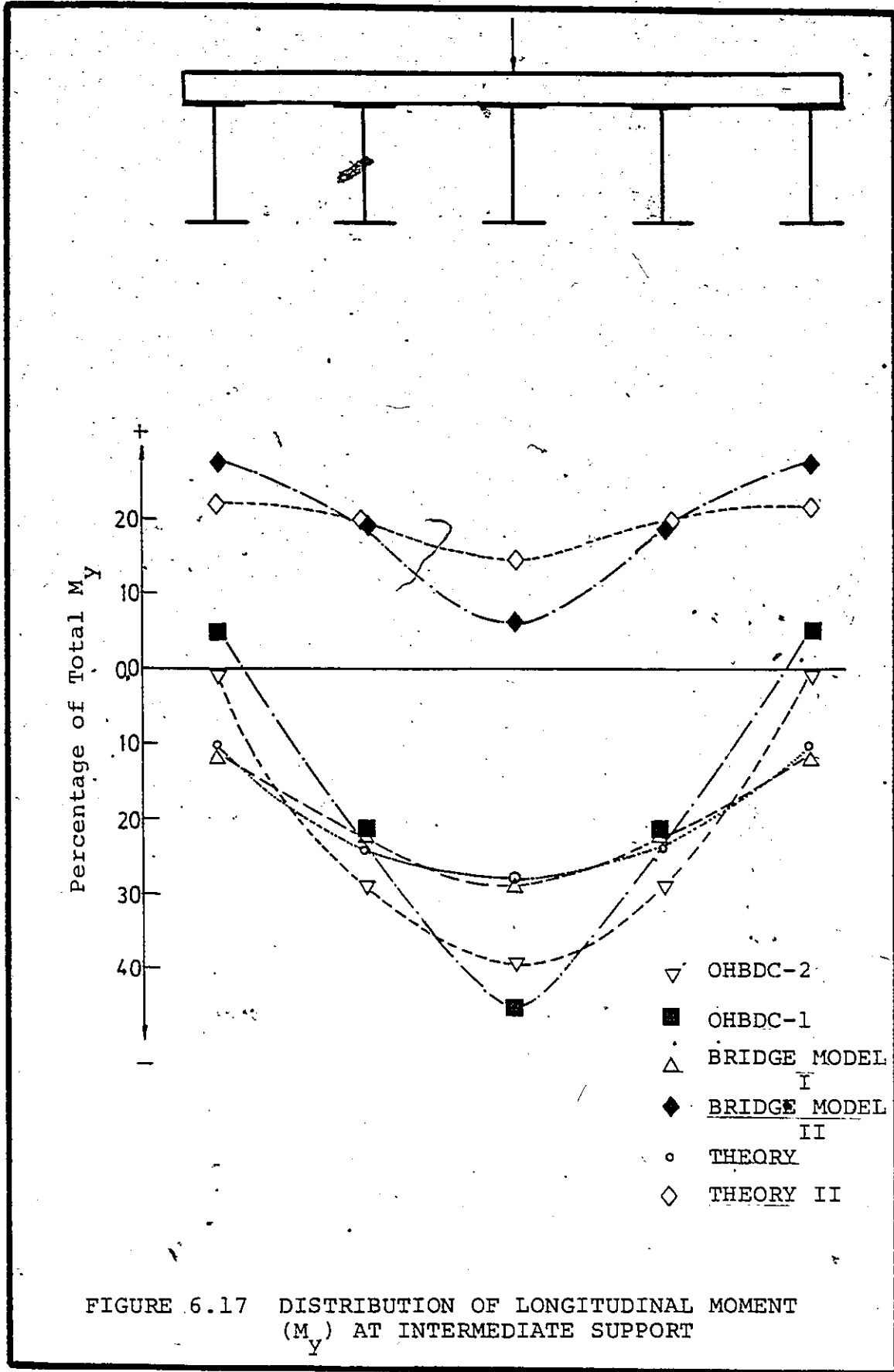(M$_X$) AT MID-SPAN.

FIGURE 6.17   DISTRIBUTION OF LONGITUDINAL MOMENT
(M$_y$) AT INTERMEDIATE SUPPORT
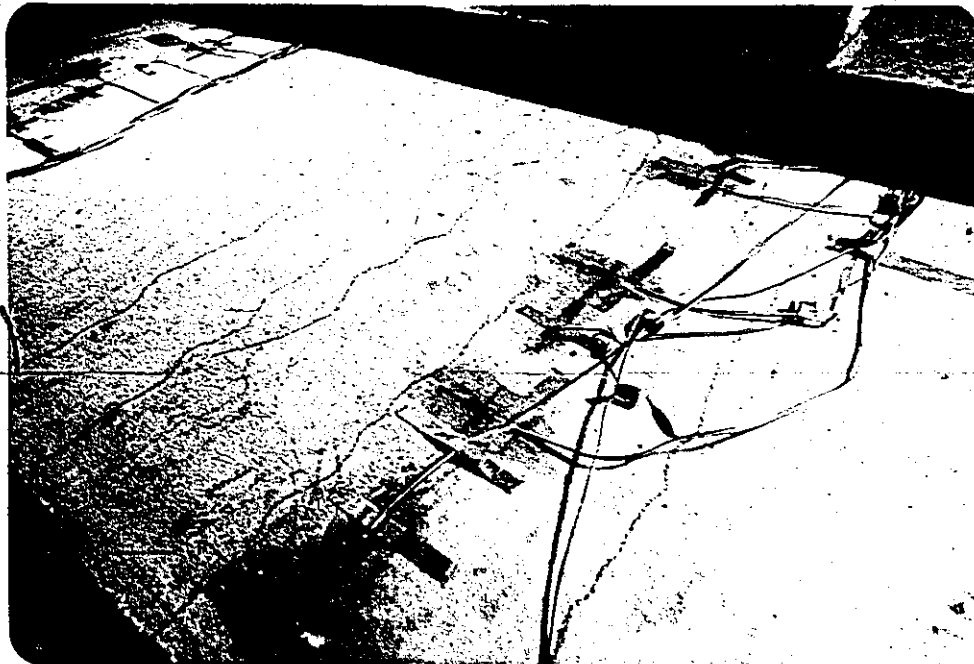
FIGURE 6.18   TRANSVERSE CRACKS AT THE INTERMEDIATE
              SUPPORT ON THE RIGHT SIDE OF LOADED
              BEAM, BRIDGE MODEL (I), (AT LOAD OF
              50 KIPS)

FIGURE 6.19   TRANSVERSE CRACKS AT THE INTERMEDIATE
              SUPPORT ON THE LEFT SIDE OF LOADED
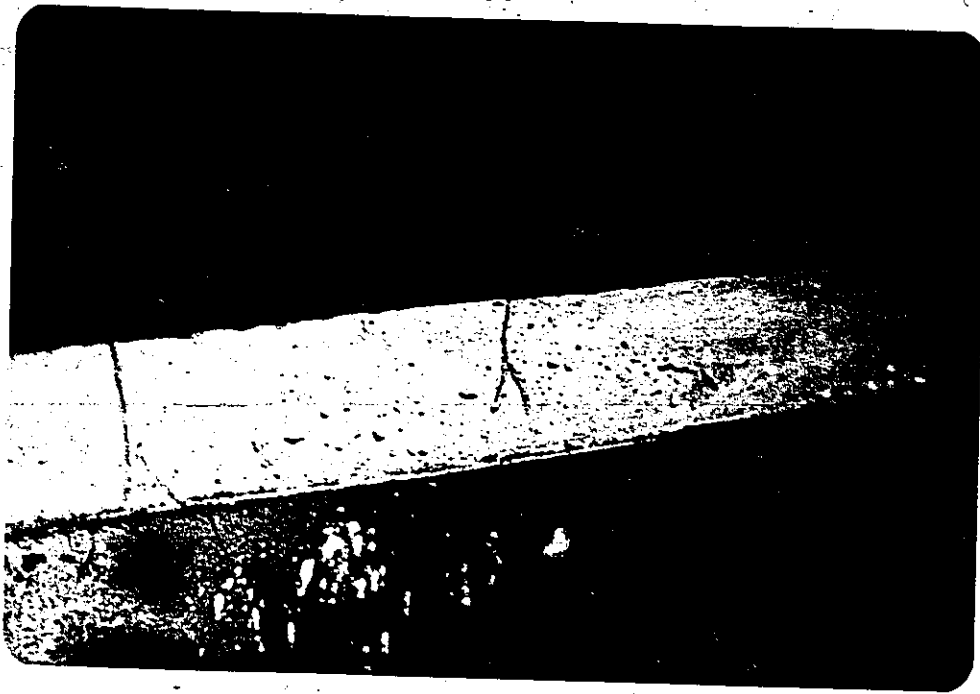   BEAM, BRIDGE MODEL (I), (AT LOAD OF
              50 KIPS).

FIGURE 6.20 DEPTH OF TRANSVERSE CRACK ON THE RIGHT
            SIDE OF THE SLAB OF BRIDGE MODEL (I),
            AT LOAD OF (50 KIPS).

FIGURE 6.21 TRANSVERSE CRACK AT THE INTERMEDIATE
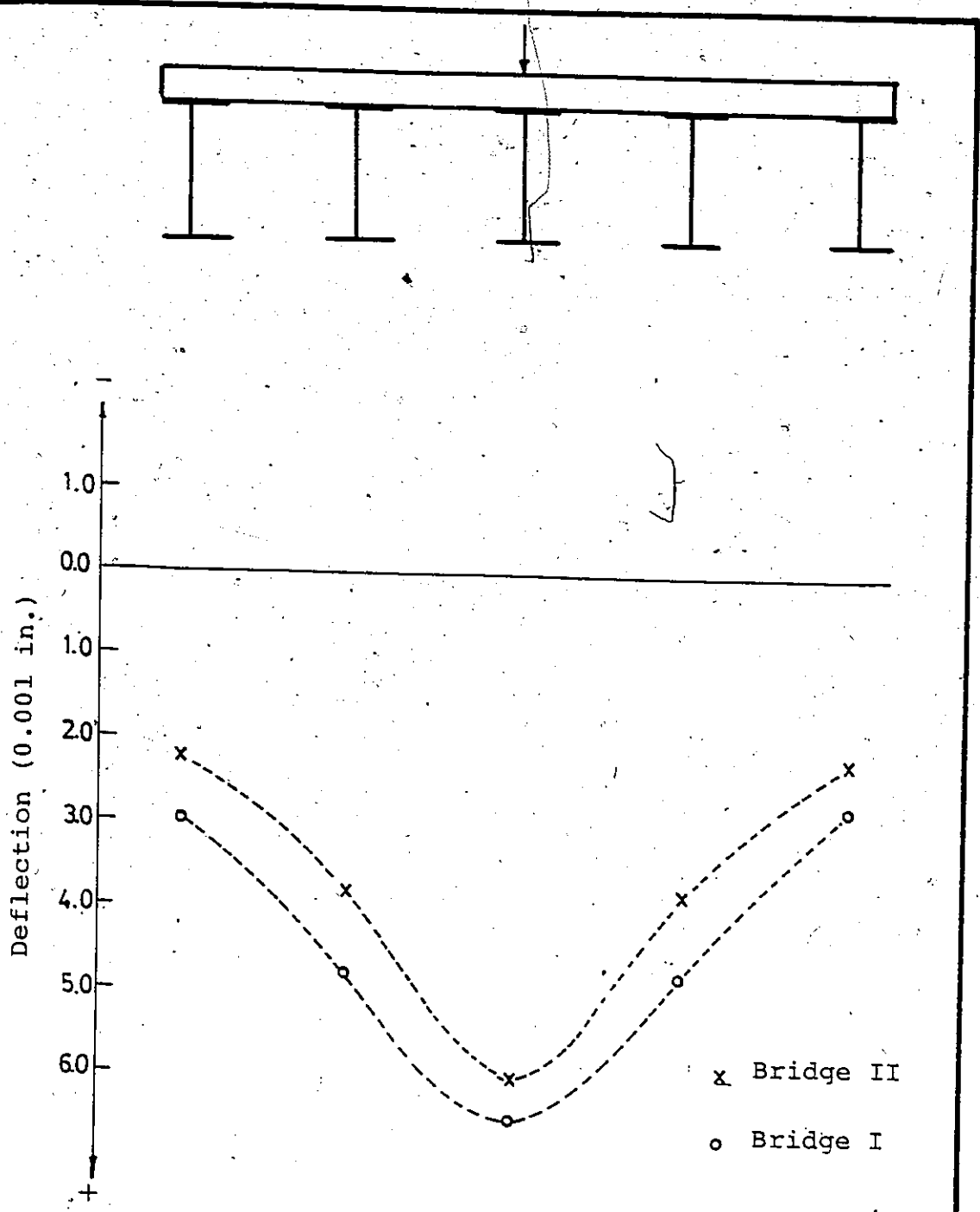   SUPPORT, BRIDGE MODEL (II), AT LOAD
            OF (180KIPS).

FIGURE 6.22   DEFLECTION DISTRIBUTION AT MID SPAN
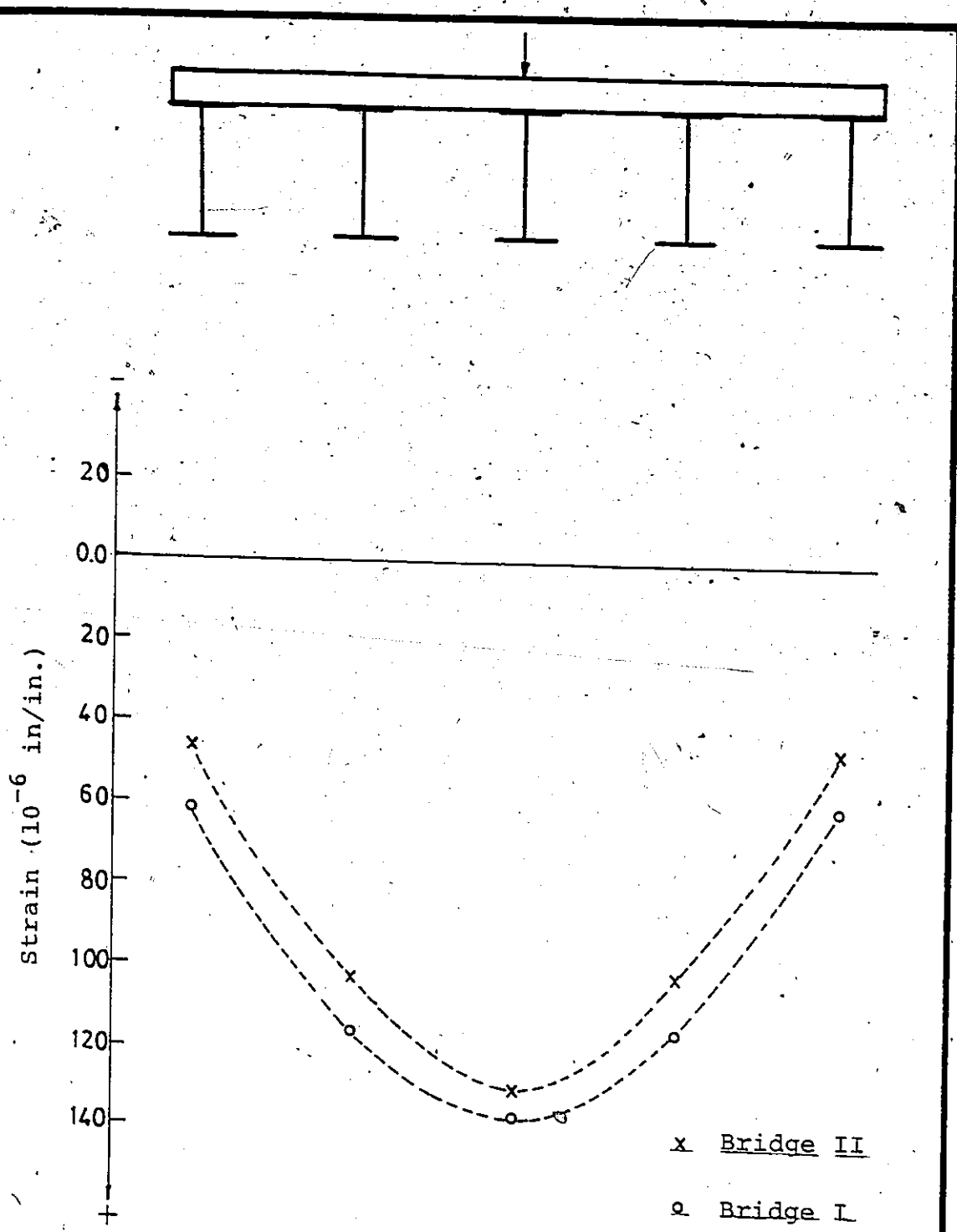UNDER WORKING LOAD.
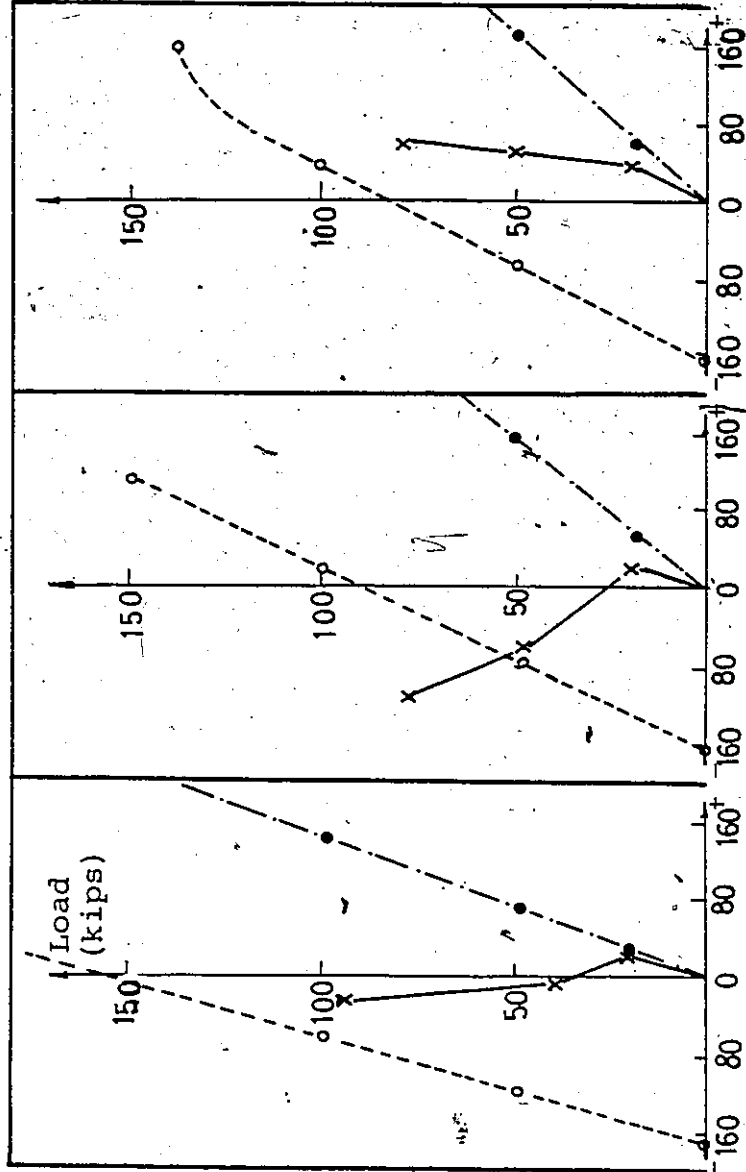
FIGURE 6.23   DISTRIBUTION OF LONGITUDINAL STRAIN
AT THE BOTTOM FACE OF THE STEEL
GIRDER UNDER THE WORKING LOAD AT
MID-SPAN.
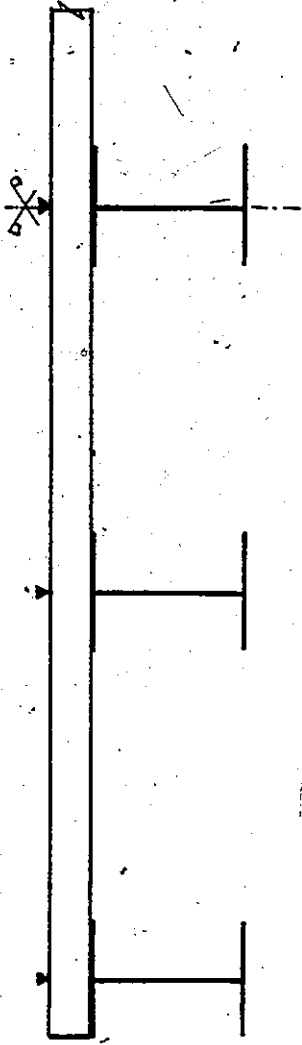
FIGURE 6.24   LONGITUDINAL STRAIN DISTRIBUTION, AT THE INTERMEDIATE SUPPORT
FOR EACH GIRDER (DUE TO TWO POINTS LOAD).

STRAIN
10-6in/in.

o   Bridge II

•   Theory

x   Bridge I

CROSS-SECTION

ELEVATION

PLAN
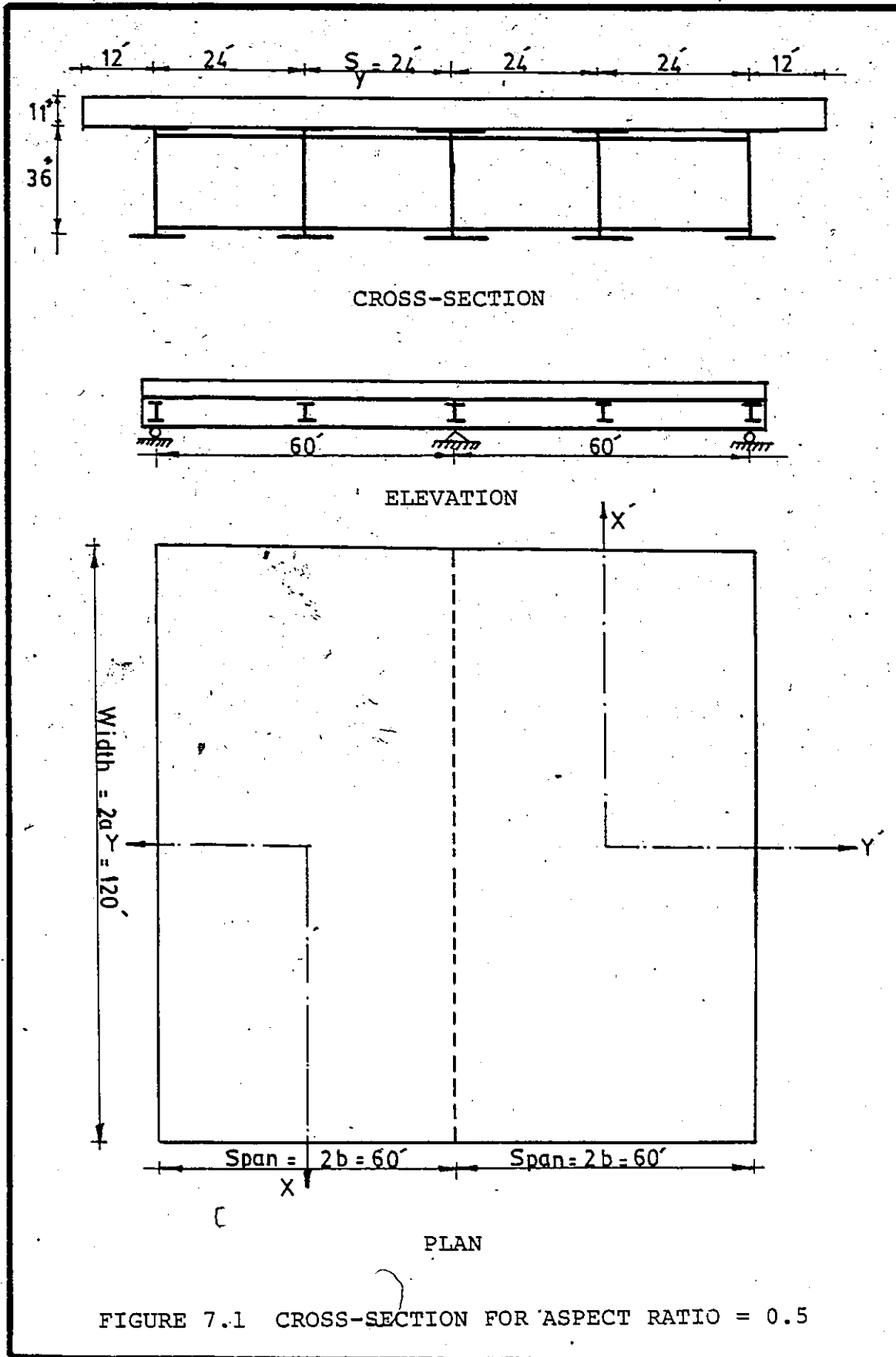
FIGURE 7.1 CROSS-SECTION FOR ASPECT RATIO = 0.5

104
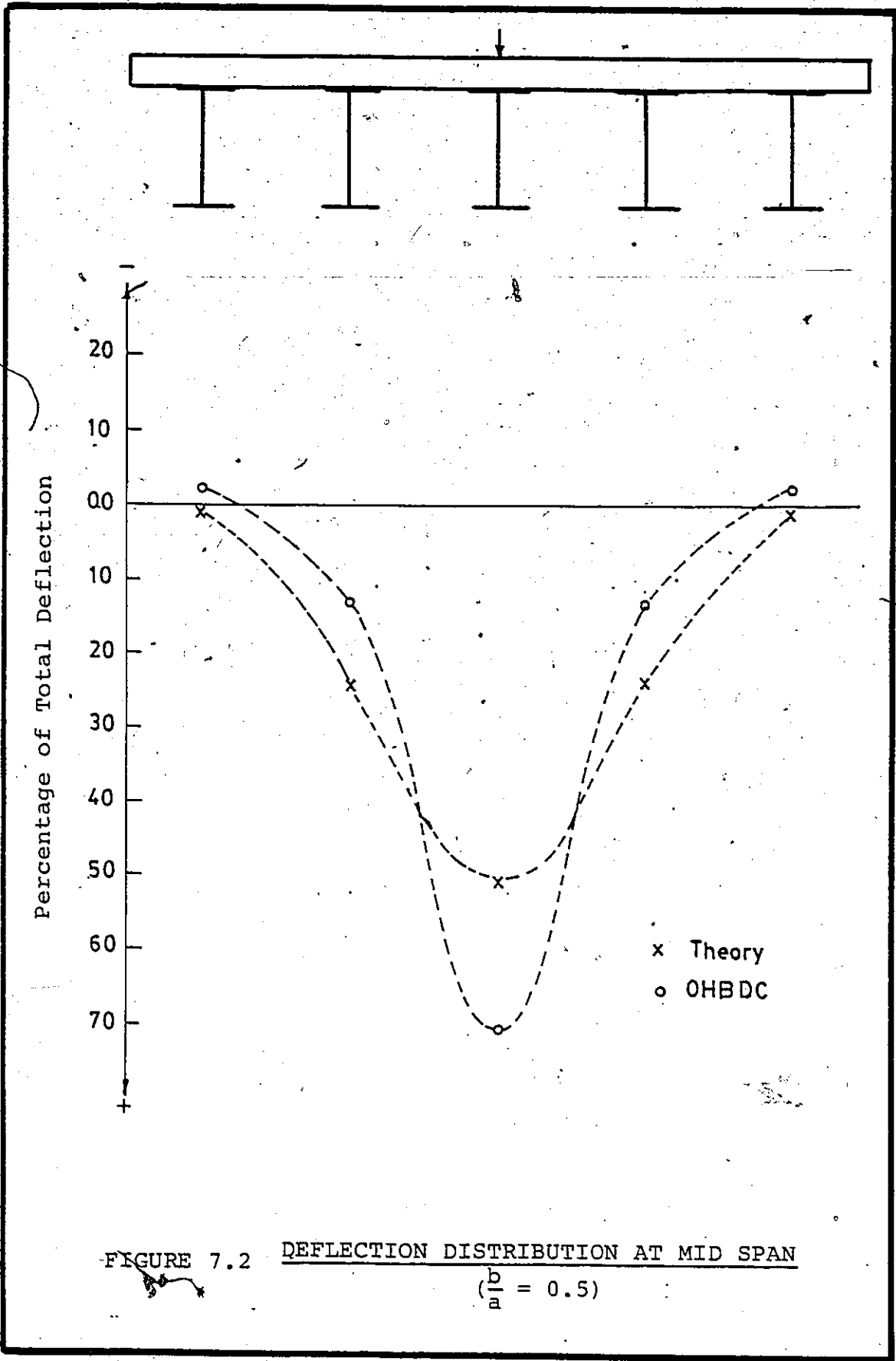
FIGURE 7.2   DEFLECTION DISTRIBUTION AT MID SPAN
$(\frac{b}{a} = 0.5)$
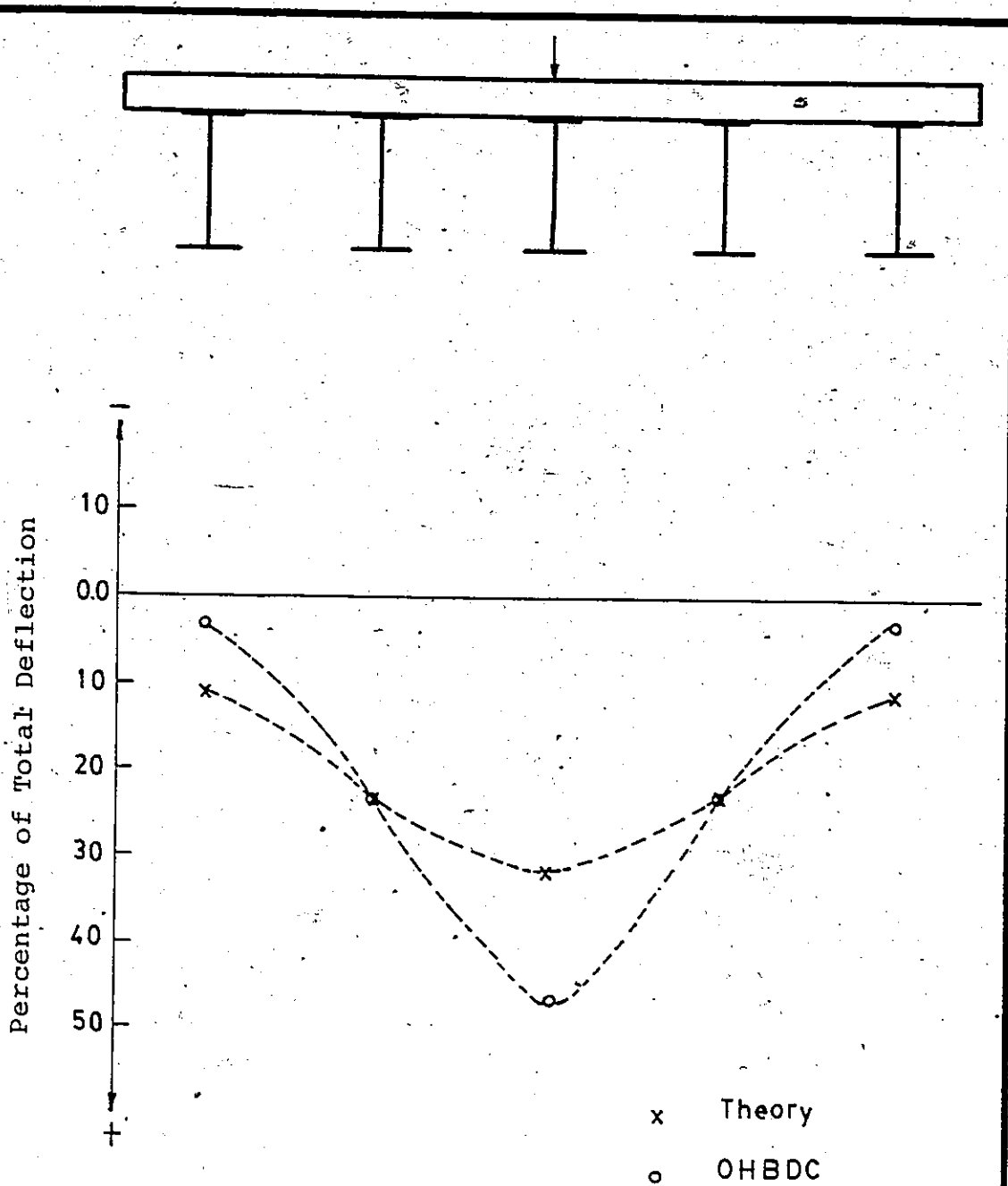
FIGURE 7.3   DEFLECTION DISTRIBUTION AT MID SPAN

$(\frac{b}{a} = 1.0)$
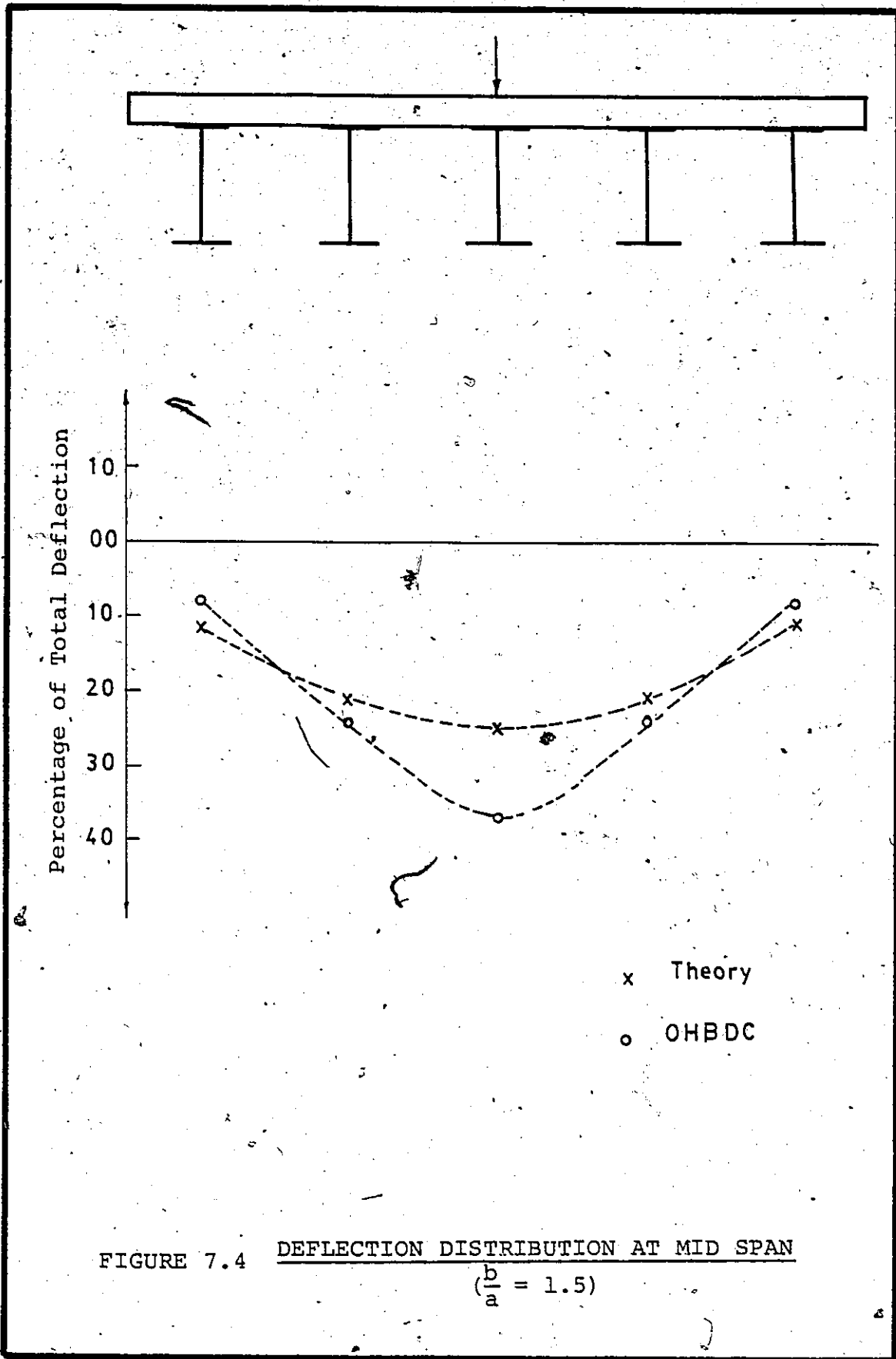
FIGURE 7.4 DEFLECTION DISTRIBUTION AT MID SPAN
$(\frac{b}{a} = 1.5)$
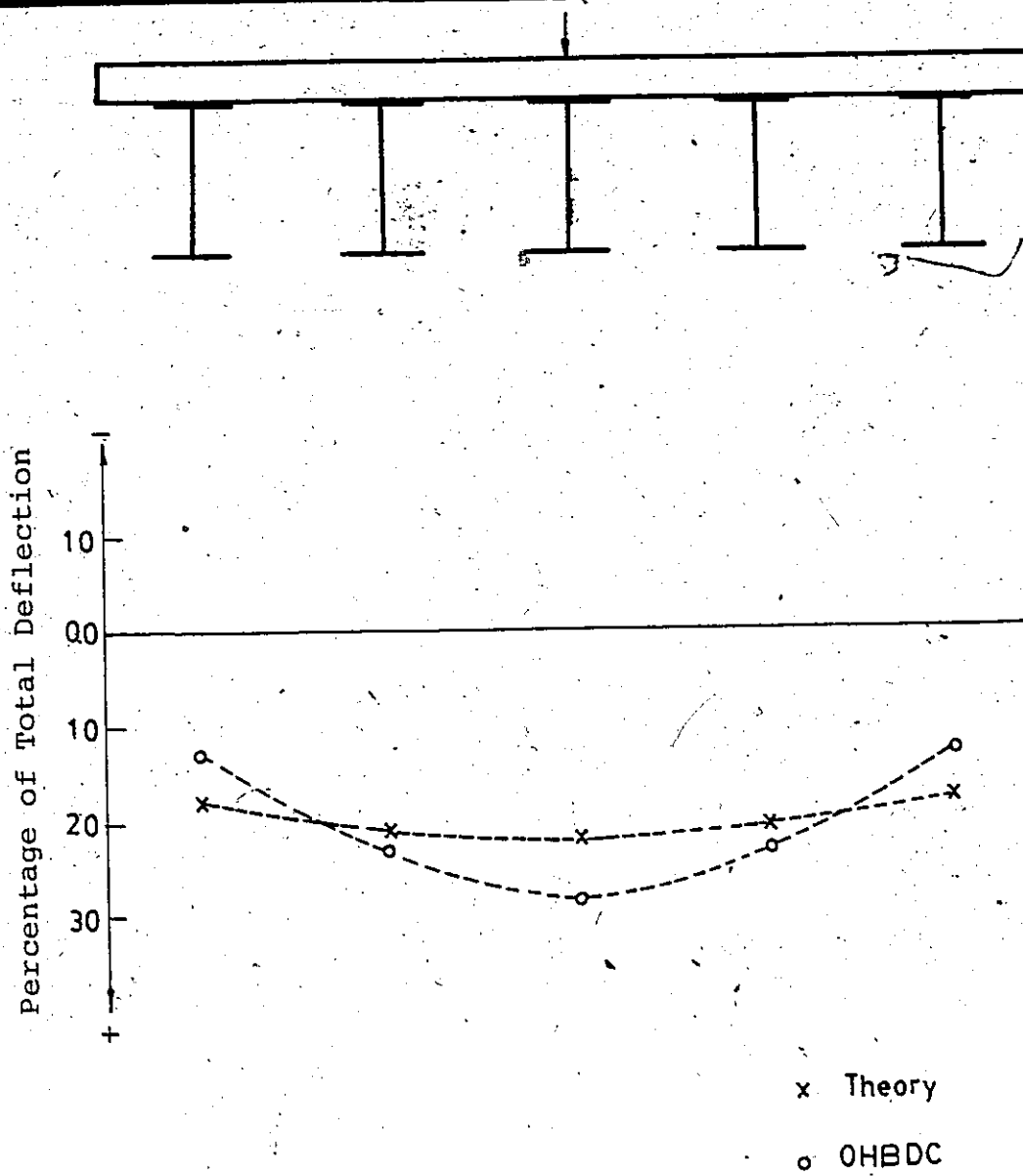
FIGURE 7.5   <u>DEFLECTION DISTRIBUTION AT MID SPAN</u>
$(\frac{b}{a} = 2.0)$

FIGURE 7.6   <u>DISTRIBUTION OF LONGITUDINAL MOMENT AT MID SPAN</u>

$(\frac{b}{a} = 0.5)$
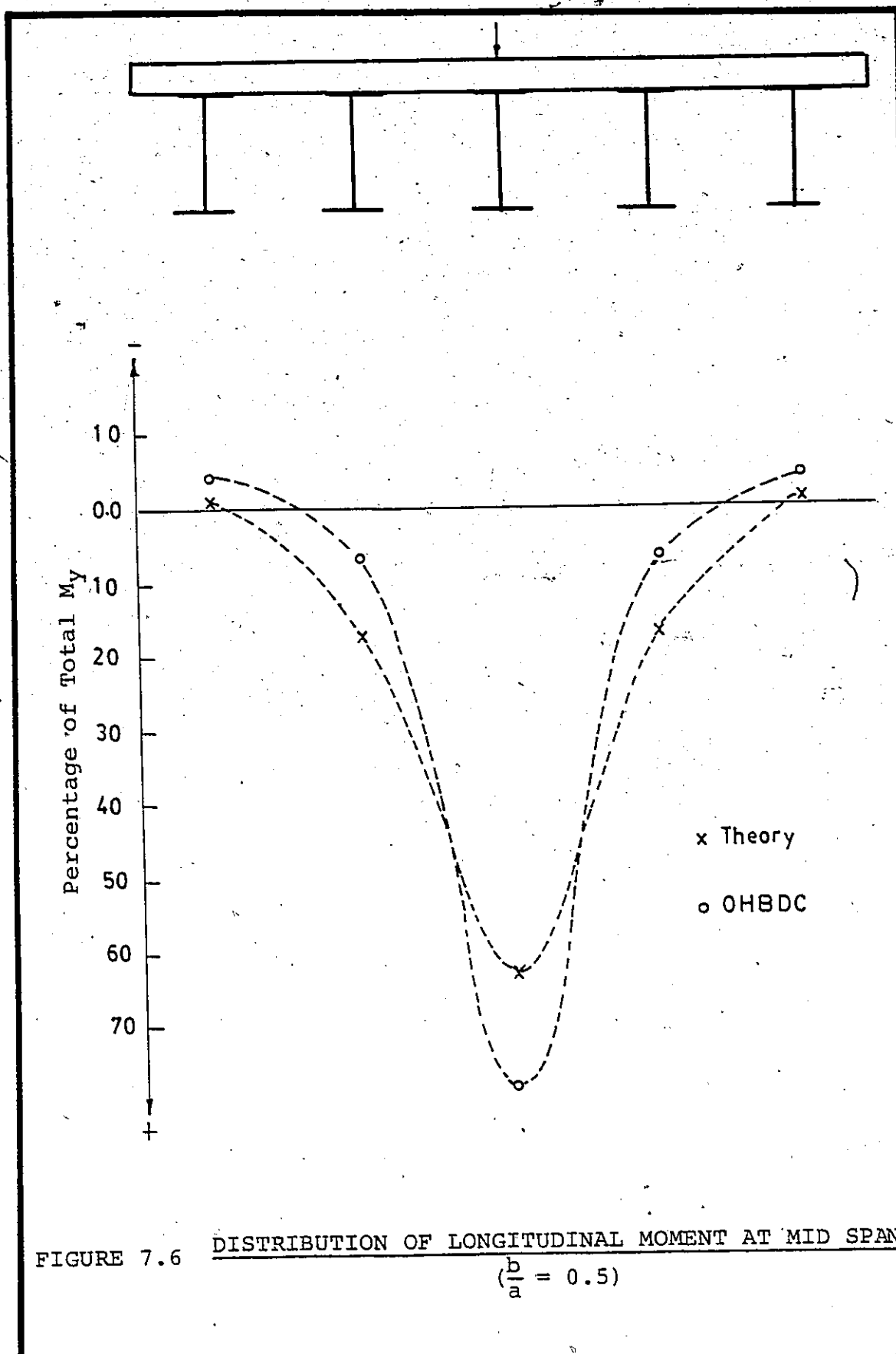
FIGURE 7.7   DISTRIBUTION OF LONGITUDINAL MOMENT AT MID SPAN
$$\left(\frac{b}{a} = 1.0\right)$$

FIGURE 7.8   DISTRIBUTION OF LONGITUDINAL MOMENT AT MID SPAN
$(\frac{b}{a} = 1.5)$
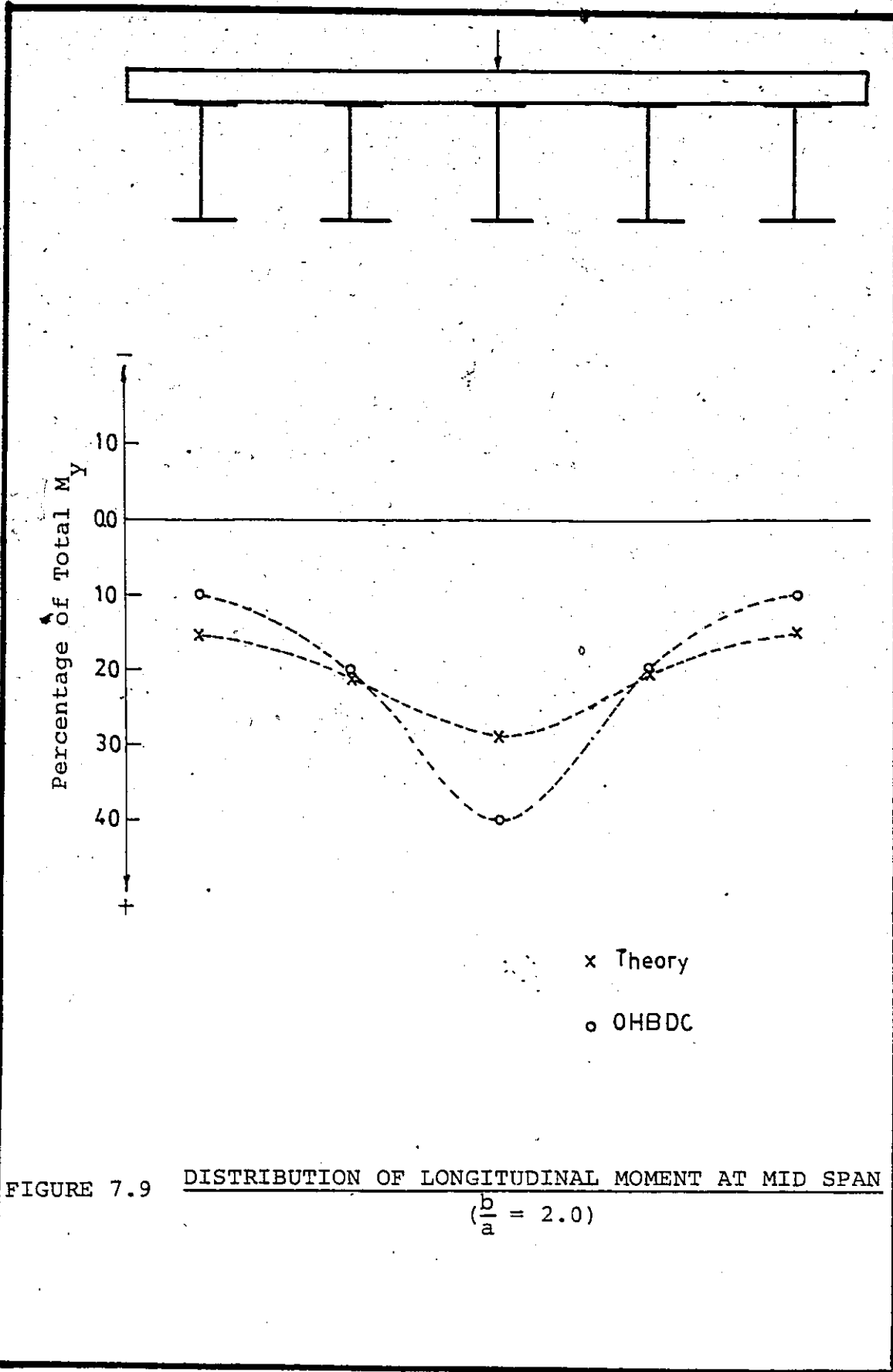
FIGURE 7.9   DISTRIBUTION OF LONGITUDINAL MOMENT AT MID SPAN
$(\frac{b}{a} = 2.0)$

FIGURE 7.10   DISTRIBUTION OF TRANSVERSE MOMENT AT MID SPAN
$(\frac{b}{a} = 0.5)$
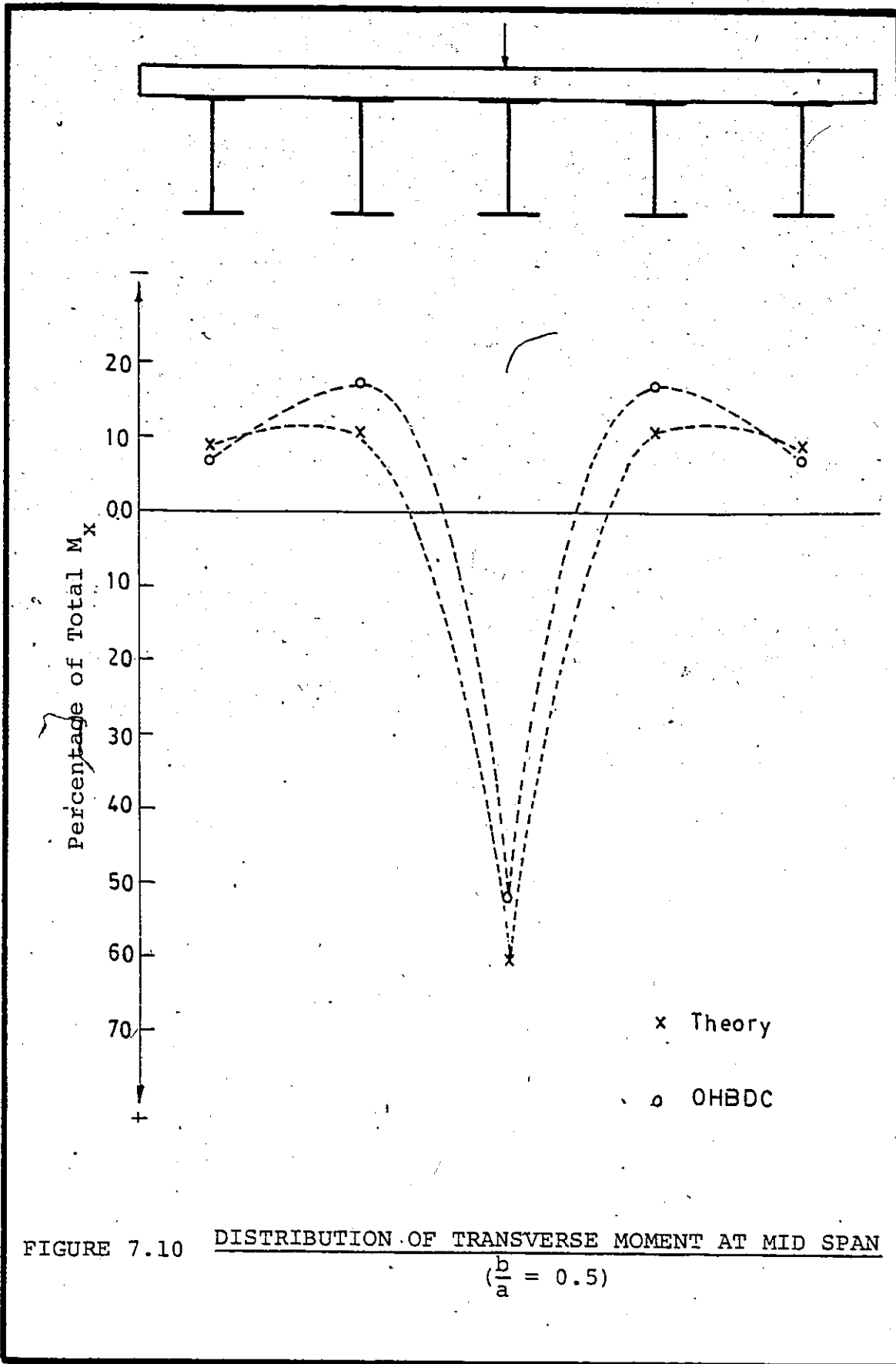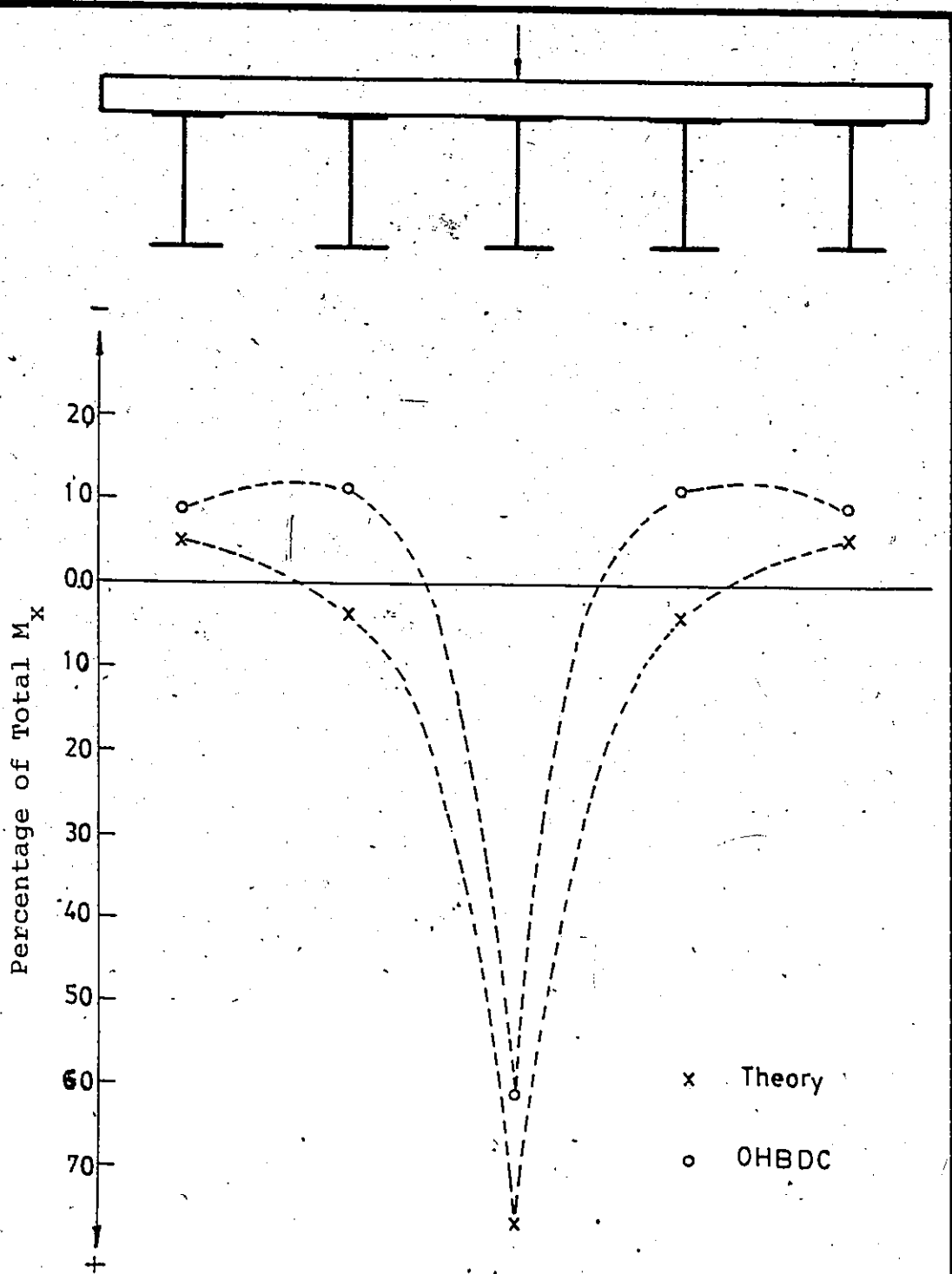
FIGURE 7.11   DISTRIBUTION OF TRANSVERSE MOMENT AT MID SPAN
$(\frac{b}{a} = 1.0)$
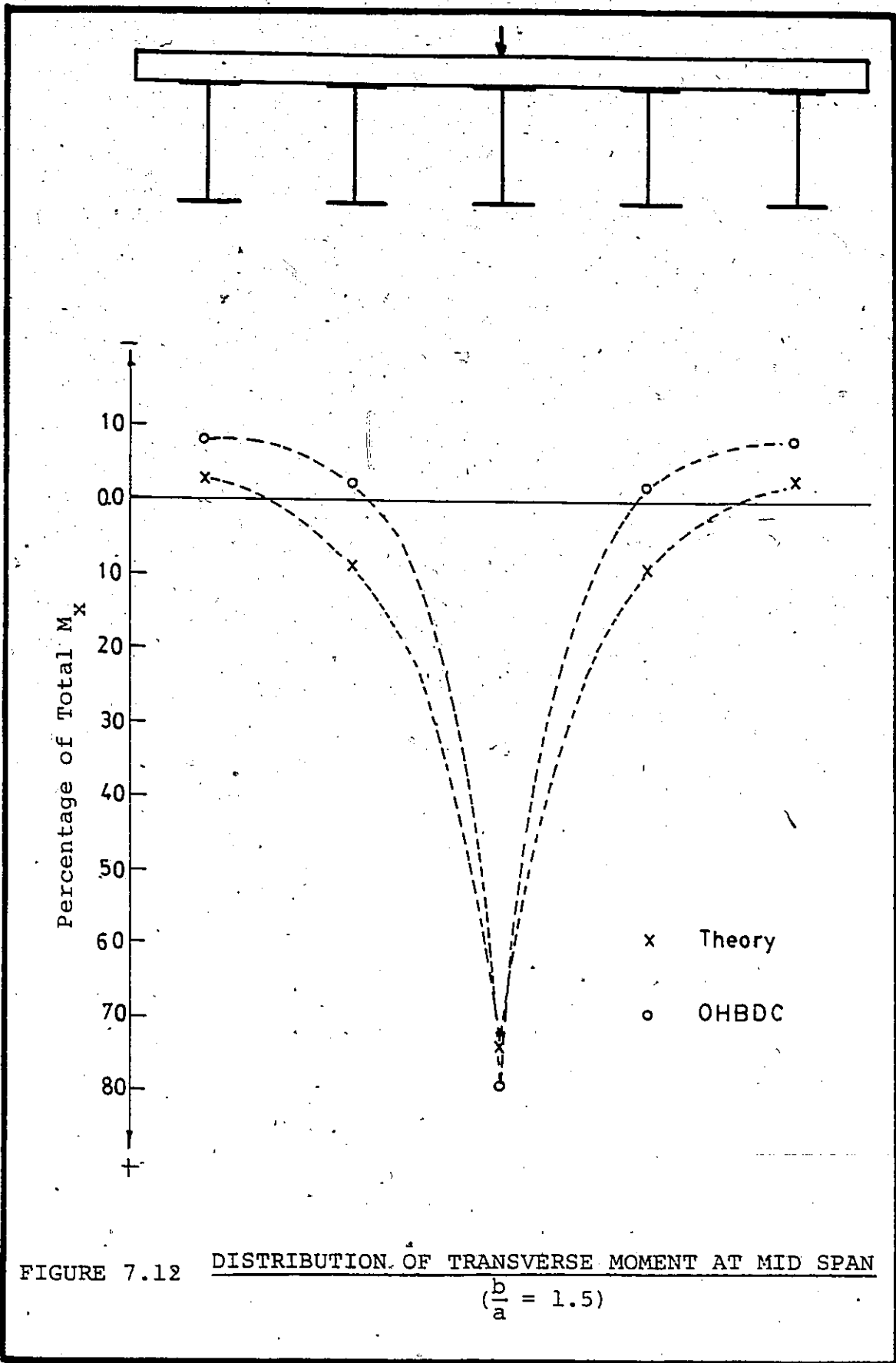
FIGURE 7.12   DISTRIBUTION OF TRANSVERSE MOMENT AT MID SPAN
$(\frac{b}{a} = 1.5)$

Percentage of Total M_x

x Theory

o OHBDC
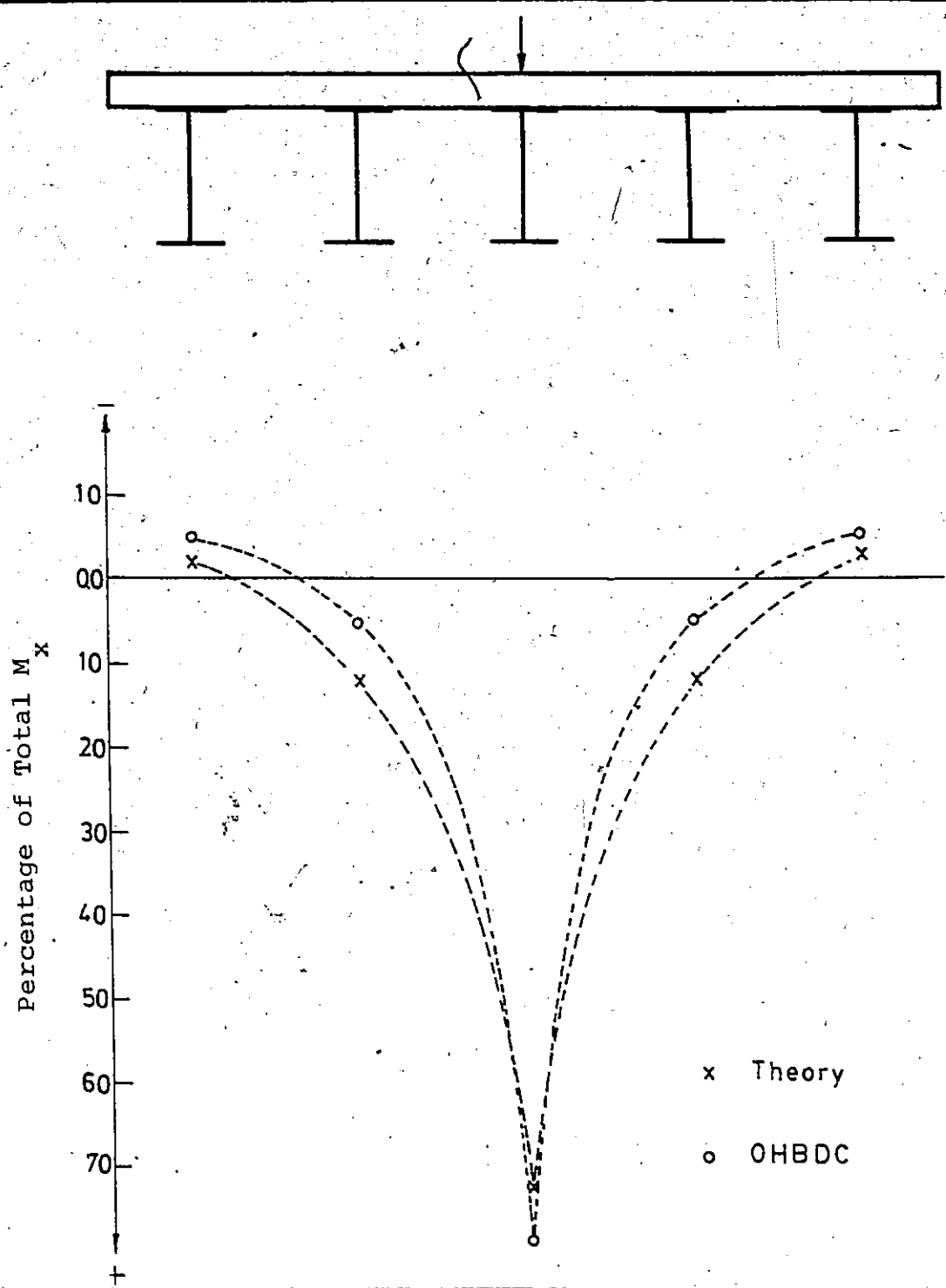
FIGURE 7.13   DISTRIBUTION OF TRANSVERSE MOMENT AT MID SPAN
$(\frac{b}{a} = 2.0)$
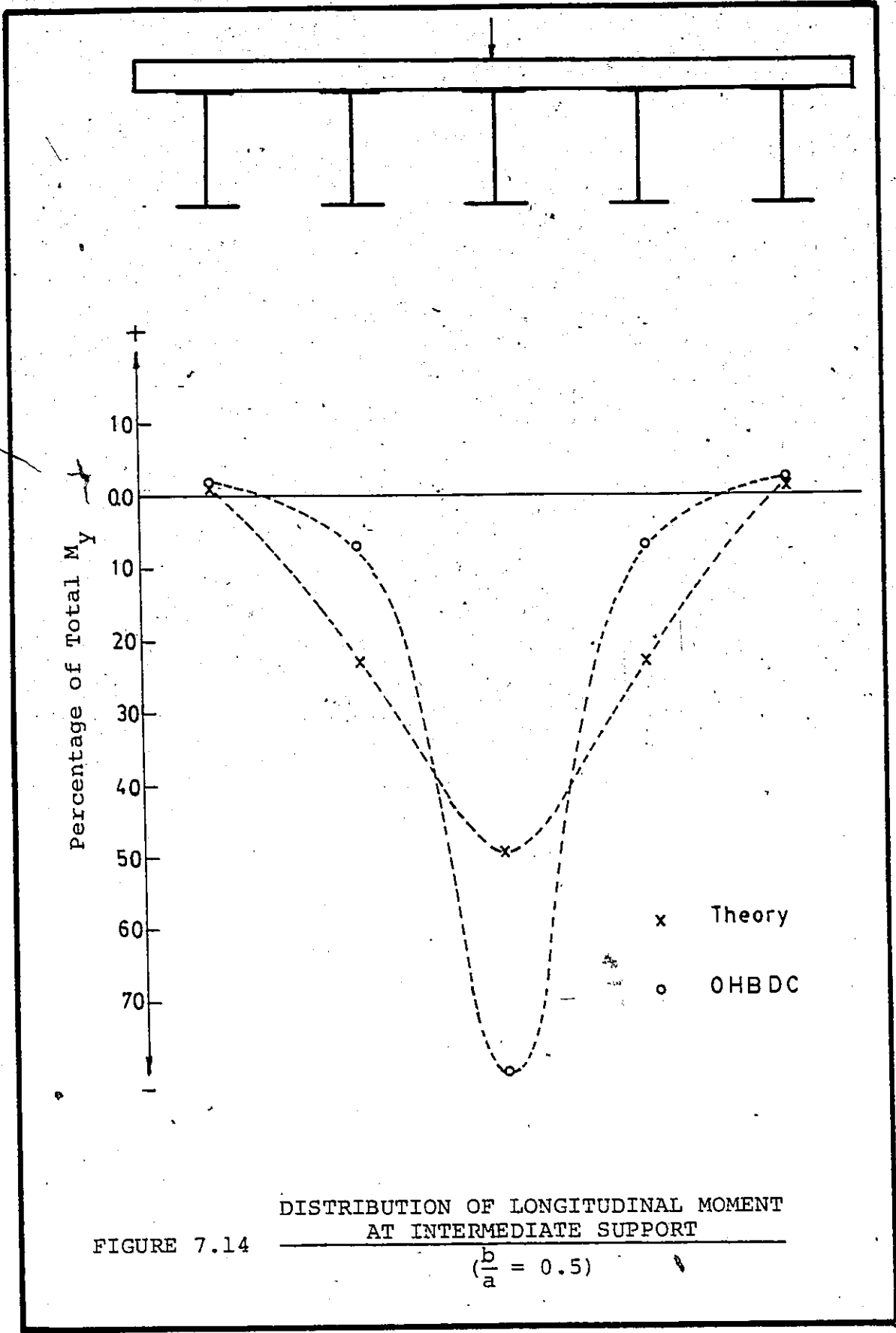
DISTRIBUTION OF LONGITUDINAL MOMENT
AT INTERMEDIATE SUPPORT
$(\frac{b}{a} = 0.5)$
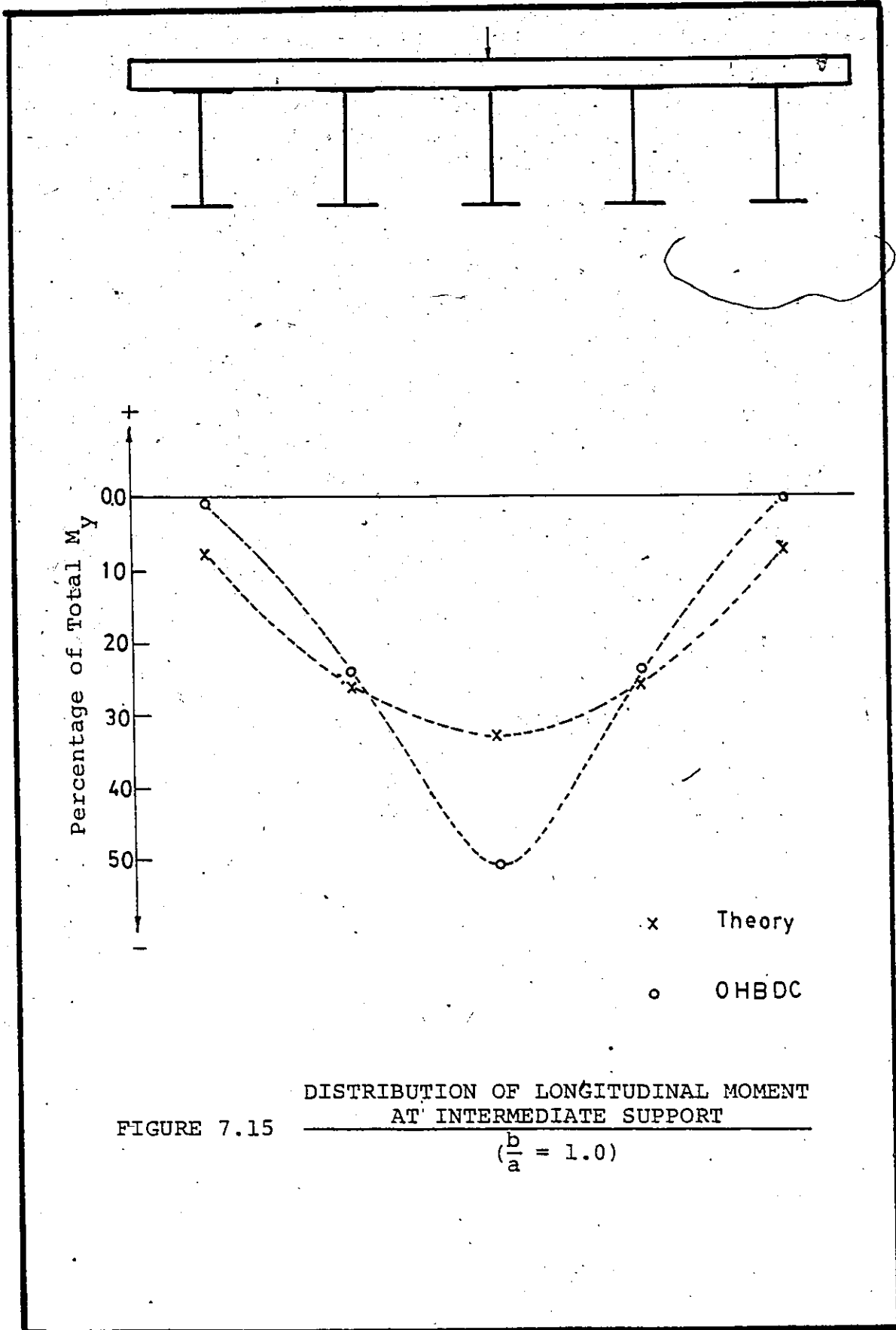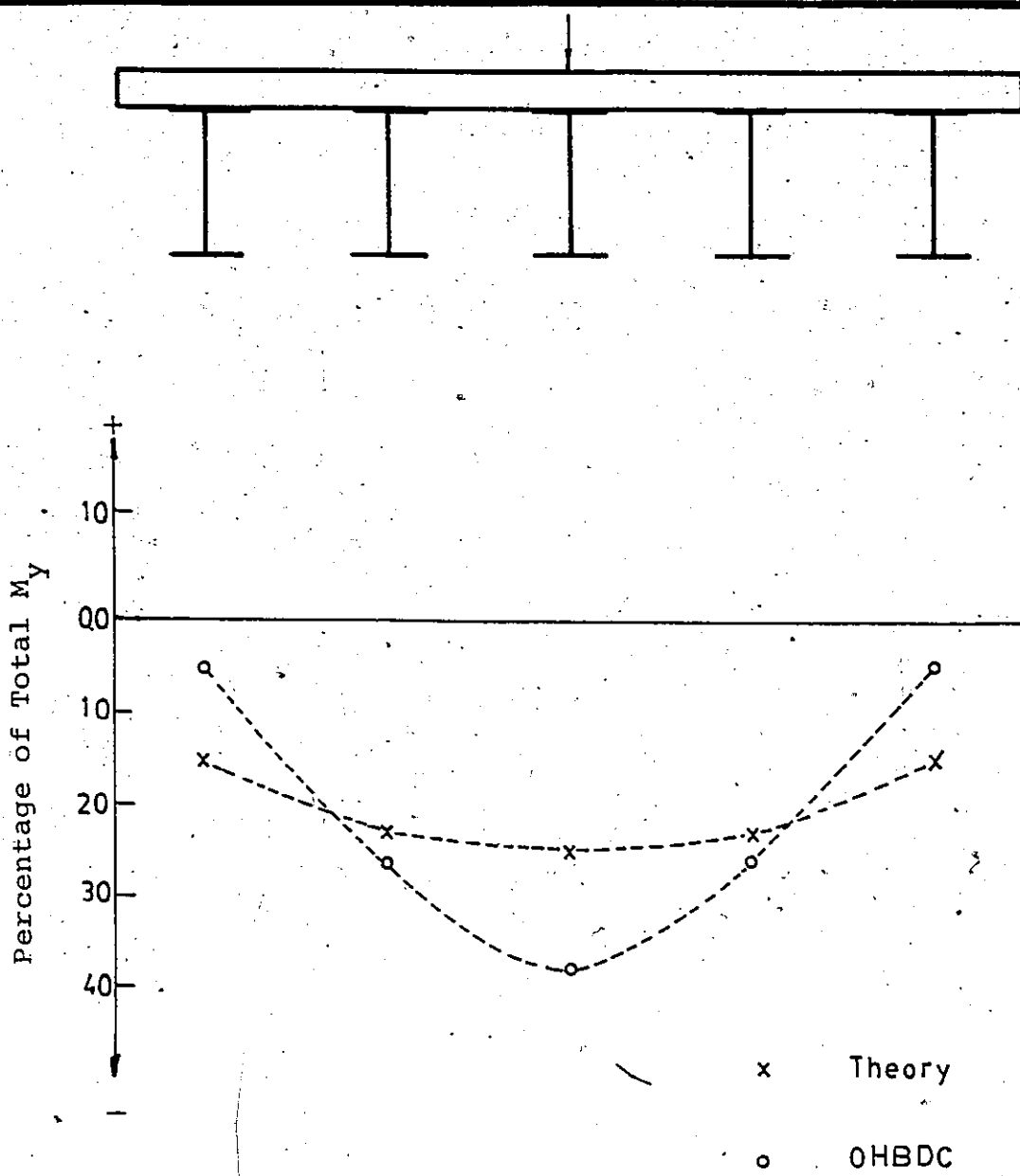
FIGURE 7.14

FIGURE 7.15   DISTRIBUTION OF LONGITUDINAL MOMENT AT INTERMEDIATE SUPPORT $(\frac{b}{a} = 1.0)$
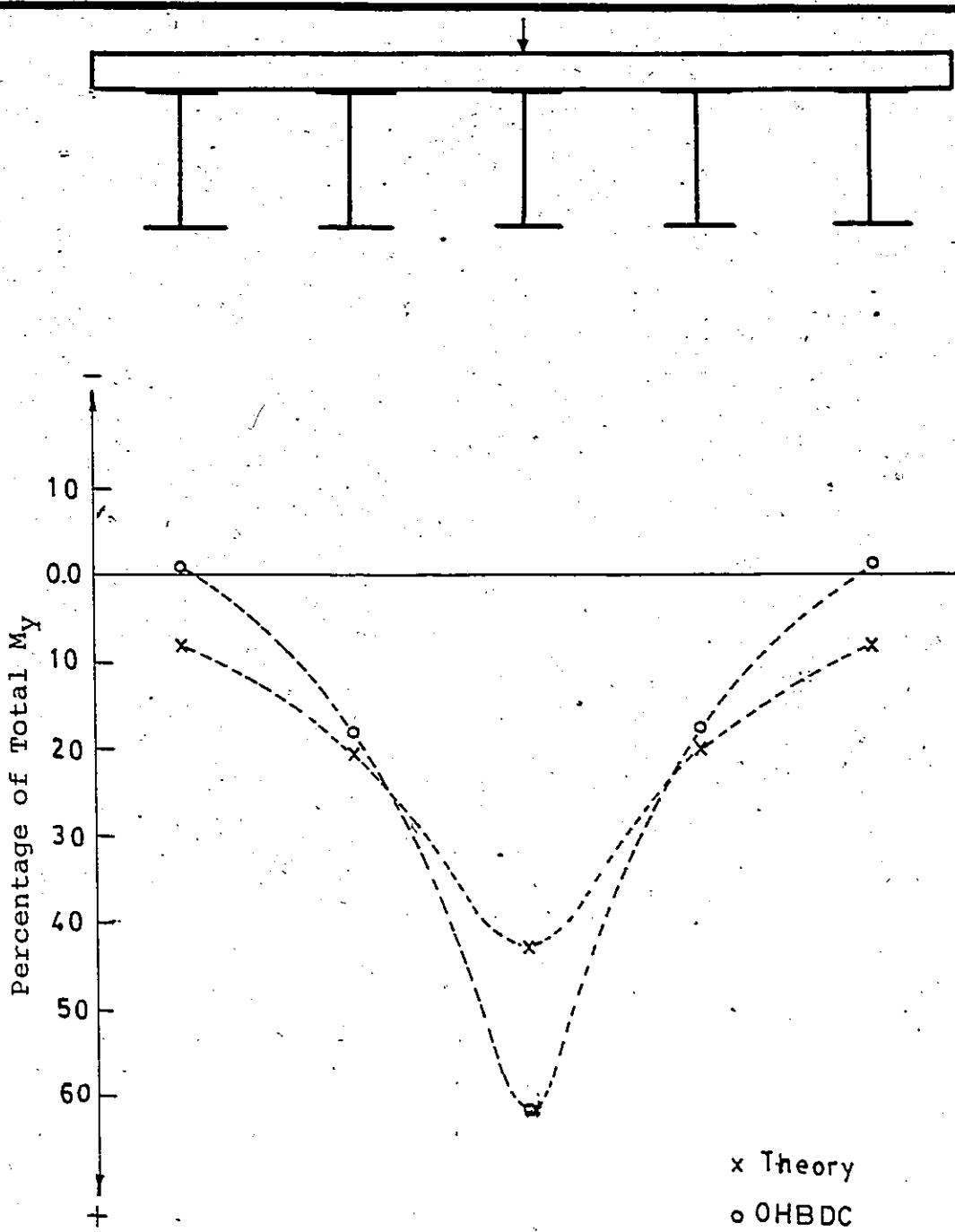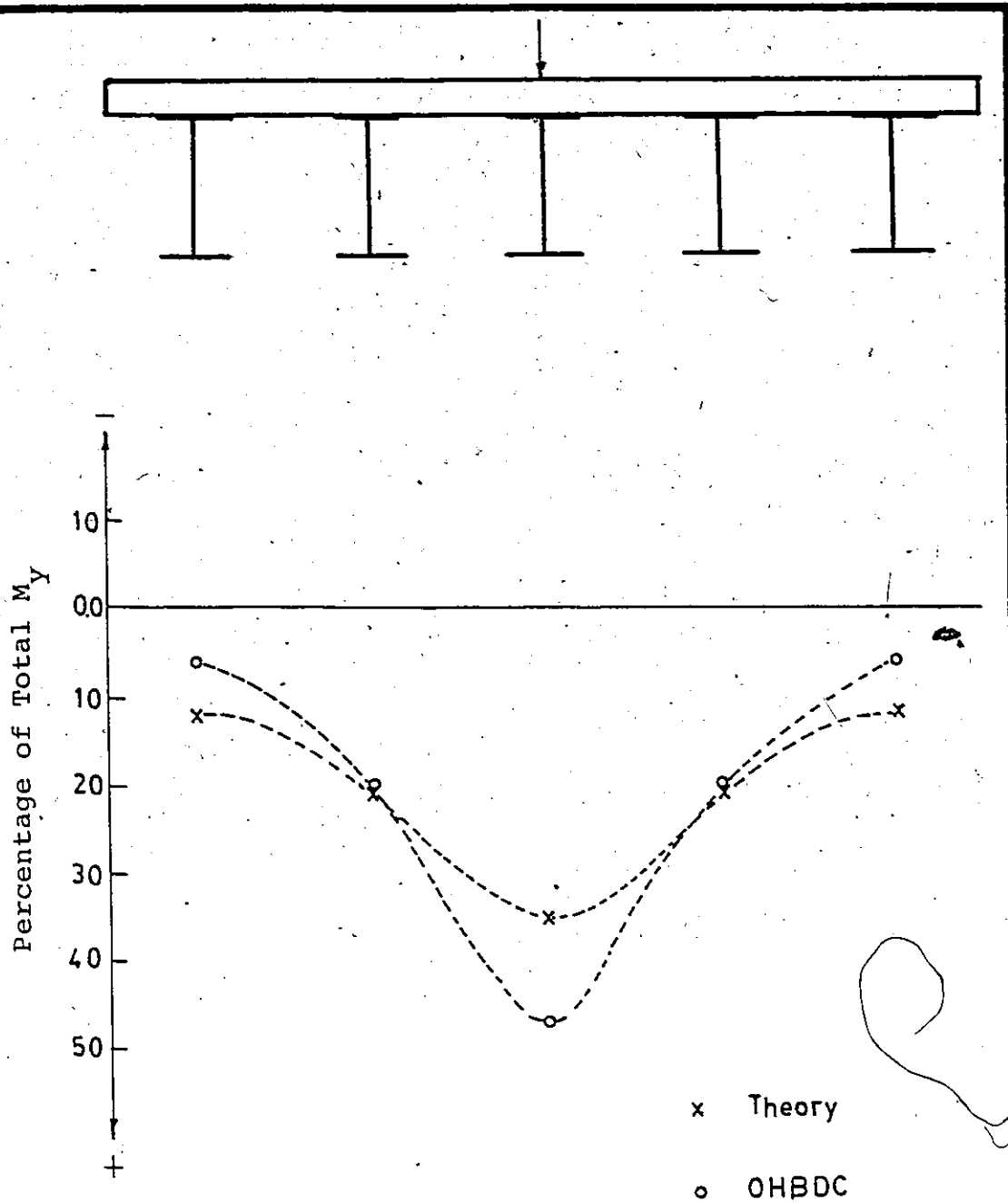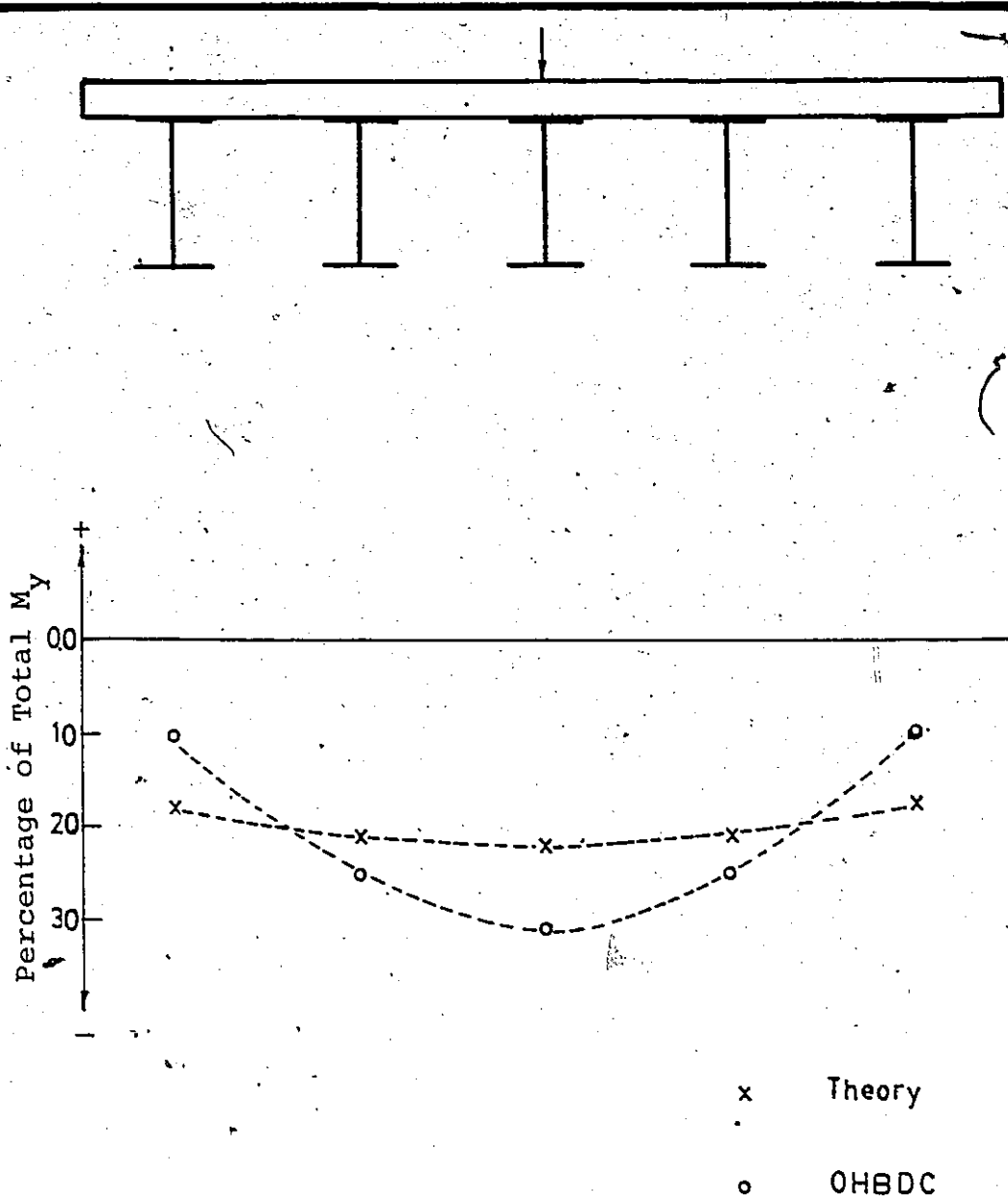
FIGURE 7.16   DISTRIBUTION OF LONGITUDINAL MOMENT
AT INTERMEDIATE SUPPORT
$(\frac{b}{a} = 1.5)$

FIGURE 7.17

DISTRIBUTION OF LONGITUDINAL MOMENT
AT INTERMEDIATE SUPPORT
$(\frac{b}{a} = 2.0)$

APPENDICES

Expressions For Matrix Elements

$A_1 = 2K_1K_2$

$A_2 = K_1^2 - K_2^2$

$A_3 = K_1(K_1^2 - 3K_2^2)$

$A_4 = K_2(3K_1^2 - K_2^2)$

$A_5 = -EI(A_2^2 - A_1^2)x_1^4$

$A_6 = 2EIx_1^4 A_1 A_2$

$A_7 = D_y$

$A_8 = -D_y x_1^2 A_2$

$A_9 = -D_y x_1^2 A_1$

$A_{10} = D_x A_3 - (D_1 + D_{xy} + D_{yx})K_1$

$A_{11} = -D_x A_4 + (D_1 + D_{xy} + D_{yx})K_2$

$A_{12} = -x_1(D_1 + D_{xy} + D_{yx})A_1$

$A_{13} = D_x - x_1^2(D_1 + D_{xy} + D_{yx})A_2$

$A_{14} = D_x A_2 - D_1$

$A_{15} = -D_x A_1$

$A_{16} = GJK_2$

$A_{17} = -D_x + D_1 x_1^2 A_2$

$A_{18} = -x_1^2 D_1 A_1$

$A_{19} = -x_1^2 GJA_1$

$A_{20} = -x_1^2 GJA_2$

$$A_{21} = 0$$

$$A_{22} = -1$$

$$A_{23} = x_1 K_1$$

$$A_{24} = -x_1 K_2$$

$$A_{25} = K_2$$

$$A_{26} = -K_2$$

$$A_{27} = 0$$

$$A_{28} = -1$$

$$B_1 = 2K_1 K_2$$

$$B_2 = K_1^2 - K_2^2$$

$$B_3 = K_1(K_1^2 - K_2^2)$$

$$B_4 = K_2(3K_1^2 - K_2^2)$$

$$B_5 = -EIx_1^4(B_2^2 - B_1^2)$$

$$B_6 = 2EIx_1^4 B_1 B_2$$

$$B_7 = D_y$$

$$B_8 = -x_1^2 D_y B_2$$

$$B_9 = x_1^2 D_y B_1$$

$$B_{10} = D_x B_3 - K_1(D_1 + D_{xy} + D_{yx})$$

$$B_{11} = -D_x B_4 + K_2(D_1 + D_{xy} + D_{yx})$$

$$B_{12} = x_1^2(D_1 + D_{xy} + D_{yx})B_1$$

$$B_{13} = -D_x + x_1^2(D_1 + D_{xy} + D_{yx})B_2$$

$$B_{14} = D_x B_2 - D_1$$

$$B_{15} = -D_x B_1$$

$$B_{16} = GJK_2$$

$$B_{17} = -D_x + D_1 x_1^2 B_2$$

$$B_{18} = -x_1^2 D_1 B_1$$

$$B_{19} = x_1^2 (GJB_1)$$

$$B_{20} = x_1^2 (GJB_2)$$

$$B_{22} = 1$$

$$B_{23} = k_1 x_1$$

$$B_{24} = -K_2 x_1$$

$$B_{26} = -K_2$$

$$B_{27} = 0$$

$$B_{28} = 1$$

$$K_{1n} = \cosh R_{1n} \cos R_{r1}$$

$$K_{2n} = \sinh R_{1n} \cos R_{r1}$$

$$K_{3n} = \sinh R_{1n} \cos R_{r1}$$

$$K_{4n} = \cosh R_{1n} \sin R_{r1}$$

$$K_{5n} = \cosh R_{2n} \cos R_{r2}$$

$$K_{6n} = \sinh R_{2n} \sin R_{r2}$$

$$K_{7n} = \sinh R_{2n} \cos R_{r2}$$

$$K_{8n} = \cosh R_{2n} \sin R_{r2}$$

$$R_{r1} = x_1 K_2 \alpha_n b$$

$$R_{r2} = K_2 \beta_n a$$

$$R_{1n} = x_1 K_1 \alpha_n b$$

$$R_{2n} = K_1 \beta_n a$$

$$S_{aa} = 2/(\beta_n^2 a^2 (\beta_n^2 a^2 / x_1^2 + 2A_2 m^2 \pi^2) + m^4 \pi^4)$$

$$S_{a1} = S_{aa} m\pi (-1)^m$$

$$S_{a2} = S_{aa} \beta_n a (-1)^m$$

$$S_{b2} = 2/(\beta_n^2 a^2 (\beta_n^2 a^2 / x_1^2 + 2B_2 m^2 \pi^2) + m^4 \pi^4)$$

$$S_{b1} = S_{ba} m\pi (-1)^m$$

$$S_{b2} = S_{ba} \beta_n a (-1)^m$$

$$S_{xa} = 2/(x_1^2 \alpha_n^2 b^2 (\alpha_n^2 b^2 + 2A_2 m^2 \pi^2) + m^4 \pi^4)$$

$$S_{x1} = S_{xa} m\pi (-1)^m$$

$$S_{ya} = 2/(x_1^2 \alpha_n^2 b^2 (\alpha_n^2 b^2 + 2B_2 m^2 \pi^2) + m^4 \pi^4)$$

$$S_{y1} = S_{ya} m\pi (-1)^m$$

$$S_{y2} = S_{ya} \alpha_n b (-1)^m$$

$$T_{a1} = A_1 \beta_n^2 a^2$$

$$T_{a2} = A_2 \beta_n^2 a^2 + m^2 \pi^2$$

$$T_{a3} = K_1 (\beta_n^2 a^2 / x_1 + m^2 \pi^2)$$

$$T_{a4} = K_2 (\beta_n^2 a^2 / x_1 - m^2 \pi^2)$$

$$T_{b1} = B_1 \beta_n^2 a^2$$

$$T_{b2} = B_2 \beta_n^2 a^2 / x_1 + m^2 \pi^2$$

$$T_{b3} = K_1 (\beta_n^2 a^2 / x_1 + m^2 \pi^2)$$

$$T_{b4} = K_2 (\beta_n^2 a^2 / x_1 - m^2 \pi^2)$$

$$T_{x1} = A_1 \alpha_n^2 b^2 x_1^2$$

$$T_{x2} = A_2 \alpha_n^2 b^2 x_1^2 + m^2 \pi^2$$

$$T_{x3} = x_1 K_1 (x_1 \alpha_n^2 b^2 + m^2 \pi^2)$$

$$T_{x4} = x_1 K_2 (x_1 \alpha_n^2 b^2 - m^2 \pi^2)$$

$$T_{y1} = B_1 \alpha_n^2 b^2 x_1^2$$

$$T_{y2} = B_2 x_1^2 \alpha_n^2 b^2 + m^2 \pi^2$$

$$T_{y3} = K_1 x_1 (x_1 \alpha_n^2 b^2 + m^2 \pi^2)$$

$$T_{y4} = x_1 K_2 (x_1 \alpha_n^2 b^2 - m^2 \pi^2)$$

$$\mu_{3n} = K_1 \beta_n x$$

$$\mu_{4n} = K_2 \beta_n x$$

Fourier Coefficients For Lateral Load

The Fourier coefficients of Equation 4.14 are evaluated below:

$$a_{00} = (1/2a) \int_{-a}^{a} f_o(x)\,dx$$

$$= (1/2a) \int_{-a}^{a} [C_{17} + C_{20}(x^2/a^2) + C_{21} + C_{24}(Tx^4/b^4 - 1)]\,dx$$

$$= C_{17} + 1/3\, C_{20} + C_{21} + C_{24}(Ta^4/5b^4 - 1)$$

$$a_{om} = (1/a) \int_{-a}^{a} f_o(x) \cos\alpha_m x \, dx$$

$$= (1/a) \int_{-a}^{a} [C_{17} + C_{20}(x^2/a^2) + C_{21} + C_{24}(Tx^4/b^4 - 1)] \cos\alpha_m x \, dx$$

$$= C_{20}I_{1m} + C_{24}T\, I_{3m}\, a^4/b^4$$

The integrals I_{1m}, I_{3m}, etc. are defined at the end of this appendix with change of index from m to n wherever necessary.

$$b_{om} = (1/a) \int_{-a}^{a} f_o(x) \sin\alpha_m x \, dx = 0$$

$$c_{no} = (1/2a) \int_{-a}^{a} f_n(x)\,dx$$

$$= (C_{1n}W_{1n} + C_{4n}W_{2n} + C_{5n}W_{3n} + C_{8n}W_{4n})(-1)^n$$

$$c_{nm} = (1/a) \int_{-a}^{a} f_n(x) \cos\alpha_m x \, dx$$

$$= (C_{1n}A_{j1} + C_{4n}A_{j2} + C_{5n}A_{j4})(-1)^n$$

$$d_{nm} = (1/a) \int_{-a}^{a} f_n(x) \sin\alpha_m x \, dx = 0$$

Fourier Expansions and Definite Integrals

$$I_{1n} = (1/a) \int_{-a}^{a} (x^2/a^2)\cos \alpha_n x \, dx$$

$$= (1/b) \int_{-b}^{b} (y^2/b^2)\cos \beta_n y \, dy$$

$$= 4(-1)^n/n^2\pi^2 \text{ , and so on.}$$

$$I_{3n} = (1/a) \int_{-a}^{a} (x^4/a^4)\cos \alpha_n x \, dx$$

$$= (1/b) \int_{-b}^{b} (y^4/b^4)\cos \beta_n y \, dy$$

$$= 8(-1)^n(1-6/n^2\pi^2)/n^2\pi^2$$

$$I_{5n} = -2(-1)^n/n\pi$$

$$I_{7n} = -2(-1)^n(1-6/n^2\pi^2)/n\pi$$

$$W_{1n} = (1/2a) \int_{-a}^{a} \cosh \mu_{3n}\cos \mu_{4n} \, dx$$

$$= x_1(K_1 K_{7n} + K_2 K_{8n})/a \beta_n$$

$$W_{2n} = x_1(K_1 K_{8n} - K_2 K_{7n})/a \beta_n$$

$$\hat{W}_{3n} = x_1(K_1 K_{7n} + K_2 K_{8n})/a \beta_n$$

$$W_{4n} = x_1(K_1 K_{8n} - K_2 K_{7n})/a \beta_n$$

$$W_{5n} = (K_1 K_{3n} + K_2 K_{4n})/b \alpha_n$$

$$W_{6n} = (K_1 K_{4n} - K_2 K_{3n})/b \alpha_n$$

$$W_{7n} = (K_1 K_{3n} + K_2 K_{4n}/b \alpha_n$$

$$W_{8n} = (K_1 K_{4n} - K_2 K_{3n})/b \, \alpha_n$$

$$A_{j1} = (1/a) \int_{-a}^{a} \cosh \mu_{3n} \cos \mu_{4n} \cos \alpha_m x \, dx$$

$$= S_{a2}(T_{a3}K_{7n} + T_{a4}K_{8n})$$

$$A_{j2} = S_{a2}(-T_{a4}K_{7n} + T_{a3}K_{8n})$$

$$A_{j3} = S_{b2}(T_{b3}K_{7n} + T_{b4}K_{8n})$$

$$A_{j4} = S_{b2}(-T_{b4}L_{7n} + T_{b3}K_{8n})$$

$$A_{j5} = S_{x2}(T_{x3}K_{3n} + T_{x4}K_{4n})$$

$$A_{j6} = S_{x2}(-T_{x4}K_{3n} + T_{x3}K_{4n})$$

$$A_{j7} = S_{y2}(T_{y3}K_{3n} + T_{y4}K_{4n})$$

$$A_{j8} = S_{y2}(T_{y4}K_{3n} - T_{y3}K_{4n})$$

$$B_{j1} = (1/a) \int_{-a}^{a} \sinh \mu_{3n} \cos \mu_{4n} \sin \alpha_m x \, dx$$

$$= S_{a1}(-T_{a2}K_{7n} - T_{a1}K_{8n})$$

$$B_{j2} = S_{a1}(T_{a1}K_{7n} - T_{a2}K_{8n})$$

$$B_{j3} = S_{b1}(-T_{b2}K_{7n} - T_{b1}K_{8n})$$

$$B_{j4} = S_{b1}(T_{b1}K_{7n} - T_{b2}K_{8n})$$

$$B_{j5} = S_{x1}(-T_{x2}K_{3n} - T_{x1}K_{4n})$$

$$B_{j6} = S_{x1}(T_{x1}K_{3n} - T_{x2}K_{4n})$$

$$B_{j7} = S_{y1}(-T_{y2}K_{3n} - T_{y1}K_{4n})$$

$$B_{j8} = S_{y1}(T_{y1}K_{3n} - T_{y2}K_{4n})$$

APPENDIX (C)

Design of Concrete Mix

Two trial mixes were made to meet the following conditions: concrete is required for reinforced and pre-stressed concrete slab for using in the composite bridges;

Concrete mix must have: 3 to 4 in. range in slump suitably vibrated and adequately cured.

Strength: Two different concrete mixes for strength equal to 5000 and 8000 psi were required for reinforced and prestressed concrete slab of composite bridges.

Cement content: High early strength portland cement manufactured by Canada Cement Company was used in all the bridges. Different cement contents range from 500 to 700 lbs. per cu. yd. and air content of 3.5% were used in the concrete mixes.

Aggregates: Maximum size of the aggregate was restricted to 0.25 inch (6.4 mm) since the concrete cover to the center of steel reinforcement was 0.5 inch (12.7 mm) with a specific gravity equal to 2.65.

Assumption: According to reference (22), the amount of water required per cubic yard 400 lb. The percentage of fine aggregate to the total aggregate was assumed between 40 to 70% for the different trial mixes.

Quantities per cubic yard: From the information given, the absolute volume occupied by the paste was calculated as:

130

Cement, abs. vol.   = 560/(3.15x62.4)   = 2.85 cu. ft.

Water, abs. vol.   = 392/(1.0x62.4)   = 6.28 cu. ft.

Air, abs. vol.   = 3.5x0.27   = 0.94 cu. ft.

Paste, total vol.   = 2.85+6.28+0.94   = 10.07 cu. ft.

Aggregate, abs. vol.   = 27-10.07   = 16.93 cu. ft.

Coarse aggregate, wt. = 16.93x0.40x2.65x62.4 = 1120 lbs.

Fine aggregate, wt.   = 16.93x0.60x2.65x62.4 = 1680 lbs.

The above quantities per cubic yard were approximate, and used as a preliminary trial batch.

For 10 lbs. of cement, a trial batch consisted of:

Cement   = 10.00 lbs.

Water   = 392 x 10/(560)   =   7.00 lbs.

Coarse aggregate = 1120 x 10/(560) = 20.00 lbs.

Fine aggregate   = 1680 x 10/(560) = 30.00 lbs.

Based on the workability and maximum strength of this trial mix, two trial mixes with different water/ cement ratio and fine aggregate content were made using reference (22).

The following table shows the properties of the two mixes and their strength after 7, 14 and 28 days.

Table (C.1)

Mix No.	Ratio by Weight in lbs.				Strength in psi		
	Cement	Water	Sand	Gravel	7 days	14 days	28 days
1	1.0	0.70	3.00	2.00	4000	4680	5500
2	1.0	0.40	2.25	1.50	6600	7500	8000

The total volume of the slab and cylinders = 11 ft^3.

and the total weight of the concrete mix required:

$$11 \times 146 = 1606 \text{ lbs.}$$

which was divided into three batches. Mix No. 1 was chosen
for the reinforced composite bridge and Mix No. 2 for the
prestressed portion of the composite bridge model (II).

APPENDIX (D)

Rigidities and Properties of Slab Models

Rigidities of Uncracked Section: (Theory)

Longitudinal Direction:
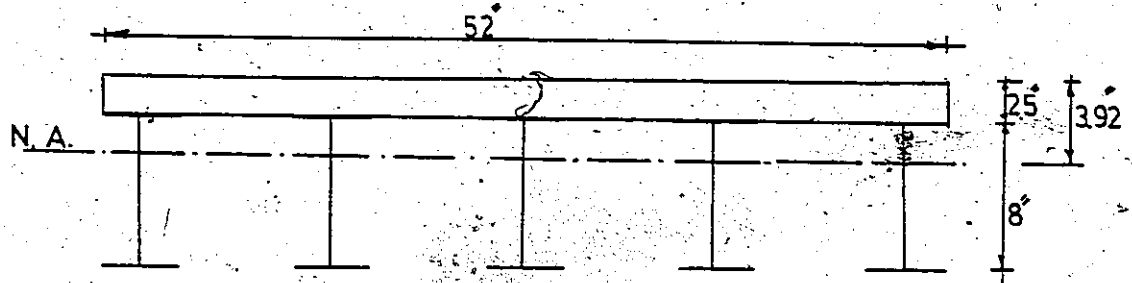
$$e_y = \frac{(52 \times 2.5) \times 1.25 + 7 \times 5(3.83 \times 6.5)}{(52 \times 2.5) + 7 \times 5(3.83)}$$

$$= 3.92 \text{ in.}$$

$$I_y = \frac{52 \times 2.5^3}{12(1-\nu^2)} + \left(\frac{52 \times 2.5}{1-\nu^2}\right) \times (3.92-1.25)^2$$

$$+ 7 \times 5[39.6 + 3.83 \times (6.5-3.92)^2]$$

$$= 1017.4 + 2278.3$$

$$= 3295 \text{ in.}^4$$

$$i = I_y/52$$

$$= 63.4 \text{ in}^4/\text{in.}$$

$$D_y = E_c \cdot i$$

$$= 280 \times 10^6 \text{ lb.in}^2/\text{in.}$$

$$i_o = \frac{h^3}{6}$$

$$= \frac{2.5^3}{6}$$

$$= 2.6 \text{ in}^4/\text{in.}$$

$$D_{yx} = G \cdot i_o$$

$$= 1.92 \times 10^6 * 2.6$$

$$= 5.00 \times 10^6 \text{ lb.in}^2/\text{in.}$$

$$D_1 = E_c \times \nu \times \frac{1}{52} [1017.4]$$

$$= 13.00 \times 10^6 \text{ lb.in}^2/\text{in.}$$

Transverse Direction:

$$e_x = \frac{(132*2.5)1.25 + 7x5(4.56x6.5)}{132x2.5 + 7x5x4.56}$$

$$= 2.96 \text{ in.}$$

$$I_x = [\frac{132x2.5^3}{12(1-\nu^2)} + (\frac{132x2.5}{1-\nu^2}) \times (2.96-1.25)^2]$$

$$+ 7x5[30.1 + 4.56(6.5-2.96)^2]$$

$$= [1160] + [3653.5]$$

$$= 4214 \text{ in}^4$$

$$j = I_y/132$$

$$= 31.92 \text{ in}^4/\text{in.}$$

$$D_x = E_c \cdot j$$

$$= 141.00 \times 10^6 \text{ lb.in}^2/\text{in.}$$

$$D_{xy} = D_{yx}$$

$$D_2 = 1160 \times \nu \times E \times \frac{1}{132}$$

$$= 5.83 \times 10^6 \text{ lb.in}^2/\text{in.}$$

Rigidities According to OHBDC-1 (neglecting the diaphragms):

Longitudinal Direction:

e_y = 3.92 in.

D_y = 280 x 10^6 lb.in^2/in.

D_{yx} = 5.0 x 10^6 lb.in^2/in.

D_1 = ν(Lesser of D_x or D_y)

Transverse Direction:

e_x = 1.25 in.

$I_x = \dfrac{2.5^3}{12(1-\nu^2)}$

= 1.33 in^4/in.

$D_x = E_c \times 1.33$

= 5.87 x 10^6 lb.in^2/in.

$D_2 = D_1$

= 0.15 x 5.87

= 0.88 x 10^6 lb.in^2/in.

$D_{xy} = D_{yx}$

= 5 x 10^6 lb.in^2/in.

Rigidities According to OHBDC-2 (by just adding the rigidity of the diaphragms to the rigidity of the slab in the transverse direction):

Longitudinal Direction:

As above

Transverse Direction:

e_x = 1.25 in.

D_x = 41.00 x 10^6 lb.in^2/in.

D_2 = D_1

= ν x 41.00

= 6.15 x 10^6 lb.in^2/in.

D_{xy} = D_{yx}

= 5 x 10^6 lb.in^2/in.

TABLE D.1

MECHANICAL PROPERTIES OF STEEL GIRDER

Type of Specimen	Yield Stress (ksi)	Tensile Strength (ksi)	% Elongation In 2"
Web & Flange	45	70	23

TABLE D.2

ROLLED STEEL BEAM PROPERTIES

Beam	Area (in^2)	Depth (in)	Flange		Web Thickness (in)	Moment of Inertia (in^4)
			Width (in)	Thickness (in)		
W 8x13	3.83	8	4.00	0.254	0.230	39.6
W 6x15.5	1.41	6	6	0.269	0.235	30.1
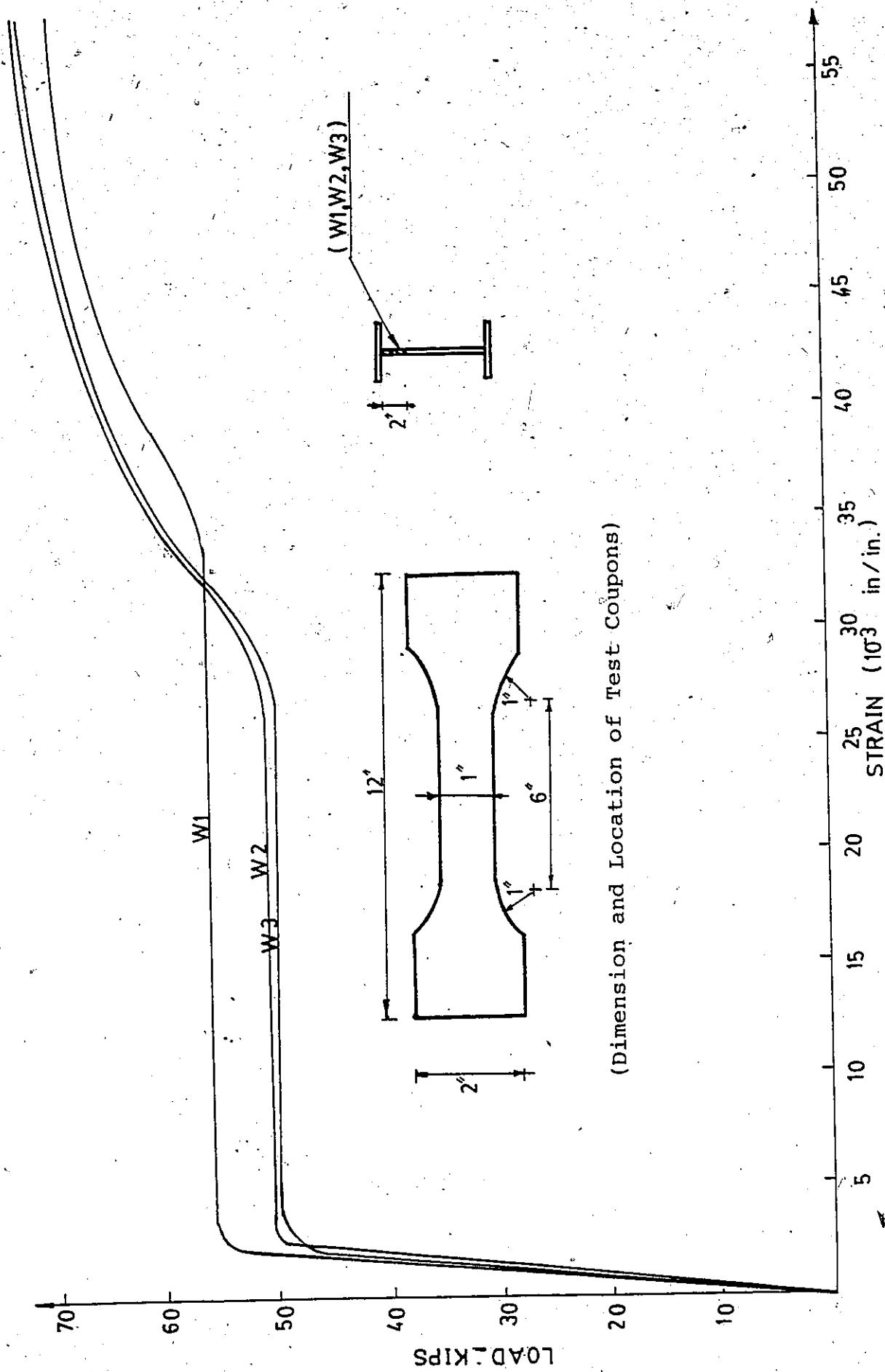
FIGURE D.1 COUPON TEST OF STEEL GIRDER

TABLE D.3

COMPARISON BETWEEN THE RIGIDITIES

				Rigidities				
	e_x	D_x	D_1	D_{xy}	e_y	D_y	D_2	D_{yx}
Theory	2.96	141	5.83	2.5	3.92	280	13	2.5
OHBDC-1	1.25	5.87	0.88	2.5	3.92	280	0.88	2.5
OHBDC-2	1.25	41.03	6.15	2.5	3.92	280	6.15	2.5

all units in lb.in^2/in. x 10^6

APPENDIX (E)

Calibration of Load Cells

FIGURE E.1 CALIBRATION OF LOAD CELL (150 KIPS)
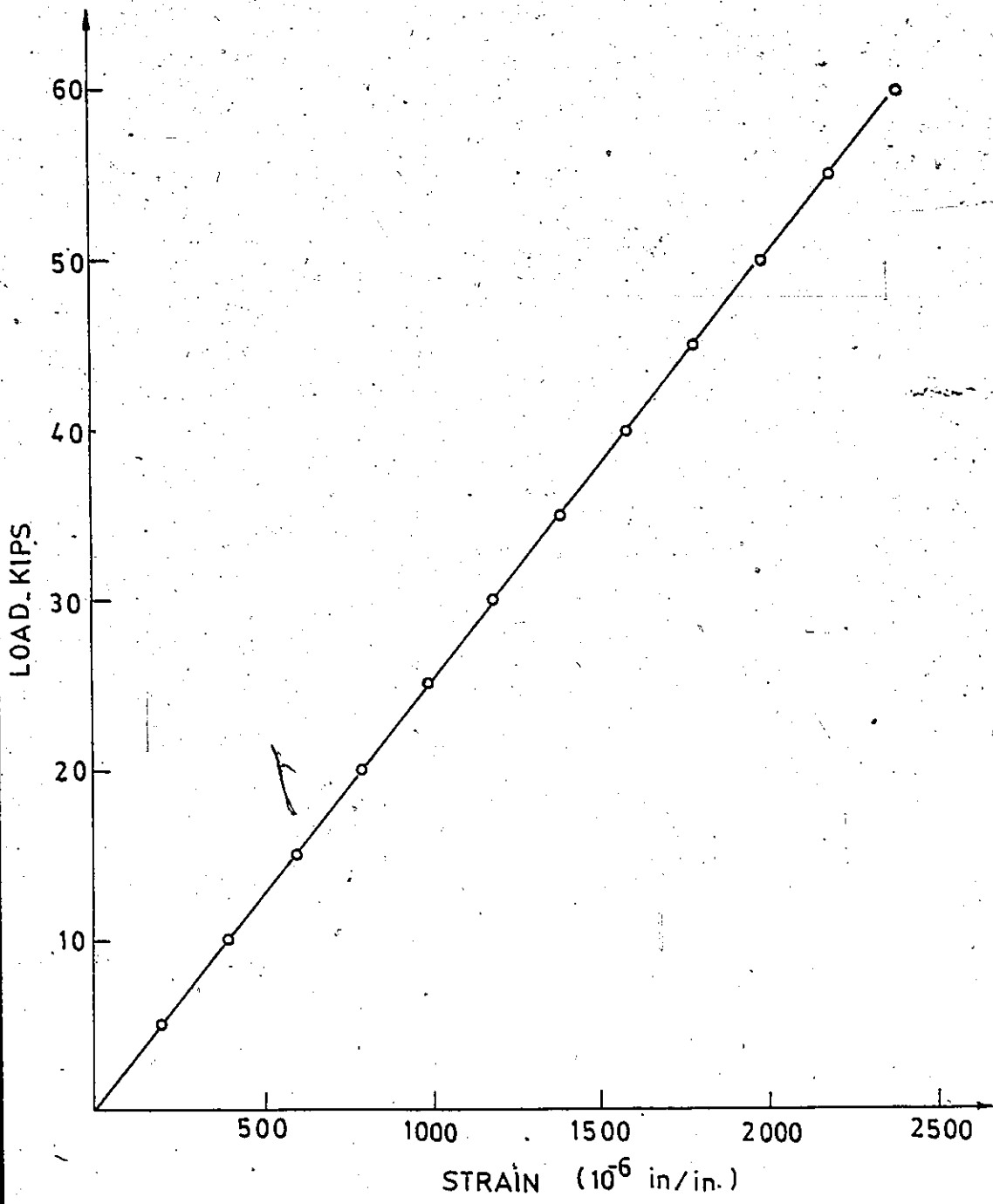
FIGURE E.2   CALIBRATION OF LOAD CELL (50 KIPS)

APPENDIX (F)

Parametric Study

TABLE F.1

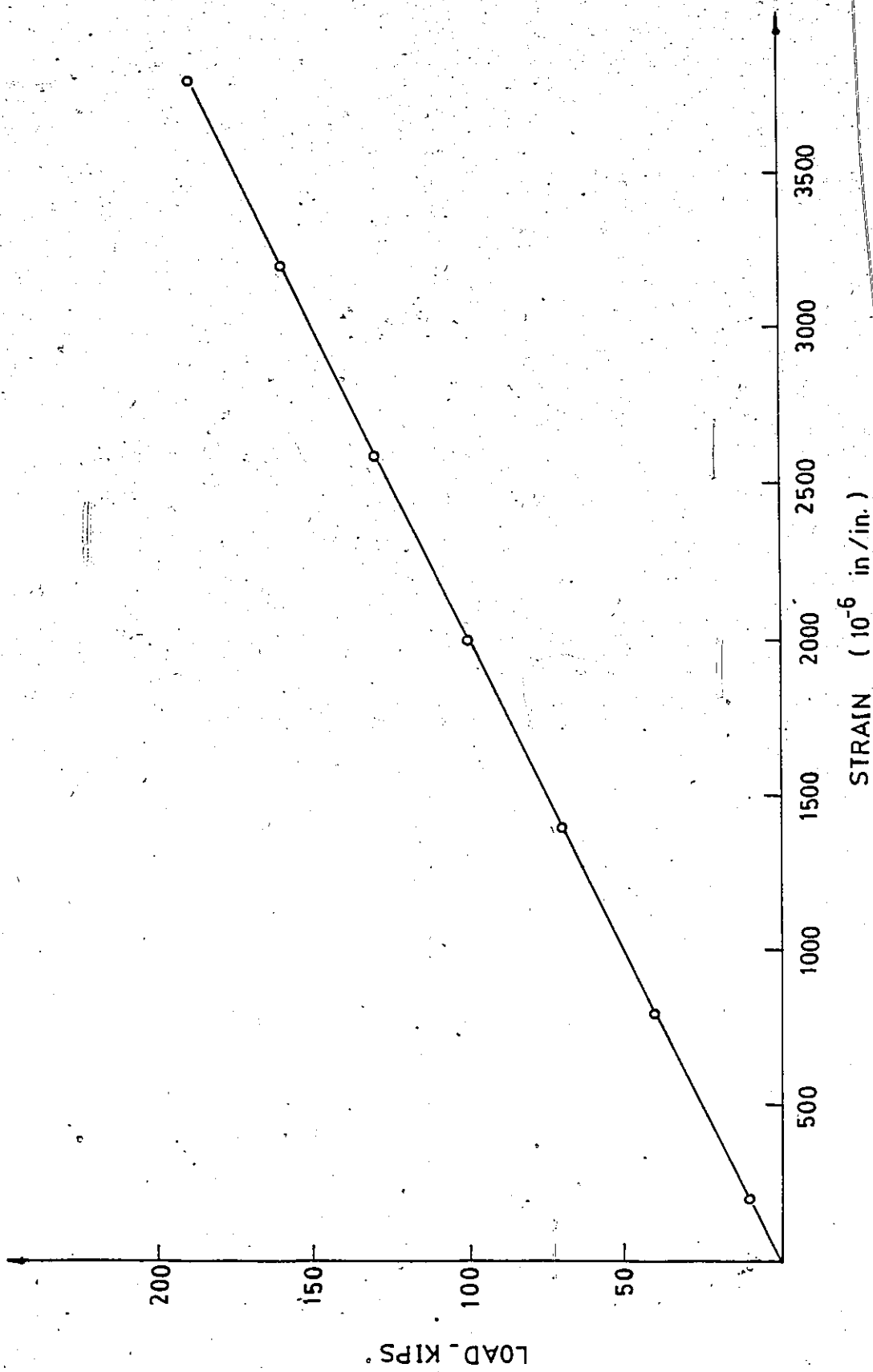| Aspect Ratio	OHBDC								THEORY							
Rigidities	e_x	e_y	D_x	D_y	D_1	D_2	D_{xy}	D_{yx}	e_x	e_y	D_x	D_y	D_1	D_2	D_{xy}	D_{yx}
b = 30' a = 60' b/a = 0.5	5.5	8.54	354	3856	53.12	53.12	301	301	7.79	8.54	2736	3856	78.9	99.8	301	301
b = 30' a = 30' b/a = 1.0	5.5	10.89	354	6804	53.12	53.12	301	301	7.79	10.89	2736	6804	78.9	201.5	301	301
b = 30' a = 20' b/a = 1.5	5.5	12.75	354	9422	53.12	53.12	301	301	7.79	12.75	2736	9422	78.9	322.5	301	301
b = 30' a = 15' b/a = 2.0	5.5	14.26	354	11643	53.12	53.12	301	301	7.79	14.26	2736	11693	78.9	446.9	301	301

All units in lb.in^2/in *10^6

ORTHOTROPIC RIGIDITIES OF DIFFERENT ASPECT RATIO

Calculation of Rigidity According to OHBDC: (by ignoring the effect of the transverse diaphragms), $b/a = 0.5$

Span = $2b = 60'$; Width = $2a = 120'$

Longitudinal Direction:

1.1 Find e_y: in units of Deck concrete, $n = 10$

$$e_y = \frac{(24 \times 12 \times 11)\, 5.5 + 10(47.1) \times 29}{(24 \times 12 \times 11) + 10(47.1)}$$

$$= 8.54 \text{ in.}$$
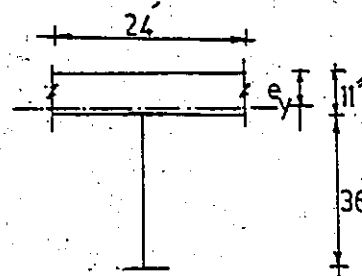
1.2 Find I_y:

$$I_y = [\, 24 \times 12 \times \frac{11^3}{12} + (24 \times 12 \times 11) \times (8.54-5.5)^2\,]$$

$$+ 10[\, 9760 + 47.1 \times (29-8.54)^2\,]$$

$$= 61414.32 + 294766$$

$$= 356180 \text{ in.}^4$$

1.3 Find i, i_o:

$$i = I_y/P_y$$

$$= 1236 \text{ in.}^4/\text{in.}$$

$$i_o = \frac{t^3}{6}$$

$$= 221.8 \text{ in.}^4/\text{in.,}$$ i.e., the torsional inertia of the steel girder is neglected.

1.4 Find D_y, D_1:

$$D_y = E \cdot i$$

$$= 3.12 \times 10^6 \times 1236$$

$$= 3856.00 \times 10^6 \text{ lb.in}^2/\text{in.}$$

$$D_1 = \nu \,(\text{Lesser of } D_x \text{ and } D_y)$$

$$= 53 \times 10^6 \text{ lb.in}^2/\text{in.}$$

$$D_{xy} = G \cdot i_o$$

$$= 1.36 \times 10^6 \times 221.8$$

$$= 301.00 \times 10^6 \text{ lb.in}^2/\text{in.}$$

Transverse Direction:

$$j = \frac{t^3}{12(1-\nu^2)}$$

$$= 113.5 \text{ in.}^4/\text{in.}$$

$$D_x = E \cdot j$$

$$= 354.00 \times 10^6 \text{ lb.in}^2/\text{in.}$$

$$D_{yx} = D_{xy}$$

$$= 301.00 \times 10^6 \text{ lb.in}^2/\text{in.}$$

$$D_2 = D_1$$

$$= 53.00 \times 10^6 \text{ lb.in}^2/\text{in.}$$

Calculation of Rigidity According to Theory: (by taking into account the transverse diaphragms), as connected rigidly to the main girder.

Longitudinal Direction:

$$e_y = 8.54 \text{ in.}$$

$$I_y = 356180 \text{ in.}$$

$$D_y = 3856.00 \times 10^6 \text{ lb.in}^2/\text{in.}$$

$$D_2 = 61414.32$$

$$= 0.5(61414.32)$$

$$= 9212 \times E/24 \times 12$$

$$= 99.8 \times 10^6 \text{ lb.in}^2/\text{in.}$$

$$D_{xy} = D_{yx}$$

$$= 301.00 \times 10^6 \text{ lb.in}^2/\text{in.}$$

Transverse Direction:

$$e_x = 7.79 \text{ in.}$$

$$I_x = 1.26 \times 10^6 \text{ in}^4$$

$$j = 877 \text{ in}^4/\text{in.}$$

$$D_x = E \cdot j$$

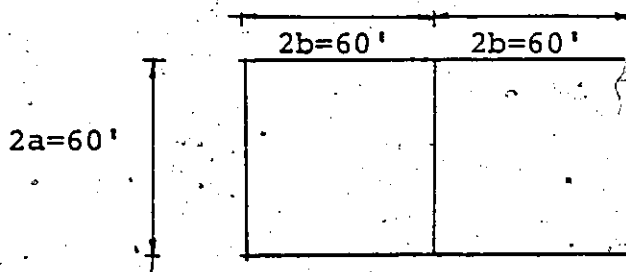$$= 2736 \times 10^6 \text{ lb.in}^2/\text{in.}$$

$$D_1 = 79.00 \times 10^6 \text{ lb.in}^2/\text{in.}$$

$$D_{yx} = 301.00 \times 10^6 \text{ lb.in}^2/\text{in.}$$

Case (2), Aspect Ratio = 1.0 = b/a

Span = 60' = 2b; Width = 2a = 60'

Plan

Calculation of Rigidity According to OHBDC:

Longitudinal Direction:

1.1 Find e_y, I_y:

$$e_y = \frac{(12 \times 12 \times 11) \times 5.5 + 10(47.1) \times 29}{(12 \times 12 \times 11) + 10(47.1)}$$

$$= 10.89 \text{ in.}$$

$$I_y = [12 \times 12 \times \frac{11^3}{12} + (12 \times 12 \times 11) \times (10.89-5.5)^2]$$

$$+ 10[9760 + 47.1(29-10.89)^2]$$

$$= 61990.5 + 252074$$

$$= 314065 \text{ in.}^4$$

1.2 Find i, i_o:

$$i = I_y / P_y$$

$$= 2181.01 \text{ in.}^4/\text{in.}$$

$$i_o = 221.8 \text{ in.}^4/\text{in.}$$

1.3 Find D_y, D_1:

$$D_y = 3.12 \times 10^6 \times 2181.01$$

$$= 6805.00 \times 10^6 \text{ lb.in}^2/\text{in.}$$

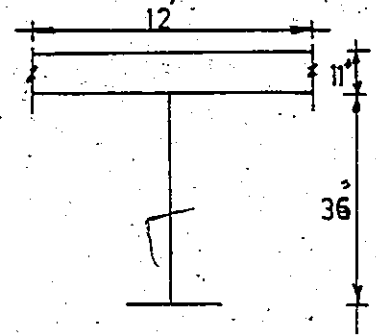$$D_1 = \nu(\text{Lesser of } D_x \text{ and } D_y)$$

$$= 53.00 \times 10^6 \text{ lb.in}^2/\text{in.}$$

$$D_{xy} = G \cdot i_o$$

$$= 301.00 \times 10^6 \text{ lb.in}^2/\text{in.}$$

Transverse Direction:

$$D_x = 354.12 \times 10^6 \text{ lb.in}^2/\text{in.}$$

$D_{yx} = D_{xy}$

$\qquad = 301.00 \times 10^6$ lb.in^2/in.

$D_2 = D_1$

$\qquad = 53.00 \times 10^6$ lb.in^2/in.

Calculation of Rigidity According To Theory:

Longitudinal Direction:

$e_y = 10.89$ in.

$D_y = 6805.00 \times 10^6$ lb.in^2/in.

$D_{xy} = 301.00 \times 10^6$ lb.in^2/in.

$D_2 = \nu[61990.5] \times E/12 \times 12$

$\qquad = 201.00 \times 10^6$ lb.in^2/in.

Transverse Direction:

$e_x = 7.79$ in.

$D_x = 2736 \times 10^6$ lb.in^2/in.

$D_1 = 79.00 \times 10^6$ lb.in^2/in.

$D_{yx} = 301.00 \times 10^6$ lb.in^2/in.

Calculation of Rigidity According to OHBDC: (b/a = 1.5)
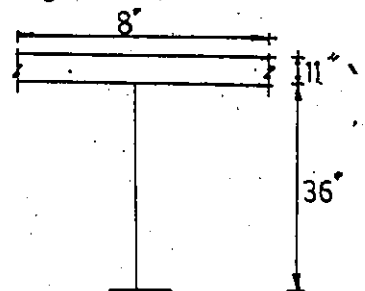
Span = 2b = 60'; Width = 2a = 40'

Calculation of Standard Parameters (Table A5.3(b)).

Longitudinal Direction:

1.1 Find e_y: (in units of Deck concrete and assuming n=10)

$$e_y = \frac{(8 \times 12 \times 11) \times 5.5 + 10(47.1) \times 29}{(8 \times 12 \times 11) + (10 \times 47.1)}$$

$\qquad = 12.75$ in.

$$I_y = [96 \times \frac{11^3}{12} + (96 \times 11) \times (12.75-5.5)^2]$$

$$+ 10[9760 + 47.1 \times (29-12.75)^2]$$

$$= 10648 + 55506 + 221973$$

$$= 2.9 \times 10^5 \text{ in.}^4$$

$$i = (I_y/P_y)$$

$$= (2.9 \times 10^5) \times \frac{1}{8 \times 12}$$

$$= 3020 \text{ in}^4/\text{in.}$$

$$j = \frac{t^3}{12(1-\nu^2)}$$

$$= \frac{11^3}{12(1-0.15^2)}$$

$$= 113.5 \text{ in.}^4/\text{in.}$$

The torsional inertia of the steel girder is neglected, so that:

$$i_o = j_o$$

$$= t^3/6$$

$$= 11^3/6$$

$$= 221.8 \text{ in}^4/\text{in.}$$

Calculation of properties of the idealized orthotropic plate using table A5.3(a):

$$D_y = E \cdot i$$

$$= (3.12 \times 10^6) \times 3020$$

$$= 9422.0 \times 10^6 \text{ lb.in}^2/\text{in.}$$

$$D_{xy} = G \cdot i_o$$

$$= (1.36 \times 10^6) \times 221.8$$

$$= 301.00 \times 10^6 \text{ lb.in}^2/\text{in.}$$

D_1 = ν(Lesser of D_x and D_y)

   = 53.00 x 10^6 lb.in²/in.

Transverse Direction:

j   = 113.5 in.⁴/in.

D_x = E·j

   = 3.12 x 10^6 x 113.5

   = 354.00 x 10^6 lb.in²/in.

D_{yx} = G·j_o

   = D_{xy}

   = 301.00 x 10^6 lb.in²/in.

D_2 = D_1

   = 53.00 x 10^6 lb.in²/in.

Calculation of Rigidity According to Theory

Longitudinal Direction:

e_y = 12.75 in.

I_y = 2.9 x 10^5 in.⁴

D_y = 9422.0   x10^6 lb.in²/in.

D_{xy} = 301.00 x 10^6 lb.in²/in

D_2·   = ν[10648 + 55506] x E x $\frac{1}{8x12}$

   = 322.50 x 10^6 lb.in²/in.

D_{xy} = D_{yx}

   = 301.00 x 10^6 lb.in²/in.

Transverse Direction:

$$e_x = \frac{(120 \times 12 \times 11) \times 5.5 + 5 \times 10 \times (34.2) \times 29}{(120 \times 12 \times 11) + 5 \times 10 \times 34.2}$$

$$= 7.79 \text{ in.}$$

$$I_x = [\, 120 \times 12 \times \frac{11^3}{12} + (120 \times 12 \times 11) \times (7.79-5.5)^2 \,]$$

$$+ 10 \times 5 \times [\, 4930 + 34.2 \times (29-7.79)^2 \,]$$

$$= [\, 159720 + 83066.5 \,] + 50[\, 20315 \,]$$

$$= 242786 + 1.02 \times 10^6$$

$$= 1.26 \times 10^6 \text{ in.}^4$$

$$j = \frac{1.26 \times 10^6}{120 \times 12}$$

$$= 877 \text{ in.}^4/\text{in.}$$
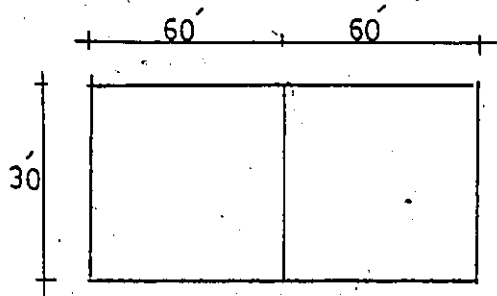
$$D_x = E \cdot j$$

$$= 2736 \times 10^6 \text{ lb.in}^2/\text{in.}$$

$$D_1 = \nu[\, 242786 \,] \times E \times \frac{1}{120 \times 12}$$

$$= 79.00 \times 10^6 \text{ lb.in}^2/\text{in.}$$

Case (4), Aspect ratio = 2.0 = b/a

Span = 2b = 60'; Width = 2a = 30'

Plane

Calculation of Rigidity According to OHBDC:

Longitudinal Direction:

$$e_y = \frac{(6 \times 12 \times 11) \times 5.5 + 10(47.1) \times 29}{(6 \times 12 \times 11) + 10(47.1)}$$

$$= 14.26 \text{ in.}$$

$$I_y = [6 \times 12 \times \frac{11^3}{12} + (6 \times 12 \times 11) \times (14.126 - 5.5)^2]$$

$$+ 10[9760 + 47.1(14.26 - 29)^2]$$

$$= 68762 + 199933.0$$

$$= 268695 \text{ in.}^4$$

$$i = 3731.8 \text{ in.}^4/\text{in.}$$

$$i_o = 221.8 \text{ in}^4/\text{in.}$$

$$D_y = 11643.00 \times 10^6 \text{ lb.in}^2/\text{in.}$$

$$D_1 = 53.00 \times 10^6$$

$$D_{xy} = 301.00 \times 10^6 \text{ lb.in}^2/\text{in.}$$

$$D_x = 354.00 \times 10^6 \text{ lb.in}^2/\text{in}$$

$$D_{yx} = D_{xy}$$

$$= 301.00 \times 10^6 \text{ lb.in}^2/\text{in.}$$

Calculation of Rigidity According to Theory:

$$e_y = 14.26 \text{ in.}$$
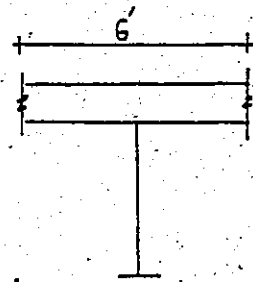
$$D_y = 11693.46 \times 10^6 \text{ lb.in}^2/\text{in.}$$

$$D_2 = 0.15 \times 68762 \times 3.12 \times 10^6 \times 1/72$$

$$= 447.00 \times 10^6 \text{ lb.in}^2/\text{in.}$$

$$e_x = 7.79 \text{ in.}$$

$$D_x = 2736 \times 10^6 \text{ lb.in}^2/\text{in.}$$

$$D_1 = 79.00 \times 10^6 \text{ lb.in}^2/\text{in.}$$

$$D_{xy} = D_{yx}$$

$$= 301 \times 10^6 \text{ lb.in}^2/\text{in.}$$

BIBLIOGRAPHY

1. American Concrete Institute, "Building Code Requirements for Reinforced Concrete," (ACI 318-71), 1971.

2. Bares, R., and Massonet, C., "Analysis of Beam Grids and Orthotropic Plates by the Guyon-Massonet-Bares Method," Frederick Unger Publishing Co., New York, 1968.

3. Barnard, P.R., and Johnson, R.P., "Plastic Behaviour of Continuous Composite Beams," Institution of Civil Engineers, Vol. 32, October 1965.

4. Botzler, P.W., and Colville, J., "Continuous Composite-Bridge Model Tests," Journal of the Structural Division, ASCE, No. ST9, Sept., 1979.

5. Daniels, J.H., and Fisher, J.W., "Prestressing the Negative Moment Region of Composite Beams," Fritz Engineering Laboratory Department of Civil Engineering, Lehigh University, Bethlehem, Pennsylvania.

6. Daniels, J.H., and Fisher, J.W., "Static Behaviour of Continuous Composite Beams," Fritz Engineering Laboratory, Department of Civil Engineering, Lehigh University, Bethlehem, Pennsylvania.

7. Fisher, J.W., Daniels, J.H., and Slutter, R.G., "Continuous Composite Beams for Bridges," International Association for Bridge and Structural Engineering, Ninth Congress, Amsterdam, May, 1972.

8. Garcia, I., and Daniels, J.H., "Tests of Composite Beams Under Negative Moment," Fritz Engineering Laboratory, Department of Civil Engineering, Lehigh University, Bethlehem, Pennsylvania, Feb., 1971.

9. Gupta, D.S.R., "Orthotropic Continuous Skew Plates," Ph.D. Thesis, 1974, Dept. of Civil Engineering, University of Windsor, Windsor, Ontario, Canada.

10. Hoppmann 2nd, and Baltimore, M.D., "Bending of Orthogonally Stiffened Plates," Journal of Applied Mechanics, Transactions, ASME, Vol. 77, June, 1955, pp. 267-271.

11. Huffington, N.J., Jr., and Blacksburg, V2., "Theoretical Determination of Rigidity Properties of Orthogonally Stiffened Plates," Journal of Applied Mechanics, Transactions, ASME, Vol. 78, 1956, Paper No. 55-A-12, pp. 15-20.

12. Hoppmann, W.H., and Huffington, N.J., Jr., and Magness, L.S., "A Study of Orthogonally Stiffened Plates," Journal of Applied Mechanics, Transactions, ASME, Vol.

78, Paper No. 56-APM-11, 1956, pp. 343-350.

13. Iwamoto, K., "On the Continuous Composite Girder," Highway Research Board, Bulletin 339, 1962.

14. Jackson, N., "The Torsional Rigidities of Concrete Bridge Decks," Concrete V_2, nH, Nov., 1968, pp. 465-474.

15. Kennedy, J.B., and Gupta, D.S.R., "Bending of Skew Orthotropic Plate Structure," Journal of the Structural Division, Proc., ASCE, Vol. 102, No. ST8, August, 1976, pp. 1559-1574.

16. Kennedy, J.B., and Bali, S.K., "Rigidities of Concrete Waffle-Type Slab Structures," Canadian Journal of Civil Engineering, Vol. 6, No. 1, 1979.

17. Kuang-Haw Chu, F., and Krishnamoorthy, G., "Use of Orthotropic Plate Theory in Bridge Design," Journal of the Structural Division, Proc., ASCE, June, 1962.

18. Ontario Highway Bridge Design Code, 1979, Volume I and Volume II.

19. Pama, R.P., and Cusens, A.R., "Load Distribution in Multi-Beam Concrete Bridges," American Concrete Institute Paper SP 23-7.

20. Portland Cement Association, "Design and Control of Concrete Mixtures," Eleventh Edition, 1968.

21. Rowe, R.E., "Load Distribution in Bridge Slabs (With Special Reference to Transverse Bending Moments Determined From Tests on Three Prestressed Concrete Slabs)," Magazine of Concrete Research, Vol. 9, No. 27, November, 1957.

22. Siess, C.P., and Viest, I.M., "Studies of Slab and Beam Highway Bridges, :V: Tests of Continuous Right I-Beam Bridges," Bulletin No. 416, University of Illinois, Engineering Experiment Station, 1953.

23. Slutter, Roger G., and Driscoll, George, C., Jr., "Flexural Strength of Steel-Concrete Composite Beams," Journal of The Structural Division, ASCE, Vol. 91, No. ST2, 1965.

24. Szilard, R., "Theory and Analysis of Plates: Classical and Numerical Methods," Prentice-Hall Inc. Englewood Cliffs, New Jersey, 1974.

25. Tachibaba, Kondo, K., and Ito, K., "Experimental Study on Composite Beams Prestressed with Wire Cables," International Association for Bridge and Structural Engineering, Preliminary Publication of the Seventh Congress, 1964.

26. Timoshenko, S., and Woinowsky-Krieger, S., "Theory of Plates and Shells," McGraw Hill Book Company, 1959.

27. Viest, I.M., Fountain, R.S., and Sieses, C.P., "Development of the New AASHO Specifications for Composite Steel and Concrete Bridges," Highway Research Board, Bulletin 174, 1958.

28. Vitols, V., and Clifton, R.J., "Analysis of Composite Beam Bridges by Orthotropic Plate Theory," Journal of Structural Division, ASCE, August, 1963.

29. Wylie, C.R., "Advanced Engineering Mathematics," McGraw-Hill Book Company, Inc., 1960.

VITA AUCTORIS

NABIL FOUAD FANOUSE GRACE

1952   Born on 23rd of July in PORT-SAID, EGYPT.

1970   Matriculated from Tanta School, TANTA, EGYPT.

1975   Graduated with Bachelor of Science (Honour) in Civil Engineering, from Cairo University, CAIRO, EGYPT.

1975   Appointed as an instructor in Civil Engineering Department, Cairo University, CAIRO, EGYPT.

1976   Joined as a part-time designer Engineer in a Consulting Firm For Civil Engineering, PORT-SAID, EGYPT.

1979   Enrolled in a Master's program in Civil Engineering Department, University of Windsor, WINDSOR, ONTARIO, CANADA.